Aus dem Lehrstuhl für Humangenetik

Prof. Dr. rer. nat. Bernhard H.F. Weber

der Fakultät für Medizin

der Universität Regensburg

NRF2-Associated Antioxidant Stress Response in Age-Related Macular Degeneration (AMD)

Inaugural – Dissertation

zur Erlangung des Doktorgrades

der Medizin

der

Fakultät für Medizin

der Universität Regensburg

vorgelegt von

Emily Webster

2023

Aus dem Lehrstuhl für Humangenetik

Prof. Dr. rer. nat. Bernhard H.F. Weber

der Fakultät für Medizin

der Universität Regensburg

NRF2-Associated Antioxidant Stress Response in Age-Related Macular Degeneration (AMD)

Inaugural – Dissertation

zur Erlangung des Doktorgrades

der Medizin

der

Fakultät für Medizin

der Universität Regensburg

vorgelegt von

Emily Webster

2023

Dekan:	**Prof. Dr. med. Dipl. Phys. Dirk Hellwig**
1. Berichterstatter:	**Prof. Dr. rer. nat. Bernhard H.F. Weber**
2. Berichterstatterin:	**PD Dr. med. habil. Caroline Brandl**
Tag der mündlichen Prüfung:	**14.04.2023**

Parts of this work have already been published (co-first authorship) in a peer-reviewed journal in an open access format:

Plössl, K., **Webster, E.**, Kiel, C., Grassmann, F., Brandl, C., & Weber, B. H. F. (2022). In vitro modeling of the complex retinal condition age-related macular degeneration. *Journal of Translational Genetics and Genomics*, *6*(1), 46-62. http://dx.doi.org/10.20517/jtgg.2021.39

Table of Contents

Zusammenfassung

Die altersbedingte Makuladegeneration (AMD) ist eine degenerative Erkrankung der zentralen Netzhaut und die führende Ursache für den Verlust der Sehkraft in Industriestaaten (Resnikoff et al., 2004). Neben dem zunehmenden Alter wird das individuelle Risiko, eine AMD zu entwickeln, von einer Konstellation aus genetischer Prädisposition und Umweltfaktoren beeinflusst. Oxidativer Stress wird als wichtiger umweltbedingter Risikofaktor gesehen, jedoch müssen die genauen Pathomechanismen bezüglich der Beteiligung an der Krankheitsentstehung noch vollständig aufgeklärt werden. Die retinalen Pigmentepithelzellen (RPE) sind einem hohen oxidativen Stress ausgesetzt. Der protektive Nuclear factor erythroid 2-related factor 2 (NRF2)-Signalweg ist ein Schlüsselelement der oxidativen Stressantwort in allen Zellarten, so auch dem RPE (Sachdeva et al., 2014; Rojo de la Vega et al., 2018).

In dieser Arbeit wurden die beiden Risikofaktoren (1) genetische Prädisposition und (2) oxidativer Stress kombiniert in einem Patienten-abgeleiteten RPE Modellsystem für AMD wiedergegeben, indem oxidativer Stress durch Natriumiodat (sodium iodate, SI) und Blaulicht (BL) in aus humanen induzierten pluripotenten Stammzellen abgeleiteten RPE (hiPSC-RPE)-Zelllinien mit genetisch hohem oder niedrigem AMD Risiko induziert wurde. Geeignete experimentelle Protokolle für akute (24 h) und chronische (72 h) SI-Behandlung und akute (9 h) BL-Bestrahlung wurden etabliert und es wurde bestätigt, dass die Morphologie der RPE-Zellen und die Integrität des Zell-Monolayers durch die Behandlungen nicht beeinträchtigt wurden. Die NRF2-assoziierte oxidative Stressantwort der hiPSC-RPE-Zellen wurde durch Expressionsanalyse der NRF2-abhängigen antioxidativen Gene Hämoxygenase-1 (*HMOX1*) und NAD(P)H Dehydrogenase [Quinone] 1 (*NQO1*) untersucht. Die analysierten Zelllinien reagierten mit erhöhter mRNA- und Proteinexpression auf die Behandlungen. Hierbei induzierten SI und BL die zwei Gene in unterschiedlichen Ausmaßen. Die *in vitro* Daten zeigten keine signifikanten Unterschiede in der oxidativen Stressantwort zwischen Hoch- und Niedrigrisikozelllinien. Hieraus wurde geschlossen, dass eine genetische Veranlagung für AMD die NRF2-assoziierte oxidative Stressantwort nicht messbar beeinflusst.

In einem zusätzlichen Projekt wurden hiPSC-RPE Zellen mit Photorezeptoraußensegmenten (photoreceptor outer segments, POS) aus der Schweinenetzhaut gefüttert und damit ein physiologischer Stressor in das Modell integriert. Nachdem bestätigt wurde, dass alle Zelllinien POS phagozytieren konnten, wurde gezeigt, dass mit dem Lipidperoxidationsprodukt 4-Hydroxynonenal (HNE) modifizierte POS gegenüber lysosomalem Abbau stabilisiert wurden. Des Weiteren wurden physiologischer und physikalischer oxidativer Stress kombiniert untersucht, indem die hiPSC-RPE-Zellen für 7 Tage mit HNE-modifizierten POS inkubiert wurden, gefolgt von BL-Bestrahlung. Die POS-Phagozytose hatte keinen Einfluss auf die BL-induzierte *HMOX1* und *NQO1* mRNA Expression in den hiPSC-RPE-Zelllinien.

Summary

Age-related macular degeneration (AMD) is a degenerative disease of the central retina and the leading cause of vision loss in developed countries (Resnikoff et al., 2004). Besides increasing age, the individual risk for developing AMD results from a combination of both genetic predisposition and environmental factors. Oxidative stress is considered to be a major environmental risk factor, but the exact pathomechanisms regarding its implication in disease development are yet to be fully resolved. The cells of the retinal pigment epithelium (RPE) are highly exposed to oxidative stress. A key element in the oxidative stress defense in the RPE, as in all cell types, is the protective nuclear factor erythroid 2-related factor 2 (NRF2) signaling pathway (Sachdeva et al., 2014; Rojo de la Vega et al., 2018).

In the present study, two risk factors, namely genetic susceptibility and oxidative stress, were replicated combined in a unique patient-derived RPE model system for AMD by inducing oxidative stress in human induced pluripotent stem cell-derived RPE (hiPSC-RPE) cell lines carrying a defined high or low genetic AMD risk. Oxidative stress was induced with the chemical stressor sodium iodate (SI) and the physical stressor blue light (BL). Suitable experimental protocols for acute (24 h) and chronic (72 h) SI treatment and acute (9 h) BL irradiation were established and it was confirmed that RPE cell morphology and monolayer integrity showed no adverse effects due to the treatments. The NRF2-associated oxidative stress response of the hiPSC-RPE cells was investigated by analyzing the expression of the NRF2-responsive antioxidant genes Heme oxygenase 1 (*HMOX1*) and NAD(P)H dehydrogenase [quinone] 1 (*NQO1*). In all studied cell lines, mRNA and protein expression of *HMOX1* and *NQO1* were increased in response to the oxidative stress conditions. SI and BL induced the two genes in different orders of magnitude. The *in vitro* data revealed no significant differences in the oxidative stress response between high and low risk cell lines. Therefore, it was concluded that genetic predisposition to AMD seems rather unlikely to influence a NRF2-associated oxidative stress response.

In an additional project, a physiological stressor was introduced into the model system by feeding the hiPSC-RPE cells with photoreceptor outer segments (POS) isolated from porcine retinae. After confirming that the cell lines were capable of POS phagocytosis, it was demonstrated that POS modified with the lipid peroxidation product 4-Hydroxynonenal (HNE) were stabilized against lysosomal degradation. Furthermore, physiological and physical oxidative stressors were studied in combination by challenging the hiPSC-RPE cells with HNE-modified POS for 7 days followed by subsequent BL irradiation. POS phagocytosis did not influence BL-induced *HMOX1* and *NQO1* mRNA expression in the hiPSC-RPE cell lines.

1 Introduction

1.1 Age-related Macular Degeneration (AMD)

Age-related macular degeneration (AMD) is a degenerative disease of the central retina, also known as the macula, and is the leading cause of vision loss in developed countries (Resnikoff et al., 2004). Following cataract, glaucoma and undercorrected refractive error, AMD is the fourth leading cause of blindness in people aged 50 years and older globally and is estimated to account for 5.6 % of blindness in that age group (GBD 2019 Blindness and Vision Impairment Collaborators, & Vision Loss Expert Group of the Global Burden of Disease Study, 2021).

AMD is a multifactorial condition with the presence of extracellular deposits as a distinguishing characteristic of the disease (Gass, 1972; Spaide et al., 2020; Yoon et al., 2022). Damage to the support system of the light-transducing photoreceptor cells can result in irreversible central vision loss (Fritsche et al., 2014). Visual impairment and blindness are highly debilitating for the affected patients and are even considered the third most formidable illness following cancer and cardiovascular disease (Fritsche et al., 2014). Visual impairment in AMD patients can have a pronounced effect on their quality of life (Brown et al., 2005) and lead to concomitant depression (reviewed in Cimarolli et al., 2016).

Since AMD is age-related, the number of people affected is expected to increase in the future due to population ageing (Wong et al., 2014; Li et al., 2020). The worldwide prevalence of all forms of AMD in 45- to 85-year-olds has been estimated to be 8.69 % in a systematic review and meta-analysis conducted by Wong et al. in 2014, with a projected number of AMD cases worldwide of 196 million in 2020 and climbing to 288 million in 2040 (Wong et al., 2014). Hereby AMD prevalence has been found to be higher in Europeans than in Asians or Africans (Wong et al., 2014). Regarding gender, no significant difference in AMD prevalence was detected (Smith et al., 2001; Wong et al., 2014; Li et al., 2020). In 2015, 67 million people in the European Union were affected by AMD, of which 50 million people were over 74 years old (Li et al., 2020). These EU case numbers of AMD are expected to increase by 15 % within the next 30 years (Li et al., 2020). Due to these high and increasing case numbers worldwide, the disease is not only burdensome to the affected individuals, but also places a substantial strain on public health and utilization of health resources with an economic impact (Brown et al., 2005; Cruess et al., 2008). Therefore, finding a cure for AMD is highly anticipated.

1.2 AMD Pathogenesis, Classification and Clinical Features

In AMD, pathogenesis takes place in the macula, the central part of the retina, which has the highest density of photoreceptor cells within the retina (Jager et al., 2008). The fovea centralis,

localized in the center of the macula region, contains the highest concentration of cone photoreceptors and is therefore specialized for high-resolution and color vision (van Lookeren Campagne et al., 2014) (see healthy retina in **Figure 1 A**). The complexity of AMD etiology and pathophysiology results in different stages and clinical manifestations of the disease, which exhibit some similar but distinguishable features and allow for various classification systems (van Lookeren Campagne et al., 2014). The currently recommended clinical classification system is based on lesions in color fundus photographs (Ferris et al., 2013).

Patients with early AMD are often asymptomatic or only experience small changes, such as slight visual distortion or reduced contrast sensitivity (Thomas et al., 2021). In early and intermediate AMD, funduscopic examinations reveal drusen (**Figure 1 B**), which are yellowish extracellular lipid and protein waste deposits between the retinal pigment epithelium (RPE) and Bruch's membrane and a hallmark sign of AMD (reviewed in Jager et al., 2008; van Lookeren Campagne et al., 2014; Al-Zamil & Yassin, 2017; Fleckenstein et al., 2021). Another indication of early AMD is RPE pigment abnormalities presenting as hypo- or hyperpigmented areas (Ferris et al., 2013). Furthermore, a population-based study conducted by Brandl et al., 2019 revealed significant thickening of the RPE/ Bruch's membrane complex and thinning of the photoreceptor layer of the retina in patients with early AMD compared to healthy controls (Brandl et al., 2019). Although patients with early AMD are usually clinically asymptomatic, they are at increased risk of disease progression to a late form of AMD accompanied by visual impairment (Brandl et al., 2022). In adults of 60+ years of age in Europe, pooled prevalences of early or intermediate AMD and late AMD have been estimated at 25.3 % and 2.4 %, respectively (Li et al., 2020).

Late AMD includes two advanced stages, geographic atrophy (GA), the dry form, and neovascular AMD (NV-AMD), the wet form (Ferris et al., 2013). GA and NV-AMD can develop and coexist in the same eye, possibly due to shared risk factors (Holz et al., 2014; van Lookeren Campagne et al., 2014). Although NV-AMD only constitutes 10 - 15 % of AMD cases, it accounts for 90 % of AMD blindness (Ferris et al., 1984; Waisbourd et al., 2007; reviewed in Frampton, 2013).

While the term choroidal neovascularization (CNV) was used to describe wet AMD for a long time, a more refined classification of NV events was deemed necessary in recent years (Fleckenstein et al., 2021). A new consensus classification for NV-AMD including three macular neovascularization subtypes was suggested by Spaide et al., 2020. Type 1 describes neovessels sprouting from the choriocapillaris into the sub-RPE space (Spaide et al., 2020). Since the neovessels are initially capillary-like, serous leakage and/or haemorrhage and fluid accumulation below the RPE can occur, which may result in detachment of the RPE and its basement membrane from the inner collagenous layer of Bruch's membrane (Campochiaro et

al., 1999; Grossniklaus & Green, 2004; Spaide et al., 2020). In Type 2, neovascularization from the choroid breaks through Bruch's membrane and the RPE monolayer and proliferates subretinally. In Type 3, neovessels don't originate from the choroid, but stem from the retinal circulation and descend towards the outer retina. When leakage exceeds the local removal capacities, fluid can accumulate subretinally and intraretinally (**Figure 1 C**) (Spaide et al., 2020). This fluid accumulation becomes clinically symptomatic with patients experiencing a distortion of straight lines, termed metamorphopsia, due to irregularity of the retinal surface (Campochiaro et al., 1999; Lim et al., 2012). Other symptoms of NV-AMD include rapid central vision loss and scotomas (Lim et al., 2012) as a result of disciform fibrovascular scars (Sarks et al., 2006).

In GA-AMD, vision loss progresses slowly and gradually over many years, in contrast to the acute vision loss observed in NV-AMD (Lim et al., 2012; van Lookeren Campagne et al., 2014). The central disease pathology in GA is loss of RPE function (McLeod et al., 2009; van Lookeren Campagne et al., 2014). RPE atrophy is clinically visible in fundoscopy as sharply demarcated area of depigmentation (Lim et al., 2012) and leads to secondary photoreceptor degeneration and loss of choriocapillaris (**Figure 1 D**) (McLeod et al., 2009; Bhutto & Lutty, 2012). If the fovea is spared initially, GA only marginally impacts vision decline in the beginning, whereas when the fovea is involved, irreversible scotomas in the visual field cause significant visual impairment (Bhutto & Lutty, 2012; van Lookeren Campagne et al., 2014).

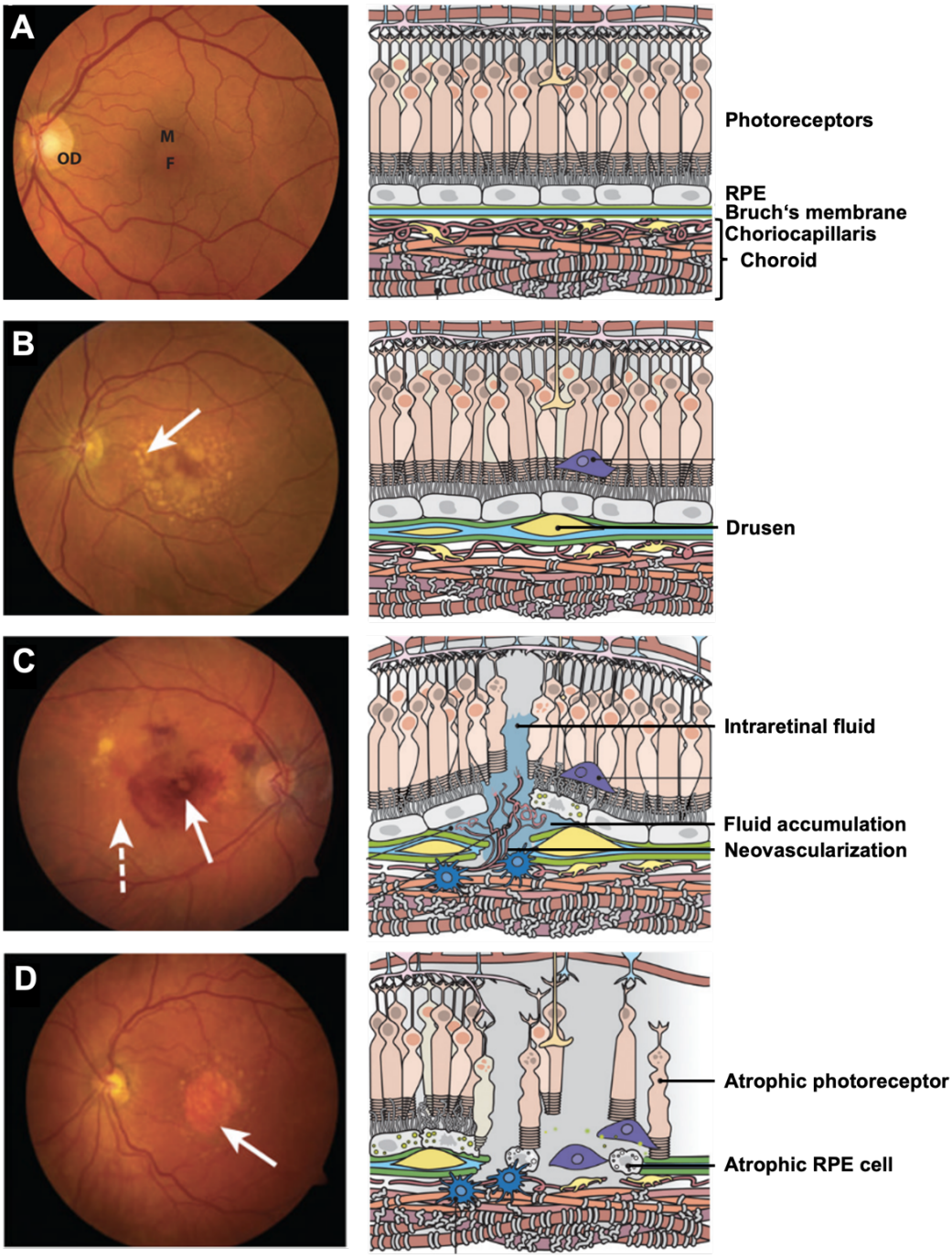

Figure 1: Fundus photographs and schematic depictions of a healthy retina and retinas with different forms of AMD

(**A**) Depiction of a normal healthy retina. OD = optic disc, M = macula, F = fovea.

(**B**) Presence of drusen under the RPE in early/ intermediate AMD. The large drusen (arrow) in the fundus photograph are an indicator of intermediate AMD.

(**C**) Retina with NV-AMD: fundus photograph showing subretinal haemorrhage (solid arrow), hard exudates (dashed arrow) and large drusen and schematic depiction of neovascularization breaking through the RPE and extending into the photoreceptor layer with sub- and intraretinal accumulation of fluid.

(**D**) Retina with GA: fundus photograph showing atrophy as sharply demarcated area of depigmentation (arrow) and schematic depiction of GA with loss of RPE cells and photoreceptors and disruption of Bruch's membrane.

Fundus photographs adapted from Swaroop et al., 2009; schematic illustrations adapted from van Lookeren Campagne et al., 2014.

1.3 Treatment for AMD

NV-AMD therapy targets the vascular endothelial growth factor VEGFA, which has been proven to be centrally involved in choroidal and retinal neovascularization regulation and increased vascular permeability (Chappelow & Kaiser, 2008). The standard of care treatment for NV-AMD consists of intravitreal injections of VEGF-inhibitors, which can halt vision loss and stabilize or improve visual acuity (reviewed in Solomon et al., 2019; review and meta-analysis by Carrasco et al., 2020). Ranibizumab, aflibercept and brolucizumab are the approved anti-VEGF agents in the EU and United States. Furthermore, bevacizumab is commonly used off-label (reviewed in Kaiser et al., 2022). In the widely applied treat and extend regimen, the injection interval can be extended according to the individual treatment needs after a loading phase of three injections in 4-week-periods (Skelly et al., 2019). In multiple studies, treat and extend regimens showed similar improvements in visual acuity and anatomical effects compared to monthly injections (reviewed in Skelly et al., 2019). Although the treatment is generally well tolerated, monthly injections are inconvenient and burdensome to patients as well as doctors, expensive, and each administration poses a potential risk for serious adverse events such as endophthalmitis (reviewed in Frampton, 2013; Solomon et al., 2019).

There have been recent advances in NV-AMD treatment. In September 2022, faricimab (Vabysmo) was approved in the EU. It is an antibody that also inhibits angiopoeitin-2 next to VEGFA and may allow for an extended injection period of up to 16 weeks, further lessening the injection burden (Heier et al., 2022). The administration of aflibercept in high dose every 12 or 16 weeks following an initiation phase is currently in phase III clinical trial (https://clinicaltrials.gov/ct2/show/NCT04423718, accessed January 6th, 2023). Susvimo, a refillable ocular implant which continuously releases ranibizumab into the vitreous for six months has recently been FDA-approved and is the first alternative to anti-VEGF injections in NV-AMD treatment (Holekamp et al., 2022; Ranade et al., 2022).

Contrary to NV-AMD, there is currently no treatment available to slow the progression of GA-AMD. However, due to advances in understanding the complex pathogenesis of GA, various potential therapeutic rationales targeting different molecular pathways are under investigation (reviewed in Holz et al., 2014; Ammar et al., 2020; Fabre et al., 2022). Gene therapy, by subretinal, intravitreal or suprachoroidal delivery of a viral vector, could be a future treatment option for GA as well as NV-AMD (reviewed in Guimaraes et al., 2021; Stradiotto et al., 2022). Preventing the onset of AMD in the first place would be favorable. The modulation of risk factors, such as adopting healthy diet and lifestyle measures may reduce the risk of disease development (reviewed in Di Carlo & Augustin, 2021).

1.4 Risk Factors for AMD

Due to the complex nature of AMD pathogenesis, the risk of disease development and progression derives from a combination of genetic and environmental risk factors unique to each affected individual. As captured in the name AMD, aging is the most significant risk factor for disease development (Chen et al., 2010; Dalvi et al., 2019). While environmental contributions to risk can be partly avoided or reduced, the genetic factors and increasing age are inevitable contributors to the individual risk of developing AMD.

As AMD heritability has been estimated to range from 46 % for overall AMD to 71 % for advanced AMD in a US twin study, genetics largely contributes to AMD etiology (Seddon et al., 2005). AMD-associated genetic variants are detected in genome-wide association studies (GWAS) including thousands of individuals as well as in candidate gene studies (reviewed in Grassmann et al., 2015a; Grassmann et al., 2015b; Warwick & Lotery, 2018). In a large GWAS of over 12 million variants, the International AMD Genomics Consortium identified 52 independent genetic variants across 34 AMD loci associated with advanced AMD, which accounts for 46.7 % of risk variability (Fritsche et al., 2016). The risk of developing an advanced form of AMD can be increased by 44-fold in individuals with an unfavorable genetic profile compared to those with an advantageous genetic profile (Fritsche et al., 2016). The understanding of early AMD genetics and its commonalities and individualities compared to advanced AMD is progressing as well. In the currently largest GWAS meta-analysis on early AMD, two novel loci, which had previously not yet been statistically significantly linked to any form of AMD, could be identified for early AMD with statistical significance (lead variant rs4844620, near *CD46*, $p = 4.7 \times 10^{-8}$; lead variant rs621313, near *TYR*, $p = 6.8 \times 10^{-4}$) (Winkler et al., 2020).

The first GWAS for AMD was conducted in 2005 and was the first study to identify a common variant (p.Y402H) in the complement factor H gene (*CFH*) located on chromosome 1q31 to be strongly associated with AMD (Klein et al., 2005). In the following years, many further genetic risk variants located on or near other complement genes, for example complement component 2 (*C2*), complement component 3 (*C3*), complement factor B (*CFB*), complement factor I (*CFI*) and complement component 9 (*C9*) were reported to strongly contribute to AMD risk, stressing the significance of the complement system and defects hereof in disease pathogenesis (Fritsche et al., 2014; Grassmann et al., 2015b; Fritsche et al., 2016). Next to the complement, other relevant pathways with AMD-associated genetic variants include angiogenesis, lipid transport, extracellular matrix remodeling, immune regulation and cell survival (Fritsche et al., 2013; Fritsche et al., 2014; Fritsche et al., 2016). A strong susceptibility locus contains the age-related maculopathy susceptibility 2/HtrA serine peptidase (*ARMS2/HTRA1*) genes on chromosome 10q26 (Jakobsdottir et al., 2005; Rivera et al., 2005; reviewed in Grassmann et

al., 2015a; Grassmann et al., 2015b; Warwick & Lotery, 2018). AMD-associated risk variants are not only studied individually. A new approach investigating epistatic interactions of GWAS variants has revealed novel risk genes, which became apparent due to additive effects of the risk variants in certain combinations (Kiel et al., 2021).

Many further risk factors as well as supplements have been associated with AMD next to aging and genetics. However, more research is warranted, as there are only a limited number of studies on these factors, which sometimes even show controversial data (Strunz et al., 2020). Solid data currently only exist for smoking (Smith et al., 2001). Cigarette smoke, a potent chemical oxidant, is the strongest and a repeatedly replicated modifiable environmental risk factor associated with AMD (Smith et al., 2001; Sachdeva et al., 2014, Wang et al., 2014a; reviewed in Lambert et al., 2016; Brandl et al., 2022). Pooled data from three continents revealed that current smokers are at higher AMD risk compared to past smokers and people who have never smoked (Tomany et al., 2004). In this study, current smoking has been calculated to increase the incidence of GA and late AMD compared to nonsmokers with odds ratios of 2.83 and 2.35, respectively (Tomany et al., 2004). Quitting smoking, even at an older age, could be seen as a prevention mechanism for disease progression, as former smoking showed no association with increased odds for progression (Brandl et al., 2022).

Other factors that have been linked to AMD risk include sunlight exposure, cardiovascular disease, hypertension, diet, cholesterol, alcohol consumption, increased plasma fibrinogen levels, iris color, age at menopause, hormone replacement therapy and ethnicity, with white individuals being at higher risk (Smith et al., 2001; Bressler et al., 2008; reviewed in Chen et al., 2010; Lambert et al., 2016). Dietary behaviors have also been proposed to influence AMD risk (Agrón et al., 2021). A diet high in fat has been shown to increase the risk of progression to advanced stages of AMD, while fish and nut consumption reduce it (Seddon et al., 2003). Furthermore, supplementation of zinc and the antioxidants vitamin C, E and beta carotene has demonstrated a reduction in the risk of progression to advanced AMD in higher-risk groups (Age-Related Eye Disease Study Research Group, 2001). However, as beta carotene supplementation has been linked to an increased risk of developing lung cancer in smokers, it is contraindicated for current and past smokers (Albanes et al., 1995; Omenn et al., 1996; Age-Related Eye Disease Study 2 (AREDS2) Research Group, 2014; reviewed in Gorusupudi et al., 2017; Chew et al., 2022). Therefore, substitution with lutein and zeaxanthin instead was evaluated in the AREDS2 cohort and is currently recommended as part of the formulation (Age-Related Eye Disease Study 2 (AREDS2) Research Group, 2014; Chew et al., 2022).

1.5 Oxidative Stress in Disease Pathology

Oxidative stress is suspected to play a major role in AMD pathogenesis, as its implication in disease development is extensively studied from many different angles (reviewed in Beatty et al., 2000; Cai & McGinnis, 2012; Lambros & Plafker, 2016). Of all tissues in the body, the retina is amongst those with the highest oxygen consumption (reviewed in Yu & Cringle, 2001). The choriocapillaris has an even higher blood perfusion than the kidney and an oxygen saturation of 90 % in its venous blood compared to 45 % in the venous blood of the retina (reviewed in Strauss, 2005). This high oxygen tension makes the retina predisposed to photooxidation and oxidative damage (Strauss, 2005; Kim et al., 2015). Additional oxidative stress sources, of which many are unique to the retina, put especially the macular region in a high oxidative stress environment (reviewed in Datta et al., 2017). Adding avoidable external oxidative stressors like cigarette smoking and a high fat diet to one's lifestyle further magnifies the oxidative stress burden (reviewed in Datta et al., 2017).

RPE cells are the most metabolically active cells in the eye (Zhao et al., 2019). The RPE is constantly exposed to extreme oxidative stress loads because of its raised metabolism, the oxygen tension between the choriocapillaris, which is rich in oxygen, and the retina, photooxidative stress through intense light exposure and the daily phagocytosis of shed photoreceptor outer segments (POS) (reviewed in Strauss, 2005; Jarrett & Boulton, 2012; Lambros & Plafker, 2016). All these sources of oxidative stress can lead to an increased production of reactive oxygen species (ROS) including free radicals, singlet oxygen and hydrogen peroxide, which can damage membrane lipids, proteins, carbohydrates and nucleic acids (reviewed in Beatty et al., 2000; Strauss; 2005). Unsaturated fatty acids, in large part docosahexanoic acid (DHA), in the photoreceptor membranes make the retina susceptible to lipid peroxidation (reviewed in Beatty et al., 2000). With increasing age, reduced antioxidative capacities of the postmitotic RPE cells may prove less sufficient to neutralize an accumulation of ROS, which can result in cell degeneration and cell death (Boulton & Dayhaw-Barker, 2001; Jarrett & Boulton, 2012; Sachdeva et al., 2014; Garcia et al., 2015; Zhao et al., 2019).

With age, lipofuscin, a waste product of lipids and proteins, accumulates in the RPE cells as a result of POS phagocytosis and incomplete lysosomal digestion thereof (reviewed in Beatty et al., 2000; Sparrow & Boulton, 2005; Kaemmerer et al., 2007; Kevany & Palczewski; 2010; Brandstetter et al., 2015). It has been reported that lipofuscin accumulation in RPE cells expands from only 1 % of an RPE cells volume in the first decade of life to 19 % in 81- to 90-year-olds (Feeney-Burns et al., 1984). These lipofuscin depositions can debilitate the RPE from functioning normally which can result in loss of function and atrophy of the RPE (reviewed in Beatty et al., 2000; Kaemmerer et al., 2007). Furthermore, lipofuscin itself can cause photooxidative damage and lipid peroxidation (reviewed in Beatty et al., 2000; Davies et al.,

2001; Kaemmerer et al., 2007; Brandstetter et al., 2015). Lipofuscin is a photosensitizer that when excited produces ROS wavelength-dependently, with blue light (BL) irradiation causing the greatest photoinducible generation of ROS (Rózanowska et al., 1995; Rózanowska et al., 1998; reviewed in Beatty et al., 2000). Lipofuscin is therefore regarded as a contributor to oxidative and photooxidative damage in the RPE and AMD pathogenesis (e.g. Rózanowska et al., 1995; Rózanowska et al., 1998; Strauss, 2005; Holz et al., 2014; van Lookeren Campagne et al., 2014).

1.6 Functions of the RPE and Implications of Loss of Function

The RPE describes a monolayer of cuboidal, hexagonally shaped and polarized cells strategically located between the photoreceptors to their apical side and Bruch's membrane and subjacent choriocapillaris to their basolateral side (reviewed in Sparrow et al., 2010; Bonilha, 2014; Tarau et al., 2019). With long apical microvilli of the RPE cells interdigitating with the outer segments of the photoreceptors, RPE and photoreceptors show close structural interaction (Strauss, 2005; Bonilha, 2014). The RPE exhibits multiple functions essential for maintaining visual function as well as health, function and viability of the photoreceptors and choriocapillaris (Strauss, 2005; Datta et al., 2017). Consequently, RPE cell impairment or loss of functionality can result in retinal degeneration and vision loss and is centrally involved in GA as well as NV-AMD pathogenesis (Strauss, 2005; Datta et al., 2017).

As outer blood-retina barrier, the RPE selects and regulates nutrient and fluid transport (Rizzolo, 2007; Bhutto & Lutty, 2012; Obert et al., 2017). Apical junctional complexes between the RPE cells consisting of tight, adherens and gap junctions are involved in maintaining the polarity and barrier function of the RPE by preventing diffusion and intercellular leakage (reviewed in Rizzolo, 2007; Sparrow et al., 2010; Bhutto & Lutty, 2012; Bonilha, 2014; Obert et al., 2017). The apical to basolateral polarity of the RPE with asymmetrical distribution of organelles enables transepithelial transport of nutrients like glucose, vitamin A and fatty acids from the choroid to the photoreceptors, and reversely ions, water and metabolic end products from the subretinal space to the bloodstream (reviewed in Strauss, 2005; Sparrow et al., 2010). Furthermore, the RPE as a pigmented epithelium helps with light absorption as a defense mechanism against photooxidation (summarized in Strauss, 2005). One of the light-absorbing pigments is melanin, which is organized in melanosomes and of higher density in the macular region where light is focused compared to the periphery (Boulton & Dayhaw-Barker, 2001; reviewed in Strauss, 2005). Along with many other antioxidants in the RPE protecting from photooxidation, e.g. carotenoids, glutathione, superoxide dismutase and catalase, melanin can also act as an antioxidant neutralizing ROS (reviewed in Boulton & Dayhaw-Barker, 2001; Strauss, 2005; Sparrow et al., 2010).

The RPE and photoreceptors form a functional unit of reciprocal dependence (Strauss, 2005). Hence, dysfunction or degeneration of either leads to secondary retinal degeneration and can result in AMD (Westenskow et al., 2012). One of the functions for which the photoreceptors depend on the RPE is maintaining their excitability. In the visual cycle, RPE cells reisomerize all-trans-retinol to 11-cis-retinal and deliver it back to the photoreceptors, since the photoreceptors cannot regenerate it themselves (summarized and reviewed in Strauss, 2005).

Another unique function of the RPE is phagocytosis of POS (Young & Bok, 1969; reviewed in Strauss, 2005). Photoreceptors are highly susceptible to oxidative stress due to constant light exposure and their high proportion of polyunsaturated fatty acids (Sparrow et al., 2010). Hence, in the course of a day, radicals and photo-damaged proteins and lipids accumulate within the POS (reviewed in Strauss, 2005). To dispose of these toxins and prevent toxic effects, the tips of POS containing the most photooxidative products are shed daily under circadian control and a POS is fully renewed from its base in approximately 10-14 days (Young, 1967; Young, 1978; reviewed in Strauss, 2005; Kevany & Palczewski, 2010; Sparrow et al., 2010). Lifelong daily phagocytosis and digestion of the shed POS make the postmitotic RPE cells the most actively phagocytic cell in the body (Mazzoni et al., 2014). Since RPE cells are postmitotic, the efficient disposal of this waste material is crucial for maintaining their health and function (Kevany & Palczewski, 2010). As the RPE is already subject to high amounts of oxidative and photooxidative stress due to intense light energy exposure and close proximity to the oxygen-rich choriocapillaris, the phagocytosis of POS enriched in light-damaged, polyunsaturated fatty acids and resulting ROS induce further stress which can eventually lead to RPE cell death and result in AMD development (Strauss, 2005; Krohne et al., 2010a; Lambros & Plafker, 2016).

1.7 Further Molecular Pathomechanisms

Besides RPE and photoreceptors, Bruch's membrane is also involved in AMD pathology. With age, Bruch's membrane thickens due to an increase in deposition and cross-linking of collagen fibers and the accumulation of RPE waste products (reviewed in Bhutto & Lutty, 2012). This leads to functional impairment of Bruch's membrane with reduced transport capacities between the RPE and choroid (reviewed in Bhutto & Lutty, 2012). As material from the RPE can no longer pass through for elimination by the choriocapillaris, it accumulates between RPE and Bruch's membrane and is termed drusen, which can become confluent and lead to larger areas of RPE detachment (reviewed in Green et al., 1985; Bhutto & Lutty, 2012; Al-Zamil & Yassin, 2017). Drusen components include cholesterol, the apolipoproteins B and E, acute phase proteins like vitronectin and CRP, amyloid-beta, oxidation by-products, complement regulators and complement components like CFH, C1q, C3, C5 and the membrane attack

complex C5b-9 (reviewed in Hageman et al., 2001; Anderson et al., 2002; Crabb et al., 2002; Johnson et al., 2002; Curcio et al., 2005; Rudolf et al., 2008; Doyle et al., 2012; Gao et al., 2015). The presence of complement regulators and components and inflammation-related proteins in drusen indicates that complement activation and local pro-inflammatory stimuli play a role in drusen formation (reviewed in Hageman et al., 2001; Anderson et al., 2002).

Additionally to drusen, so-called reticular pseudodrusen, deposits in the subretinal space between the photoreceptor layer and the RPE, occur in eyes affected by AMD and have been, with advances in imaging, regarded as markers for disease progression in recent years (reviewed in Datta et al., 2017; Yoon et al., 2022). They have been reported to be positive for CFH, vitronectin, apolipoprotein E and unesterified cholesterol, which are components of conventional drusen (Rudolf et al., 2008). Furthermore, reticular pseudodrusen have been found to contain CD59, which is released by the RPE (Ebrahimi et al., 2013; Datta et al., 2017). This allowed the conclusion that the formation of reticular pseudodrusen could be influenced by complement activation via the RPE (Datta et al., 2017).

With complement components and inflammation-related proteins found in drusen as well as findings of AMD-associated genetic variants in *CFH* and various other complement genes, the role of the innate immune system in AMD pathogenesis has been one of the major foci in AMD research, with chronic inflammation generally considered a centrally involved mechanism in AMD pathogenesis next to oxidative stress. Studies have even implied that oxidative stress and inflammation can augment or induce each other (reviewed in Cano et al., 2010; Datta et al., 2017). Complement regulatory proteins like CFH, CD46 and CD59 protect cells from disproportionate activation of complement (Ebrahimi et al., 2013). Dysregulation of complement is considered to be significantly involved in AMD pathology (Ebrahimi et al., 2013). Studies have shown that CFH is significantly lowered in the Bruch's membrane/ choriocapillaris complex in eyes with all forms of AMD (Bhutto et al., 2011), CD46 immunolabeling is reduced in the RPE of early AMD and GA (Vogt et al., 2011; Ebrahimi et al., 2013) and CD59 is reduced in GA areas of the RPE (Ebrahimi et al., 2013). Furthermore, levels of the systemic inflammation marker CRP are elevated in the Bruch's membrane/ choriocapillaris complex in early and wet AMD eyes, hinting at local inflammation and cellular damage at the interface of RPE and choroid (Bhutto et al., 2011). Changes in complement not only occur locally in the retina. Elevated concentrations of complement factors and activation products of the alternative pathway including C3, C3a, C3d, Ba, C5a and C5b-9 have been found in plasma of AMD patients, allowing the hypothesis that AMD is a systemic disease that locally manifests in the macular region (Scholl et al., 2008).

The nucleotide-binding oligomerization domain-like receptor family, pyrin domain-containing protein 3 (NLRP3) inflammasome, a signaling receptor of the innate immune response

activated by danger signals, is also involved in AMD pathogenesis (reviewed in Ambati et al., 2013; Ildefonso et al., 2016). Activators in the retina include drusen components C1q (Doyle et al., 2012) and amyloid-beta (Liu et al., 2013), as well as the lipid peroxidation product 4-Hydroxynonenal (HNE), the latter indicating that oxidative stress can activate the NLRP3 inflammasome in RPE cells (Kauppinen et al., 2012). Furthermore, it has been specifically shown that the NLRP3 inflammasome is activated by BL-induced photooxidative stress in RPE cells, which is intensified by lipofuscin accumulation (Brandstetter et al., 2015). Inflammasome activation has been ascribed a protective role in AMD progression (Doyle et al., 2012), however when chronic it can become harmful and lead to disease (reviewed Datta et al., 2017).

1.8 The NRF2 Signaling Pathway

Nuclear factor erythroid 2-related factor 2 (NRF2) is considered the master antioxidant transcription factor (TF) in all cell types throughout the body and regulates a large assortment of genes including antioxidant genes, phase II detoxification enzymes and transport molecules (Itoh et al., 1997; Zhang, 2006; Sachdeva et al., 2014; Wang et al., 2014a; Lambros & Plafker, 2016; Oh & Jun, 2018). NRF2 has been studied to have a protective role against many diseases including cardiovascular disease and Alzheimer's disease (reviewed in Zhang, 2006; Huang et al., 2015). Regarding cancer, NRF2 may not only be tumor suppressive, but could also show tumor promoting effects (reviewed in Rojo de la Vega et al., 2018). In the healthy RPE, the NRF2 signaling pathway is responsible for neutralizing oxidative stress and preserving cellular redox homeostasis (reviewed in Zhang, 2006; Cano et al., 2010; Lambros & Plafker, 2016).

In absence of oxidative stress, NRF2 is bound to the negative regulator Kelch-like ECH-associated protein 1 (KEAP1). KEAP1 is responsible for ubiquitination and proteasomal degradation of the NRF2 protein in the cytoplasm, and so limits its activity. In the presence of oxidative stress resulting in ROS, the conformation of KEAP1 is modified and it releases NRF2, which becomes phosphorylated (Huang et al. 2002), for translocation to the nucleus. Here, NRF2 heterodimerizes with Maf proteins (Itoh et al., 1997) and binds to antioxidant response elements (ARE) to initiate transcription of target genes, e.g. Heme oxygenase 1 (*HMOX1*) and NAD(P)H dehydrogenase [quinone] 1 (*NQO1*) (**Figure 2**) (summarized in Zhang, 2006; Sachdeva et al., 2014; Wang et al., 2014a; Lambros & Plafker, 2016; Oh & Jun, 2018).

Studies with Nrf2 knockout mice have shown that with the aging process, the cell protective NRF2 system becomes impaired and less efficient, which therefore leaves the RPE more vulnerable to oxidative damage and could consequently contribute to developing AMD (Sachdeva et al., 2014). Therefore, a possible therapeutic aim is to rejuvenate the

physiological NRF2 signaling response with NRF2 activators in order to prevent oxidative damage to the aging RPE and slow down disease progression (Sachdeva et al., 2014).

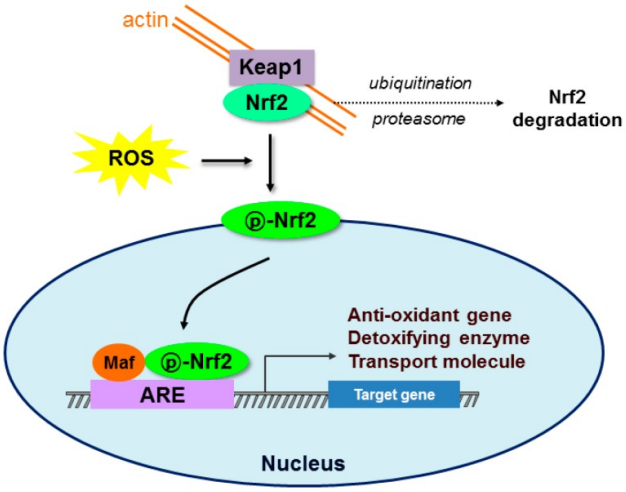

Figure 2: Schematic illustration of the NRF2 signaling pathway
In absence of oxidative stress, NRF2 is bound to the negative regulator KEAP1, which is responsible for ubiquitination and proteasomal degradation of the NRF2 protein in the cytoplasm. In the presence of oxidative stress (ROS), the conformation of Keap1 is modified and it releases NRF2, which becomes phosphorylated, for translocation to the nucleus. Here, NRF2 heterodimerizes with Maf proteins and binds to the ARE of target genes to initiate their transcription. Figure from Oh & Jun, 2018.

Next to its antioxidant properties, it is postulated that with some of the NRF2 downstream target genes involved in the inflammatory response, NRF2 also suppresses inflammation, protects against innate immune response dysregulation, e.g. during sepsis (Thimmulappa et al., 2006) and prevents oxidative stress mediated by inflammation (reviewed in Chen & Kunsch, 2004; Zhang, 2006; Cano et al., 2010). Regarding the RPE, findings have shown that the oxidant cigarette smoke increased the NRF2 signaling response and led to complement activation, and that NRF2 deficiency magnified the complement response, indicating that NRF2 deficiency not only promotes oxidative damage but also a pro-inflammatory environment (Wang et al., 2014a). Furthermore, a study revealed that Nrf2-deficient mice develop age-related retinal pathology with the AMD characteristics degeneration of RPE, thickening of Bruch's membrane, drusen, lipofuscin accumulation, spontaneous CNV as well as inflammatory protein deposition in the sub-RPE area (Zhao et al., 2011).

1.9 The hiPSC-RPE Cell Model System

A genetic cell model system for human induced pluripotent stem cell-derived RPE (hiPSC-RPE) cell lines developed at the Institute of Human Genetics was implemented in this thesis. The cells which the hiPSC-RPE cell lines are derived from had been selected and acquired through an innovative and complex procedure. The aim was to obtain multiple cell lines that carry either very high or very low genetic risk for developing AMD. By comparing the cell lines of these two extremes on both ends of the genetic risk spectrum in different experimental settings, the genetic influence in various mechanisms involved in AMD pathogenesis was to be elucidated. Firstly, 161 individuals who had been recruited at the Eye Clinic of the University Hospital Regensburg together with PD Dr. Caroline Brandl were categorized as AMD patients

or controls without any signs of early or late AMD. After genotyping the participants for 13 AMD-associated genetic variants at 8 loci (*CFH*, *ARMS2/HTRA1*, *CFB*, *C3*, *APOE*, *PLA2G12A*, *LIPC* and *TIMP3*) (Grassmann et al., 2012) which had been shown to strongly correlate with the risk for AMD (Fritsche et al., 2013; Fritsche et al., 2016), genetic risk scores were generated according to the model by Grassmann et al., 2012. Of the participants classified as of very high (risk score 5) or very low (risk score 1) genetic AMD risk, four individuals were selected from risk group 5 who all had late-stage NV-AMD along with four individuals from risk group 1 serving as controls lacking any AMD phenotype. Fibroblasts from skin biopsies or peripheral blood mononuclear cells (PBMCs) from blood samples were isolated and subsequently reprogrammed to induced pluripotent stem cells (iPSCs). These in turn were differentiated into RPE cells (Brandl et al., 2014). Consequently, these hiPSC-RPE cell lines carry a known and defined genetic AMD risk. Not only are these cells the most suitable model system for *in vivo* RPE cells, but they also enable the analysis of the influence of the complex genetic situation in patients on AMD pathogenesis.

1.10 Study Objective

A unique model for replicating a combination of two major AMD risk factors, genetic susceptibility and oxidative stress, was developed in the scope of this thesis, thus constituting a further stepping stone in unraveling AMD pathologies. This was achieved by inducing oxidative stress in patient-derived hiPSC-RPE cell lines with known genetic risk. Experimental protocols were established to investigate the effects of sodium iodate (SI), a potent chemical stressor of RPE cells (e.g. Wang et al., 2014b; Moriguchi et al., 2018), and BL irradiation, two oxidative stressors that were novel to this collection of hiPSC-RPE cell lines. Antioxidative stress responses in the NRF2 signaling pathway were analyzed after induction of oxidative stress. By studying a large number of cell lines in the experiments, with four carrying a very high and four carrying a very low genetic risk for AMD, observed effects could be verified across multiple cell lines and comparisons between high and low risk cell lines could be made. This, in turn, allowed for conclusions to be drawn regarding potential effects of either a genetically high or low AMD risk on the NRF2-dependent oxidative stress response or any further pathways of interest in future studies. The hiPSC-RPE cells were furthermore fed with POS to replicate the effect of a physiological stressor in the model system. By combining phagocytosis of POS with the physical oxidative stressor BL, it could be examined whether straining the cells by inducing their natural phagocytotic activity modified their oxidative stress response to the additional external oxidative stress of BL irradiation.

2 Material

2.1 hiPSC-derived RPE Cell Lines

Table 1: hiPSC-derived RPE cell lines analyzed in this study
PBMCs/ Fibroblast samples originated from a single patient per cell line.
For a clear presentation, cell lines were given the following IDs, with H standing for “high risk” and L standing for “low risk”.
Analysis of H5* was included for experiment establishment purposes in 4.1.1 and 4.1.3.

ID	Cell line	Source	AMD Status	Risk Score
H1	AMD 2	Fibroblasts	CNV	5 (high risk)
H2	AMD 5	PBMCs	CNV	5 (high risk)
H3	AMD 6	PBMCs	CNV	5 (high risk)
H4	AMD 8	Fibroblasts	CNV	5 (high risk)
L1	AMD 7K	PMBCs	Control	1 (low risk)
L2	AMD 10K	Fibroblasts	Control	1 (low risk)
L3	AMD 11K	PBMCs	Control	1 (low risk)
L4	AMD 12K	PBMCs	Control	1 (low risk)
H5*	AMD 1	PBMCs	CNV	5 (high risk)

PBMCs = peripheral blood mononuclear cells; CNV = choroidal neovascularization

2.2 Cell Culture Media and Additives / Reagents

Table 2: Cell culture media and additives / reagents

Component	Supplier
β-Mercaptoethanol, C_2H_6OS	Sigma-Aldrich, St. Louis, MO, USA
Corning® Matrigel® Growth Factor Reduced (GFR) Basement Membrane Matrix	Corning Inc., Corning, NY, USA
Dulbecco’s Modified Eagle’s Medium/Nutrient Mixture F-12 Ham (without phenol red) (D6434)	Sigma-Aldrich, St. Louis, MO, USA
Gentamicin solution (50 mg/ml)	Sigma-Aldrich, St. Louis, MO, USA
Gibco™ Dulbecco's phosphate-buffered saline (DPBS), no calcium, no magnesium (Ref 14190094)	Thermo Fisher Scientific, Waltham, MA, USA
Gibco™ Fetal Bovine Serum (FBS), qualified, Brazil (Ref 10270106)	Thermo Fisher Scientific, Waltham, MA, USA
Gibco™ KnockOut™ Dulbecco's Modified Eagle Medium (DMEM) (Ref 10829018)	Thermo Fisher Scientific, Waltham, MA, USA
Gibco™ KnockOut™ Serum Replacement (KOSR)	Thermo Fisher Scientific, Waltham, MA, USA
Gibco™ L-Glutamine 200 mM (100x)	Thermo Fisher Scientific, Waltham, MA, USA
Gibco™ MEM Non-Essential Amino Acids Solution (100x)	Thermo Fisher Scientific, Waltham, MA, USA
Gibco™ Opti-MEM® I Reduced Serum Medium	Thermo Fisher Scientific, Waltham, MA, USA

Gibco™ Penicillin-Streptomycin (10000 U/ml)	Thermo Fisher Scientific, Waltham, MA, USA
Nicotinamide, $C_6H_6N_2O$	Sigma-Aldrich, St. Louis, MO, USA
TrypLE™ Express	Thermo Fisher Scientific, Waltham, MA, USA

2.3 Oligonucleotides used as Primers for qRT-PCR and Corresponding Probes

Table 3: Oligonucleotides used for qRT-PCR and corresponding probe numbers from the Roche Universal ProbeLibrary

The oligonucleotides were purchased from metabion international AG, Planegg, Germany.
Probes are part of the Universal ProbeLibrary from Roche, Basel, Switzerland.

Gene	Name	Sequence (5' - 3')	Probe Number
CD46	hCD46-qRT-F hCD46-qRT-R	AAT TTG TGT TGT CCC GTA CAG A TCT GTG GGT CTC ATC AGT TAG G	# 69
HPRT1	hHPRT-qRT-F hHPRT-qRT-R	TGA CCT TGA TTT ATT TTG CAT ACC CGA GCA AGA CGT TCA GTC CT	# 73
NQO1	hNQO1-qRT-F hNQO1-qRT-R	ATG TAT GAC AAA GGA CCC TTC C TCC CTT GCA GAG AGT ACA TGG	# 87
HMOX1	hHMOX1-qRT-F hHMOX1-qRT-R	TGA ACT CCC TGG AGA TGA CTC AGC TCC TGC AAC TCC TCA AA	# 13
VEGFA	hVEGF-qRT-F hVEGF-qRT-R	GCA GCT TGA GTT AAA CGA ACG GGT TCC CGA AAC CCT GAG	# 12

2.4 Antibodies

2.4.1 Primary Antibodies

Table 4: Primary antibodies used for immunocytochemistry and Western blot analysis

Antibodies used for Western blot analysis were diluted in 5 % skimmed milk powder in TBS-T.
Antibodies used for Immunocytochemistry were diluted in primary antibody solution listed in Table 9.

Antibody	Type	Species	Dilution	Application	Supplier
anti-ß-Actin (#A2228)	mAb	mouse	1:10000	WB	Sigma-Aldrich, St. Louis, MO, USA
anti-HMOX1	mAb	rabbit	1:1000, 1:100	WB	Cell Signaling Technology, Danvers, MA, USA
anti-NQO1	mAb	mouse	1:1000, 1:100	WB	Cell Signaling Technology, Danvers, MA, USA
anti-Rhodopsin (1D4)	mAb	mouse	1:2000	WB	Prof. Dr. Robert Molday, Department of Ophthalmology and Visual Sciences, University of British Columbia, Canada
anti-ZO-1	pAb	rabbit	1:500	ICC	Thermo Fisher Scientific, Waltham, MA, USA

pAb = Polyclonal antibody, mAb = Monoclonal antibody, ICC = Immunocytochemistry, WB = Western blot

2.4.2 Secondary Antibodies

Table 5: Secondary antibodies used for immunocytochemistry and Western blot analysis
Antibodies used for Western blot analysis were diluted in 5 % skimmed milk powder in TBS-T.
Antibodies used for immunocytochemistry were diluted in secondary antibody solution listed in Table 9.

Antibody	Dilution	Application	Supplier
Goat Anti-Mouse IgG, Alexa Fluor ® 488	1:800	ICC	Thermo Fisher Scientific, Waltham, MA, USA
Goat Anti-Mouse IgG, Alexa Fluor ® 594	1:800	ICC	Thermo Fisher Scientific, Waltham, MA, USA
Goat Anti-Rabbit IgG, Alexa Fluor ® 488	1:800	ICC	Thermo Fisher Scientific, Waltham, MA, USA
Goat Anti-Rabbit IgG, Alexa Fluor ® 594	1:800	ICC	Thermo Fisher Scientific, Waltham, MA, USA
Goat Anti-Mouse IgG, Peroxidase Conjugated	1:10000	WB	(Calbiochem®) Merck Chemicals GmbH, Darmstadt, Germany
Goat Anti-Rabbit IgG, Peroxidase Conjugated	1:10000	WB	(Calbiochem®) Merck Chemicals GmbH, Darmstadt, Germany

ICC = Immunocytochemistry, WB = Western blot

2.5 Molecular Weight Standard

Table 6: Molecular weight standard for SDS-PAGE

Molecular Weight Standard	Application	Supplier
PageRuler™ Prestained Protein Ladder	Size standard for protein analysis (10 – 180 kDa) via SDS PAGE and Western blot	Thermo Fisher Scientific, Waltham, MA, USA

2.6 Assay Kits

Table 7: List of assay kits

Kit	Supplier
CytoTox 96® Non-Radioactive Cytotoxicity Assay	Promega Corporation, Madison, WI, USA
Cytotoxicity Detection Kit^{PLUS} (LDH)	Roche, Basel, Switzerland
PureLink® RNA Mini Kit	Thermo Fisher Scientific, Waltham, MA, USA
RevertAid H Minus First Strand cDNA Synthesis Kit	Thermo Fisher Scientific, Waltham, MA, USA

2.7 Chemicals

Table 8: List of chemicals

Chemical/ Reagent	Supplier
2x TaqMan Gene Expression Master Mix	Eurogentec, Seraing, Belgium
3-(4,5-Dimethylthiazol-2-yl)-2,5-diphenyltetrazoliumbromide (MTT)	Sigma-Aldrich, St. Louis, MO, USA

4′,6-diamidino-2-phenylindole (DAPI), $C_{16}H_{15}N_5$	Thermo Fisher Scientific, Waltham, MA, USA
4-Hydroxynonal (HNE)	(Calbiochem®) Merck Chemicals GmbH, Darmstadt, Germany
Ammonium persulfate (APS), $(NH_4)_2S_2O_8$	AppliChem GmbH, Darmstadt, Germany
ß-Mercaptoethanol, $HSCH_2CH_2OH$	Sigma-Aldrich, St. Louis, MO, USA
Bovine Serum Albumin (BSA)	New England Biolabs, Ipswich, MA, USA
Clarity Max Western ECL Substrate	Bio-Rad Laboratories GmbH, Feldkirchen, Germany
Clarity Western ECL Substrate	Bio-Rad Laboratories GmbH, Feldkirchen, Germany
Dako Fluorescence Mounting Medium	Agilent, Santa Clara, CA, USA
dNTPs (dATP, dGTP, dCTP, dTTP)	Genaxxon bioscience GmbH, Ulm, Germany
Ethanol ≥99,8 % p.a, C_2H_6O	Carl Roth GmbH + Co. KG, Karlsruhe, Germany
Glycerol 87 %, $C_3H_8O_3$	University of Regensburg, Chemical Supplies
Glycine, $C_2H_5NO_2$	Merck Chemicals GmbH, Schwalbach, Germany
Hydrochloric acid (HCl), 1 M	Merck Chemicals GmbH, Schwalbach, Germany
Isopropanol, C_3H_8O	Merck Chemicals GmbH, Schwalbach, Germany
Methanol, CH_4O	Merck Chemicals GmbH, Schwalbach, Germany
Paraformyaldehyde (PFA), $(CH_2O)_n$	AppliChem GmbH, Darmstadt, Germany
Potassium chloride, KCl	Merck Chemicals GmbH, Schwalbach, Germany
Potassium dihydrogen phosphate, KH_2PO_4	Merck Chemicals GmbH, Schwalbach, Germany
Rotiphorese® Gel 40 % Acrylamide/ Bisacrylamide	Carl Roth GmbH + Co. KG, Karlsruhe, Germany
Roti®-Quant	Carl Roth GmbH + Co. KG, Karlsruhe, Deutschland
Skimmed Milk Powder	Carl Roth GmbH + Co. KG, Karlsruhe, Germany
Sodium chloride, NaCl	VWR International Germany GmbH, Darmstadt, Germany
Sodium dodecyl sulfate (SDS) ≥99 %, $C_{12}H_{25}NaO_4S$	Merck Chemicals GmbH, Schwalbach, Germany
Sodium iodate, 99 % min, $NaIO_3$	Alfa Aesar, Haverhill, MA, USA
Tetramethylethylenediamine (TEMED), $(CH_3)_2NCH_2CH_2N(CH_3)_2$	Merck Chemicals GmbH, Schwalbach, Germany
Tris(hydroxymethyl)-aminomethane (Tris), $NH_2C(CH_2OH)_3$	Affymetrix, Santa Clara, CA, USA
Triton® X-100	AppliChem GmbH, Darmstadt, Germany
Tween® 20	Sigma-Aldrich, St. Louis, MO, USA

2.8 Buffers and Solutions

Table 9: Composition of buffers and solutions

Buffer/ Solution	Composition	Amount
0.1 M HCl in Isopropanol	Isopropanol 1 M HCl	90 % (v/v) 10 % (v/v)
1x Protein Isolation Buffer	25x protein isolation buffer 1x PBS	4 % (v/v)
25x Protein Isolation Buffer	Roche cOmplete™ Protease Inhibitor Cocktail 1x PBS	1 tablet 2 ml
5x Laemmli Buffer	Bromphenolblue Tris-HCl pH 6.8 β-Mercaptoethanol SDS Glycerol H_2O dest.	0.01 % 60 mM 5 % (v/v) 2 % (w/v) 10 % (v/v)
Antibody Solution (WB)	Skimmed Milk Powder 1x TBS-T	5 % (w/v)
Blocking Solution (ICC)	Goat serum 20 % Triton-X-100 1x PBS	10 % (v/v) 0.15 % (v/v)
Blocking Solution (WB)	Skimmed Milk Powder 1x TBS-T	5 % (w/v)
HNE Solution	4-Hydroxynonenal (HNE) Pen/Strep Opti-MEM™ I Reduced Serum Medium	5 mM 1% (v/v)
MTT Solution	MTT 1x PBS	0.05 % (w/v)
PBS, pH 7.4	NaCl KCl Na_2HPO_4 KH_2PO_4 H_2O dest.	137 mM 0,27 mM 10 mM 1.8 mM
PFA Solution	PFA 1x PBS	2 % (w/v)
Primary Antibody Solution (ICC)	Goat serum 20 % Triton-X-100 2 % NaN_3 1x PBS	2.5 % (v/v) 0.05 % (v/v) 0.1 % (v/v)
SDS Running Buffer, pH 8.6	Tris-HCl Glycine SDS H_2O dest.	0.25 mM 0.2 M 1 % (w/v)
Secondary Antibody Solution (ICC)	Goat serum 20 % Triton-X-100 1x PBS	2.5 % (v/v) 0.05 % (v/v)
TBS, pH 7.5	Tris NaCl H_2O dest.	50 mM 150 mM
TBS-T	Tween® 20 1x TBS	0.1 % (v/v)

Towbin	Glycine Tris Methanol H_2O dest.	190 mM 0.25 mM 20 % (v/v)

ICC = Immunocytochemistry, WB = Western blot

2.9 Consumables

Table 10: List of consumables

Consumable	Supplier
6-well CELLSTAR® cell culture plates	Greiner Bio-One GmbH, Kremsmünster, Austria
12-well CELLSTAR® cell culture plates	Greiner Bio-One GmbH, Kremsmünster, Austria
38.5 ml ultracentrifuge tubes (# 326823)	Beckman Coulter, Krefeld, Germany
96-well CELLSTAR® cell culture microplates	Greiner Bio-One GmbH, Kremsmünster, Austria
96-well microplates (clear, flat bottom)	Greiner Bio-One GmbH, Kremsmünster, Austria
Cell scrapers	Orange Scientific, Braine-l'Alleud, Belgium
ClipTip Pipette Tips	Thermo Fisher Scientific, Waltham, MA, USA
Cover glasses (24 x 50 mm)	VWR International Germany GmbH, Darmstadt, Germany
Cuvettes	Sarstedt AG & Co., Nümbrecht, Germany
ep Dualfilter T.I.P.S® (20-300 µl)	Eppendorf AG, Hamburg, Germany
Falcon tubes (15 ml/ 50 ml)	Greiner Bio-One GmbH, Kremsmünster, Austria
Immobilon®-P PVDF Membrane (pore size 0.45 µl)	Merck Chemicals GmbH, Schwalbach, Germany
MicroAmp™ Optical 384-well Reaction Plate	Thermo Fisher Scientific, Waltham, MA, USA
MicroAmp™ Optical Adhesive Film	Thermo Fisher Scientific, Waltham, MA, USA
Microtubes (0.5 ml/ 1.5 ml/2 ml)	Sarstedt AG & Co., Nümbrecht, Germany
Multiply® µStrip 0.2 ml chain	Sarstedt AG & Co., Nümbrecht, Germany
Nitrile gloves	HARTMANN, Heidenheim a.d. Brenz, Germany
Pipette tips (10 µl/ 100 µl, 1000 µl)	VWR International Germany GmbH, Darmstadt, Germany
Pipette tips, sterile, with filter (10 µl/ 100 µl, 1000 µl)	Nerbe Plus GmbH, Winsen, Germany
pluriStrainer® 5 µm	PluriSelect, Leipzig, Germany
QIAshredder	QIAGEN N.V., Hilden, Germany
Reagent reservoir (25 ml)	VWR International Germany GmbH, Darmstadt, Germany
Serological plastic pipettes (5 ml/ 10 ml/ 25 ml/ 50 ml)	Sarstedt AG & Co., Nümbrecht, Germany
SuperFrost® Plus Microscope Slides	VWR International Germany GmbH, Darmstadt, Germany
ThinCert™ Cell Culture Inserts (6 well, 12 well)	Greiner Bio-One GmbH, Kremsmünster, Austria

Tissue culture dish (10 cm)	Sarstedt AG & Co., Nümbrecht, Germany
Weighing boats	VWR International Germany GmbH, Darmstadt, Germany
Whatman paper (3 mm)	Carl Roth GmbH + Co. KG, Karlsruhe, Germany

2.10 Instruments

Table 11: List of instruments

Instrument	Supplier
AF100 Flake Ice Machine	Scotsman Industries Inc, Vernon Hills, IL, USA
Accu-jet® pro Pipette Controller	BRAND GMBH + CO KG, Wertheim, Germany
Autoclave „Autoklav V-150“	Systec GmbH, Wettenberg, Germany
Axioskop 2	Carl Zeiss Microscopy GmbH, Jena, Germany
Blue Light LED Light Source	LUMITRONIX® LED-Technik GmbH, Hechingen, Germany
Centrifuge Biofuge fresco	Heraeus Holding GmbH, Hanau, Germany
Centrifuge Megafuge 1.0R	Heraeus Holding GmbH, Hanau, Germany
Centrifuge 5810	Eppendorf AG, Hamburg, Germany
CO_2 Incubator	BINDER Gmbh, Tuttlingen, Germany
E1-ClipTip™ Multichannel Equalizer Pipette	Thermo Fisher Scientific, Waltham, MA, USA
Eclipse Ts2 Inverted Routine Microscope	Nikon Corporation, Minato, Tokio, Japan
Epithelial Volt/Ohm Meter (EVOMX)	World Precision Instruments, Sarasota, FL, USA
Eppendorf Research® plus 8 channel pipette	Eppendorf AG, Hamburg, Germany
Fine scale “Explorer®”	OHAUS Europe GmbH, Nänikon, Switzerland
Heracell™ 150i CO2-Incubator	Thermo Fisher Scientific, Waltham, MA, USA
Integra Biosciences™ Vacusafe™ Comfort Aspiration system	Thermo Fisher Scientific, Waltham, MA, USA
Millipore Milli-Q-Synthesis Water Purification System	Merck Chemicals GmbH, Darmstadt, Germany
Mini-PROTEAN® Short Plates	Bio-Rad Laboratories GmbH, Munich, Germany
Mini-PROTEAN® Spacer Plates (1.5 mm)	Bio-Rad Laboratories GmbH, Munich, Germany
Mini-PROTEAN® Tetra Cell	Bio-Rad Laboratories GmbH, Munich, Germany
NanoDrop® ND1000 Spectrophotometer	Thermo Fisher Scientific, Waltham, MA, USA
Odyssey FC Imager	LI-COR Biosciences, Lincoln, NE, USA
Picus® NxT electronic pipette, 12-channel, 10-300 µl	Sartorius AG, Göttingen, Germany
Power Pack Blue Power 500	SERVA Electrophoresis GmbH, Heidelberg, Germany
QuantStudio™ 5 Real-Time PCR System	Thermo Fisher Scientific, Waltham, MA, USA
RM5 Roller	(Assistent®) Glaswarenfabrik Karl Hecht GmbH & Co KG, Sondheim/Rhön, Germany

Safety Cabinet BDK-SK1800	Weiss Umwelttechnik GmbH, Reiskirchen, Deutschland
Scales	SCALTEC Instruments GmbH, Heiligenstadt, Germany
Spectral photometer Ultraspec 2100 pro	Amersham Biosciences, Life Technologies, Carlsbad, CA, USA
SW 40 Ti Swinging-Bucket Rotor	Beckman Coulter, Krefeld, Germany
TECAN SPARK® Multimode Microplate Reader	Tecan Trading AG, Männedorf, Switzerland
Thermocyler peqSTAR 2x Gradient	VWR International Germany GmbH, Darmstadt, Germany
ThermoMixer® compact	Eppendorf AG, Hamburg, Germany
Titramax 101	Heidolph Instruments GmbH & Co. KG, Schwabach, Germany
Trans-Blot® SD Semi-Dry Transfer System	Bio-Rad Laboratories GmbH, Munich, Germany
Trans-Blot® Turbo™ Transfer System	Bio-Rad Laboratories GmbH, Munich, Germany
Transferpette™ S single channel pipette (10 µl/ 100 µl/ 1000 µl)	BRAND GMBH + CO KG, Wertheim, Germany
Ultrasonic water bath SONOREX SUPER 10P	BANDELIN electronic GmbH & Co KG, Berlin, Germany
Vortex-Genie 2	Scientific Industries, Bohemia, NY, USA
Water bath W12	Labortechnik Medingen, Arnsdorf, Germany
Water distiller	GFL GmbH, Burgwedel, Germany

2.11 Software

Table 12: List of software

Software	Supplier
AxioVision Rel. 4.8	Carl Zeiss Microscopy GmbH, Jena, Germany
CorelDRAW® 2019	Corel Corporation, Ottawa, ON, Canada
Image Studio 5.2	LI-COR Biosciences GmbH, Lincoln, NE, USA
ImageJ 1.52n	Wayne Rasband, National Institutes of Health, Bethesda, MD, USA
Microsoft Office 2013	Microsoft Cooperation, Redmond, WA, USA
QuantStudio™ Design & Analysis Software v1.4.3	Thermo Fisher Scientific, Waltham, MA, USA
R 3.4.4	R Foundation, Vienna, Austria
Spark®Control MethodEditor	Tecan Trading AG, Männedorf, Switzerland

3 Methods

3.1 Human iPSC-derived RPE Cells (hiPSC-RPE Cells)

3.1.1 Origin of hiPSC-RPE Cells

The hiPSC-RPE cell lines cultivated and studied in various experimental settings in the scope of this thesis had previously been differentiated from iPSCs at the Institute of Human Genetics following the protocol published in Brandl et al., 2014. The iPSCs in turn had been reprogrammed from adult human dermal fibroblasts out of biopsied skin tissue (Brandl et al., 2014) as well as PBMCs from patients with an extremely high (risk score 5) or extremely low (risk score 1) genetic risk for AMD according to the genetic risk scores published in Grassmann et al., 2012.

3.1.2 Cultivation of hiPSC-RPE Cells

hiPSC-RPE cells were handled under sterile conditions in a laminar flow workbench and were kept in a Heracell™ 150i CO_2-Incubator at a constant temperature of 37°C and 5 % CO_2. They were maintained in cell culture medium consisting of Gibco™ KnockOut™ Dulbecco's Modified Eagle Medium (DMEM) supplemented with the components listed in Table 13, unless stated otherwise. All media was kept at 4°C, warmed to room temperature before application to cells and used for a maximum of 14 days after adding any supplements.

Table 13: Composition of the iPSC-RPE cell culture medium
KnockOut™ DMEM served as basis and was supplemented with the following components:

Component	Concentration
Gibco™ KnockOut™ Serum Replacement (KOSR)	5 % (v/v)
Gibco™ L-Glutamine 200 mM (100x)	2 mM
Gibco™ MEM Non-Essential Amino Acids Solution (100x)	0.1 mM
Nicotinamide	10 mM
Gentamicin solution (50 mg/ml)	5 µg/ml
β-Mercaptoethanol	0.1 mM

The hiPSC-RPE cells had been cryopreserved in liquid nitrogen. After thawing they were plated on 6-well cell culture plates coated with Corning® Matrigel® Growth Factor Reduced (GFR) Basement Membrane Matrix (Matrigel) in cell culture medium with 25 µg/ml Plasmocin. 14 days later, cells were passaged onto new Matrigel-coated 6-well plates at a ratio of 1:6 and cultivated for another 14 days.

In preparation for passaging the cells onto the new plates, transwell filter inserts as well as 96-well plates were coated with a 1:30 dilution of Matrigel (Brandl et al., 2014) and subsequently were washed with plain DMEM once. In order to divide the cells onto the Matrigel-coated transwell filter inserts in a 6- or 12-well-format, they were passaged in a ratio of 1:6 or 1:12, respectively. Additionally, cells were passaged onto Matrigel-coated 96-well plates in a ratio of 1:100. To detach the cells, they were incubated with TrypLE™ Express for 15 min at 37°C and then washed from the plates and centrifuged for 5 minutes at 1200 rpm before they were resuspended the desired volume of cell culture medium.

Cells in 6- and 12-well formats were cultured for six to eight weeks before inclusion into experiments, whereas cells cultured on 96-well plates could already be implemented in further studies after four weeks of cultivation. During the cultivation period, cell culture medium was changed three times a week, at the latest after 72 h. In 6-well plates, 2 ml of medium was used above (750 µl in 12-well plates) and below (1.5 ml in 12-well plates) the transwell filters and 150 µl per well was used in 96-well plates. Cell morphology and growth as well as the confluency of the forming monolayer were monitored regularly under the microscope during the cultivation period and before using the cells in any experiments.

3.2 Induction of Oxidative Stress with SI

For SI studies, SI was dissolved in cell culture medium without KOSR and diluted until reaching the desired concentrations of SI. Through various preliminary tests, ultimately concentrations of 0 mM and 0.5 mM SI were chosen for 24 h stress experiments. For a chronic stress model, cells were exposed to concentrations of 0 mM, 0.125 mM and 0.25 mM SI over a period of three days.

For experiments in a 6-well format, 1.5 ml of the respective solution was added above as well as below the transwell filter inserts, in a 12-well format 0.5 ml of the respective solution was applied above and 1 ml below. Cells cultured in a 96-well format were treated with 150 µl of the solution. In 24 h experiments, cells were further analyzed 24 h after incubation in the solutions. For 72 h experiments, the solutions were changed daily for a total of three times after every 24 h. Cells were further analyzed on the fourth day, 24 h after the third change of solutions.

3.3 Induction of Oxidative Stress through BL Irradiation

For BL irradiation experiments, the Blue Light LED Light Source used for studies with ARPE-19 cells and primary human RPE cells in Brandstetter et al., 2015 was custom built by LUMITRONIX® LED-Technik GmbH and installed in a CO_2 Incubator (BINDER GmbH). As

described before, the light source contains a 3x3 arrangement of blue LEDs (XLamp XP-E royal blue; Cree, Durham, NC, USA), with the peak wavelength of the LED spectrum at 448 nm. LED-cell distance was decreased to 26 cm due to the height of the incubator, as compared to the distance of 35 cm leading to an irradiance of 0,8 mW/cm^2 in Brandstetter et al., 2015.

Before beginning the BL irradiation experiments, cell culture medium was switched to irradiation medium consisting of the phenol red free Dulbecco's Modified Eagle's Medium/Nutrient Mixture F-12 Ham supplemented according to Table 13, but without KOSR. For cells cultured in a 6- or 12-well format, 1 ml of irradiation medium was added above as well as below the transwell filter inserts. For cells cultured on 96-well plates, 150 µl of irradiation medium was applied to each well. The optimal irradiation time was set to be 9 h. Hourly temperature measurements inside the incubator as well as in the medium affirmed that temperature wasn't substantially affected by the light source's irradiance. The incubator temperature was set to 34°C, since the heat emitted by the cooling element of the light source warmed the incubator by another 3°C to the desired cultivation temperature of 37°C. For every irradiated plate, a control plate treated with the same medium was incubated at 37°C for the same time period in a separate incubator without irradiation.

3.4 Induction of Oxidative Stress through POS and HNE-modified POS

3.4.1 POS Isolation

POS were collected from porcine retinae. Retinae and POS were handled on ice. In preparation for POS isolation, 48 fresh, qualitatively suitable pig eyes, chilled in cold 0.9 % NaCl, were cut in half using a scalpel. Retinae were carefully detached from the tapetum and stored at -80°C until further use. After thawing, retinae were homogenized in three steps, first by filtering them through porous material in form of a gauze bandage and then homogenizing them further using 5 ml pipettes und finally 1000 µl pipettes.

Four gradients made up of taurine buffer (composition listed in Table 14) and 20-60 % sucrose in taurine buffer were prepared according to Table 15.

Table 14: Taurine buffer composition for POS isolation gradient
For the 100 mM taurine buffer solution, 1.25 g of taurine was dissolved in 100 ml distilled H2O.

Component	Volume
5 N NaCl	5.2 ml
1 M MgCl2	400 µl
1 M Tris-Buffer (pH = 7.5)	4 ml
100mM Taurine	10 ml
ad 200 ml with dest. H2O	

Table 15: Preparation of gradient solutions for POS isolation gradients
For the four gradients together, 24 ml of each of the here listed gradient solutions were prepared.

%	Volume Taurine Buffer	Volume of 60 % Sucrose Solution
20	16 ml	8 ml
27	13.2 ml	10.8 ml
33	10.8 ml	13.2 ml
41	7.6 ml	16.4 ml
50	4 ml	20 ml
60	-	24 ml

Density gradients with increasing sucrose percentage from top to bottom were prepared in 38.5 ml ultracentrifuge tubes by undercoating 5 ml of the prepared gradient solutions one by one, beginning with the 20 % sucrose solution and ending with the 60 % sucrose solution according to Table 15. Next, each gradient was overlayed with 10 ml of the retina homogenate. The gradients were ultracentrifuged at 26.000 rpm in an SW 40 Ti Swinging-Bucket Rotor for 2 h. The annularly enriched pink POS-containing fraction was taken off and aliquoted into 2 ml tubes. In the course of three washing steps with Opti-MEM® I, samples were spun at 12.000 rpm for 5 min, pellets were resuspended and combined step by step. Lastly, now purified POS were resuspended in Opti-MEM® I with 1 % Pen/ Strep and stored frozen at 80°C until further use.

3.4.2 Bradford Assay for Determination of POS Concentration

The concentration of previously purified POS was determined via Bradford assay. Bovine serum albumin (BSA) was used as a protein standard. To begin, a BSA solution with a concentration of 2000 µg/ml was prepared by diluting 100 mg/ml BSA in Millipore H_2O with Opti-MEM® I. By serial dilution in Opti-MEM® I, a calibration curve with BSA concentrations of 2000 µg/ml, 1000 µg/ml, 500 µg/ml, 250 µg/ml, 125 µg/ml, 62,5 µg/ml, 31,12 µg/ml and 0 µg/ml was pipetted and cooled on ice. Roti®-Quant was diluted 1:5 in Millipore H_2O. 5 µl of the respective standard concentration or the POS sample to be measured was added to 995 µl of the Roti®-Quant dilution. After vortexing and incubating for 20 min at room temperature, absorbance at 595 nm was measured photometrically. The BSA concentration of 0 µg/ml served as blank measurement sample. The POS concentration was calculated from the calibration curve measurements.

3.4.3 POS Modification with HNE

In order to reduce lysosomal POS-degradation in the cells (Kaemmerer et al., 2007), POS were modified with 5 mM of the lipid peroxidation product HNE (Krohne et al., 2010a). For modification, the required volume of POS was thawed and centrifuged for 5 min at 14.000 rpm

and 4°C, after which the supernatant was discarded and POS were resuspended in 5 mM HNE in Opti-MEM® I with 1 % Pen/ Strep. After incubating the POS in the HNE solution for 24 h at room temperature, the solution was centrifuged at 14.000 rpm and 4°C for 5 min. The supernatant was discarded and POS were washed three times to remove unbound HNE (Krohne et al., 2010a) with 500 µl Opti-MEM® I with 1 % Pen/ Strep, centrifuging at 14.000 rpm and °C for 5 min after each washing step. After washing for the third time, the pellet was resuspended in the required volume of Opti-MEM® I with 1 % Pen/ Strep and stored at -80°C.

3.4.4 POS Feeding

This protocol applies to feeding of POS and HNE-POS alike. POS were fed to hiPSC-RPE cells cultured in a 12-well format. A POS concentration of 4 µg/cm^2 for analysis of POS phagocytosis in RPE cells served as point of reference (Krohne et al., 2010a; Westenskow et al., 2012), which is in accordance with the typical number of 20 POS fed per hiPSC-RPE cell for 24 h in various POS feeding experiments (Brandl et al., 2014; Singh et al., 2015; Dalvi et al., 2019; Nachtigal et al., 2020).

After thawing the POS-aliquot prepared for all wells of a feeding day, the volume was filled up to 1 ml with Opti-MEM® I with 1 % Pen/ Strep in an Eppendorf tube and placed in an ultrasonic water bath for 5 min at 10 % intensity. Next, the POS solution was vacuum sucked through a 5 µm cell strainer. The cell strainer was rinsed twice with 2 ml cell culture medium to make sure that no excess POS remained in the filter. The resulting 5 ml were filled up with cell culture medium to the required end volume. One milliliter of the resulting solution was applied in the apical compartment above the transwell filters.

POS were fed to the hiPSC-RPE cells for 6 or 7 consecutive days. Cells were incubated in the POS solution for 24 h at 37°C, replacing it daily by freshly prepared POS solution. The normal cell culture medium below the transwell filters was changed every day of POS feeding. Cells fed with POS were harvested for later protein or RNA analyses.

3.5 MTT Assay to Determine Cell Viability

MTT (3-(4,5-dimethylthiazol-2-yl)-2,5-diphenyltetrazolium bromide) assays were executed to determine cell viability of confluent hiPSC-RPE cells on 96-well plates after treatment with SI or BL irradiation.

For the assays with SI, cells were incubated for 24 h with 100 µl of different concentrations of SI ranging from 0 to 10 mM. After removing the media and washing the cells with PBS, 100 µl of a 0.5 mg/ml MTT solution in cell culture medium without KOSR were added to each well to start the assay. Cells were incubated in this solution for at least 30 min at 37°C, until visible

violet crystals had formed. After removing the MTT solution and washing with PBS, 150 µl of 0.1M HCl in isopropanol were added to each well, which dissolved the crystals within 10 minutes of gentle shaking. After transferring 100 µl of the solution into measurement plates (clear flat bottom 96-well microplates from Greiner), absorbance at 540 nm was measured using the TECAN SPARK® Multimode Microplate Reader.

For BL assays, cell culture medium was replaced by irradiation medium immediately before incubating the cells for various durations up to 24 h in the BL incubator at a constant temperature of 37°C +/- 0.5°C. The MTT assays was performed as described above for SI, but with the MTT solution prepared in irradiation medium instead of cell culture medium without KOSR.

3.6 LDH Assay to Quantify Cytotoxicity of Oxidative Stressors

As an extension to the MTT assays, cytotoxicity and cytolysis in hiPSC-RPE cells caused by oxidative stress were quantified by measuring lactate dehydrogenase (LDH) release from cells upon plasma membrane damage and cytolysis. For 24 h SI experiments, the Cytotoxicity Detection Kit^{PLUS} (LDH) was used by following the official assay protocol (Version 06 from May 2011, chapter 2.3, steps 6-10). For 72 h SI experiments and 9 h BL experiments, the CytoTox 96® Non-Radioactive Cytotoxicity Assay was applied following the assay protocol (Technical Bulletin, revised 7/16, chapter 4). The colorimetric assays were performed with the supernatant of cells cultured in a 96-well format. In each assay, media background controls were included, as well as maximum LDH release controls (high controls) in wells with 0 mM SI or 0 h BL exposure, respectively, for each cell line.

In 24 h SI experiments, 150 µl of 0 mM, 0.5 mM or 3 mM SI were applied to cells. After 24 h of incubation, the assay was performed according to the manufacturer's protocol. Absorbance was measured in the supernatants in clear flat bottom 96-well microplates from Greiner using the TECAN SPARK® Multimode Microplate Reader at 490 nm with a reference wavelength of 620 nm.

For 72 h SI experiments, cells were exposed to 150 µl of different concentrations of SI (0 mM, 0.125 mM, 0.25 mM, 1.5 mM) for three days with media change after every 24 h. In BL experiments, after application of 150 µl irradiation medium, cells were irradiated for 9 h. Control plates were incubated for 9 h without BL exposure. After the respective incubation times, the assay protocol was followed from step 4 to the end of chapter 4.B. Since high control absorbance values exceeded absorbance maxima in the plate reader, measurements were repeated with 100 µl of each well content diluted 1:1 in 1x PBS.

3.7 Immunocytochemistry

In order to assess the integrity of the RPE monolayer as well as the quality of treated and untreated hiPSC-RPE cells as a prerequisite for further experiments, immunocytochemical stainings of ZO-1 were performed. In all samples, nuclei were stained with 4',6-Diamidin-2-phenylindol (DAPI).

hiPSC-RPE cells cultured on transwell filters of 12-well plates were treated with 0 mM or 0.5 mM SI for 24 h, 0 mM, 0.125 mM or 0.25 mM SI for 72 h or 0 h or 9 h BL. A piece of the transwell filters was cut out and transferred into wells of a 48-well plate containing 1x PBS. After fixing the cells with 2 % PFA for 10 min followed by 3 washing steps for 5 min with 1x PBS, the filters were coated in blocking solution (Table 9). After 30 min of incubation at room temperature, the blocking solution was replaced by the primary antibody solution (Table 9) containing the primary antibody (Table 4) and incubated at 4°C overnight. The next day, the filter pieces were washed 3 times for 5 min with 1x PBS and incubated in the corresponding secondary antibody solution (Table 9) containing the secondary antibody (Table 5) in a dilution of 1:800 and DAPI in a dilution of 1:2.000 in the dark for at least 30 min at room temperature or at 4°C overnight. After removing the secondary antibody solution, filters were washed 3 times for 5 min with 1x PBS. The stained filters were mounted onto microscope slides using Dako Fluorescence Mounting Medium and were secured with a cover slip.

The stainings were visualized under the Fluorescence Microscope Axioskop 2 of the Carl Zeiss Microscopy GmbH. Images were taken in 40x magnification with the microscopy software AxioVision Rel. 4.8 from Carl Zeiss with an exposure of 800 ms for ZO-1 and 120 ms for DAPI. The pictures were saved as TIFF-files and were adjusted in brightness and contrast in ImageJ 1.52n.

3.8 Transepithelial Electrical Resistance (TEER) Measurements

Transepithelial electrical resistance (TEER) measure the integrity of tight junctions in the RPE cell monolayer and therefore serve as a quality control for the barrier function of the RPE (Brandl et al., 2014; Srinivasan et al., 2015; Chen et al., 2015). Measurements were taken with an epithelial Volt / Ohm Meter (EVOMX) according to the manufacturer's instructions. In preparation for the measurements, the electrodes were sterilized in 70 % ethanol for 15 min and then immersed in a 150 mM NaCl solution for 15 min to allow equilibration. Measurements were taken by gently positioning the longer electrode vertically onto the well bottom below the filter (basolateral compartment), whereby the shorter electrode was dipped into the cell culture medium above the filter (apical compartment) (Srinivasan et al., 2015). Hereby, the electrodes had no contact to the walls of the wells or the RPE monolayer. Measurements were performed by calmly holding the electrode, until a value had stabilized. This procedure was repeated for

all wells of each plate. Blank resistance was determined by measuring the TEER in wells with Matrigel-coated transwell filters which did not contain any cells. In the evaluation, after deducting the mean of the blank values from the resistance measurements, cell specific resistance values were multiplied with the surface area of the filter membrane in order to obtain values in the dimension Ω^*cm^2 (Brandl et al., 2014; Srinivasan et al., 2015).

3.9 Quantitative Expression Analysis of NRF2-Regulated Antioxidant Genes

3.9.1 RNA Isolation

Preceding RNA isolation, cells were detached and scraped from transwell filters in lysis buffer containing 10 µl ß-Mercaptoethanol per 1 ml with cell scrapers and transferred into Eppendorf tubes. 700 µl or 350 µl lysis buffer were used for cells in a 6- or 12-well format, respectively. Samples were stored at -80°C until starting RNA isolation.

RNA isolation from the thawed cell lysate samples was achieved using PureLink® RNA Mini Kits, according to the manufacturer's protocol (Quick reference, revised 21 May 2012) with minor changes.

To begin, samples were transferred onto QIAshredder homogenizers placed in collection tubes and centrifuged for 3 min at 12.000g. Steps 1 to 5 of RNA purification were completed according to the protocol. Opposite to the manufacturer's protocol, only 350 µl Wash Buffer I was added to the spin cartridges in step 6 and was centrifuged at 12.000g for 30 s, followed by a DNAse digestion with 80 µl DNAse diluted 1:8 in Buffer RDD. This was again washed with 350 µl of Wash Buffer I and centrifuged at 12.000g for 30 s. Continuing with step 8, the RNA Purification protocol was followed to the end. After the final step of eluting the RNA in 30 µl of RNAse-free water, RNA concentrations of the eluates were measured using the NanoDrop® ND1000 Spektrophotometer. The purified RNA was kept at -80°C until further use.

3.9.2 cDNA Synthesis

To synthesize cDNA from isolated RNA samples, the RevertAid H Minus First Strand cDNA Synthesis Kit was used. The reaction mixture consisted of 300 ng, 500 ng or 1.000 ng RNA sample, 1 µl Random Hexamere Primer and RNAse-free water added ad 12.5 µl to standardize RNA concentrations across all samples of an experiment. After incubating the reaction mixture for 5 min at 65°C in the Thermocycler (step 1 in Table 16), the samples were returned onto ice to cool. 7.5 µl of the cDNA synthesis reaction mix (Table 17) was added to each sample. The samples were placed back into the Thermocycler which continued its program from step 2 in Table 16. cDNA was stored at -20°C until further use.

Table 16: Thermocycler program for cDNA synthesis

Reaction Step	Temperature	Duration
Step 1: Annealing	65°C	5 min
Step 2: cDNA Synthesis and Heat Inactivation	25°C 42°C 70°C	10 min 60 min 10 min

Table 17: Composition of the cDNA synthesis reaction mix
Volume given per sample.

Component	Volume
RNAse-free H_2O	0.5 µl
5x Reaction Buffer	4 µl
dNTPs (10 mM each)	2 µl
RevertAid Reverse Transcriptase	1 µl

3.9.3 Quantitative Real-Time PCR (qRT-PCR) for Expression Analysis in hiPSC-RPE Cells

mRNA expression was determined via quantitative real-time PCR (qRT-PCR). First, 40 µl Millipore H_2O was added to previously synthesized cDNA samples. For each gene of interest, a separate reaction mixture with gene-specific primers and probes was prepared according to Table 18. Samples were pipetted into 384-well measurement plates in triplicates per gene with *HPRT1* serving as housekeeping gene. The qRT-PCR program described in Table 19 was run in the QuantStudio™ 5 Real-Time PCR System. The mean values of the triplicates per sample were further analyzed in Excel using the Delta-Delta C_T ($\Delta\Delta C_T$) method (Livak & Schmittgen, 2001).

Table 18: Composition of the qRT-PCR reaction mix
Gene-specific primers and probes were used for the genes examined. The reaction mixture with a total volume of 7.5 µl per sample was added to 2.5 µl cDNA in the 384-well measurement plate.

Component	Volume
2x TaqMan Gene Expression Master Mix	5 µl
Primer forward (50 µM)	1 µl
Primer reverse (50 µM)	1 µl
Probe	0.125 µl
H_2O (Millipore)	0.375 µl

Table 19: qRT-PCR program for gene amplification

Reaction Step	Temperature	Duration	Cycles
Step 1: Denaturation	95°C	40 s	40
Step 2: Annealing	60°C	60 s	
Step 3: Elongation	72°C	2 min	

3.10 Protein Analysis of NRF2-Regulated Antioxidant Genes and Rhodopsin in hiPSC-RPE Cells after Feeding of POS/ HNE-POS

3.10.1 Harvesting Samples for Western Blot Analysis

For Western blot analysis of HMOX1 and NQO1 protein, cells seeded on transwell filters (6-well format) were harvested after treatment with SI or BL. For protein analysis of rhodopsin, cells cultured on 12-well filters which had been fed POS or HNE-POS were harvested.

To prepare cells for subsequent Western blot analysis, media on the transwell filters was replaced by 250 µl of cold 1x protein isolation buffer consisting of 1x Roche cOmplete™ Protease Inhibitor in PBS. Cells were scraped from filters and transferred into Eppendorf tubes. Another 250 µl of the isolation buffer was used to rinse the filters and was also transferred into the respective tubes. After centrifugation for 5 min at 4°C and 1.000 rpm, the supernatant was removed and the pellet was resuspended in 150 µl of the isolation buffer. Each sample was sonicated for 10 s at 30 % intensity. After adding 30 µl Laemmli buffer, the protein samples were boiled at 95°C for 5 min before loading them onto the gels. Remaining samples were stored at -20°C.

3.10.2 Sodiumdodecylsulfate Polyacrylamide Gel Electrophoresis (SDS PAGE)

Before proteins could be detected via Western blot analysis, proteins were separated by reducing Sodiumdodecylsulfate Polyacrylamide Gel Electrophoresis (SDS PAGE) using gels composed of a separating gel containing 12.5 % polyacrylamide and a stacking gel containing 3 % polyacrylamide. The gel solutions were mixed according to Table 20 and poured into MiniPROTEAN® casting frames. Spacer plates with 1.5 mm integrated spacers were used for all gels.

Previously harvested protein samples were boiled at 95°C for 5 min immediately before loading 20 µl per sample. 5 µl of the PageRuler™ Prestained Protein ladder (10-180 kDa) served as a size standard and was loaded onto each gel. The gels were run at 50 V in SDS running buffer for approximately 30 min until the protein samples had left the stacking gel. The run continued

at 150 V for 1 to 1.5 h for the proteins to be separated by molecular weight in the separating gel.

Table 20: Composition of acrylamide gels used for SDS PAGE
Calculated for a final volume of 10 ml.

Component	Separating Gel (12.5 %)	Stacking Gel (3 %)
1 M Tris-HCl pH 8.8	3.8 ml	-
1 M Tris-HCl pH 6.8	-	5.5 ml
H2O dest.	3.0 ml	3.4 ml
Polyacrylamide (40 %)	3.1 ml	1.1 ml
SDS (20 %)	100 µl	100 µl
APS (10 %)	100 µl	100 µl
TEMED	10 µl	20 µl

3.10.3 Western Blot

After the proteins had been separated via reducing SDS PAGE, they were blotted from the gels onto a Polyvinylidene Difluoride (PVDF) membrane by semi-dry protein transfer using the Trans-Blot® SD Semi-Dry Transfer System or the Trans-Blot® Turbo™ Transfer System. The gels, two 3 mm Whatman papers per gel and PVDF membranes previously activated in methanol for 30 s were equilibrated in 1x Towbin buffer. Each gel was placed on a PVDF membrane between the Whatman papers for the proteins to be transferred from the gel onto the membrane during a 40 min run at 24 V in the blotting instrument. Blocking of the membranes took place for 1 h at room temperature in 5 % skimmed milk powder in TBS-T. Membranes were then incubated in the primary antibody (Table 4) in 5 % skimmed milk powder in TBS-T over night at 4°C. The next day, the membranes were rinsed 3 times for 5 min in TBS-T and incubated for 1 h at room temperature in the secondary antibody (Table 5) diluted 1:10.000 in 5 % skimmed milk powder in TBS-T. After rinsing 3 times for 5 min in TBS-T, Clarity Western ECL Substrate was spread over the membranes for bound protein bands to be visualized by chemiluminescence in an Odyssey® Fc Imager. Clarity Max Western ECL Substrate as a substrate with higher sensitivity was used when signal intensity needed to be enhanced. Anti-ß-Actin (Table 4) served as a loading control in all experiments.

3.11 Statistical Analysis

For statistical analysis of data consisting of two conditions, the Shapiro-Wilk Normality Test implemented in R (R Development Core Team, 2011) was performed to assess normal distribution of the data. It was followed by a two-tailed Student's T-Test for normally distributed data and a Wilcoxon Test for not normally distributed data. The T-Test was only considered

for statistical evaluation of an experiment as long as all tested data within the experiment qualified for the T-Test.

For data consisting of more than two conditions, a Kruskal Wallis Test was carried out. To determine differences between groups, a Dunn's Multiple Comparison Test implemented in the FSA package (Ogle et al., 2019) was applied to retrieve raw p-values for comparisons of interest. Correction for multiple testing was executed by employing the Benjamini-Hochberg method (Benjamini & Hochberg, 1995) implemented in the multtest package (Pollard et al., 2005). Irrespective of the statistical model, corrected p-values below 0.05 were considered statistically significant.

4 Results

4.1 Establishing Experimental Conditions for Acute Chemical Oxidative Stress with SI

The experimental conditions for SI treatment of hiPSC-RPE cell lines needed to be established before commencing the oxidative stress experiments of this thesis. The first step was to determine the suitable concentration of SI, which ought to oxidatively stress the cells without significantly reducing their viability and causing cytotoxicity.

4.1.1 Determination of Optimal SI Concentration for 24 h SI Experiments by Cell Viability Analysis

The MTT assay is a commonly used method to assess cell viability, as only viable cells can metabolically reduce MTT tetrazolium to formazan, which is quantitatively measured (Riss et al., 2013). MTT assays were performed after 24 h treatment with various concentrations of SI ranging from 0 mM to 10 mM. This concentration range was chosen based on SI studies with ARPE-19 cells in Juel et al., 2013, Hanus et al., 2016 and Zhang et al., 2016. In **Figure 3**, results for all tested concentrations (0 mM, 0.125 mM, 0.25 mM, 0.5 mM, 1 mM, 1.5 mM, 2 mM, 2.5 mM, 5 mM, 6 mM, 7 mM, 8 mM, 9 mM, 10 mM SI) are summarized combined from four independent experiments, of which each included some of the concentrations. Cell viability after exposure to the highest concentration of 10 mM SI was reduced to 0-10 % for all examined cell lines. This validated the tested concentration range to be chosen adequate for the viability analysis in the hiPSC-RPE cells. Overall, 0.5 mM SI was the highest concentration for which cell viability was not significantly decreased after statistical assessment. This concentration was therefore selected for the further acute oxidative stress experiments.

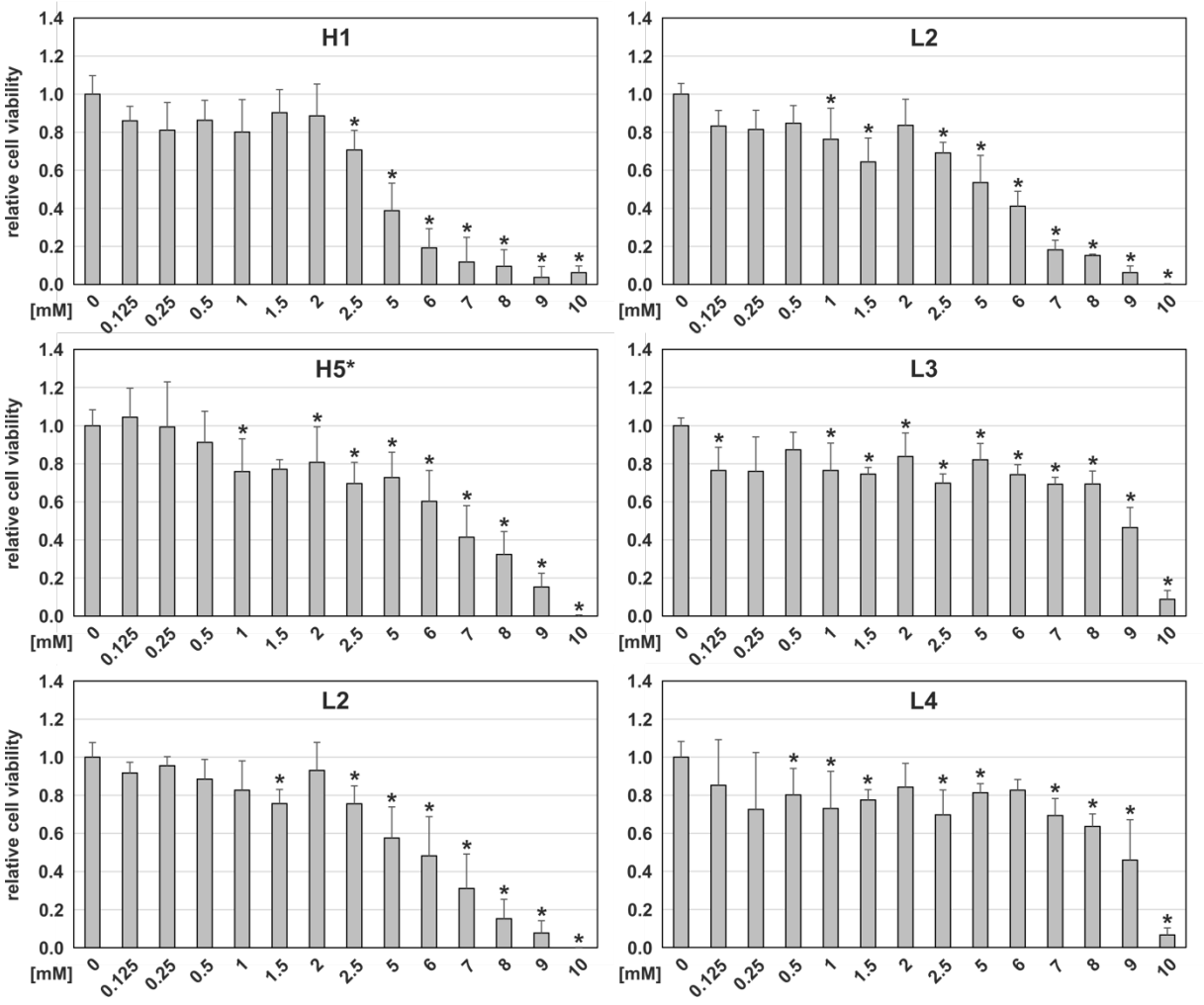

Figure 3: Influence of different concentrations of SI on cell viability of hiPSC-RPE cell lines
Two high risk (H1, H5*) and three low risk (L2, L3, L4) cell lines were treated with concentrations of 0 to 10 mM SI for 24 h in four independent experiments. After 24 h, cell viability was assessed via MTT assay. After adjusting to blank values (only 0.1 M HCl in isopropanol), measurement values were calibrated against the control (0 mM SI). Data are presented as means + SD (n = 4-16). Statistical significance (*: $p < 0.05$) was determined with the Kruskal Wallis Test with post hoc Dunn's Multiple Comparison Test and multiple testing correction using the Benjamini-Hochberg method.

4.1.2 Confirmation of Selected SI Concentration by Quantification of Cytotoxicity

To independently confirm that the concentration of 0.5 mM SI is not cytotoxic for the hiPSC-RPE cells, LDH release assays were performed. As opposed to the MTT assay, which reflects the amount of viable cells (Riss et al., 2013), the LDH assay estimates the amount of dead cells by measuring the amount of LDH released into the supernatant upon cell membrane damage and cytolysis.

After incubating the hiPSC-RPE cells with SI for 24 h in two independent experiments, the supernatants were used for the LDH assays. Concentrations of 0 mM, 0.5 mM and 3 mM SI were tested (**Figure 4**). As expected and in agreement with the data from the MTT assays, there was no significant change in cytotoxicity in cells treated with 0.5 mM SI as compared to

untreated cells. On the other hand, cells treated with 3 mM SI revealed a significant increase in cytotoxicity for two high risk cell lines (H1 and H3) as well as a clear trend for the remaining cell lines (**Figure 4 A**). Between high and low risk cell lines, there was no significant difference in cytotoxicity for 0.5 mM (p = 0.44) or 3 mM SI (p = 0.55) (**Figure 4 B**), suggesting that the treatment had a similar effect on all cells, regardless of the genetic background.

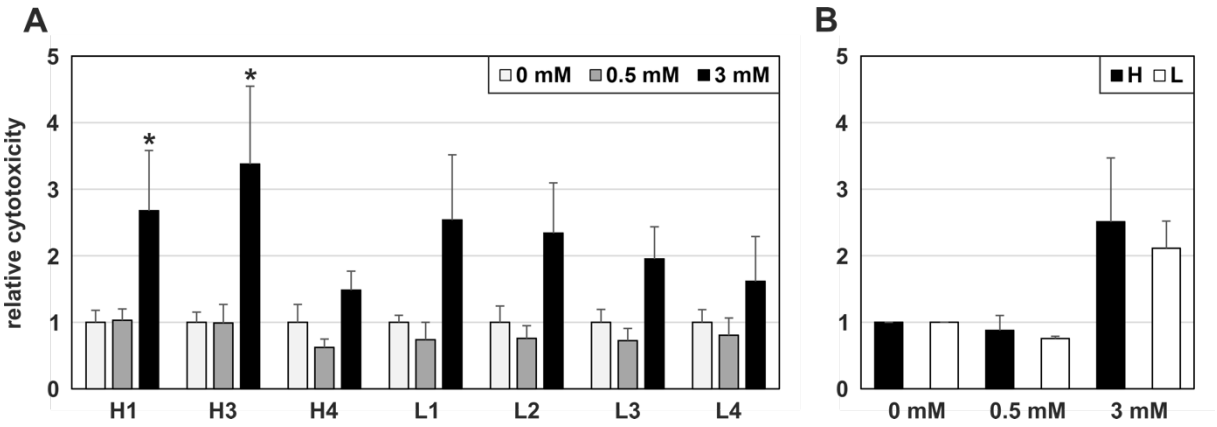

Figure 4: Effect of acute oxidative stress with SI on cytotoxicity in hiPSC-RPE cells
(**A**) Three high risk (H1, H3, H4) and four low risk (L1, L2, L3, L4) hiPSC-RPE cell lines were incubated with 0 mM, 0.5 mM and 3 mM SI for 24 h in two independent experiments. After 24 h, cytotoxicity was quantified by measuring LDH release in the supernatants. After adjusting for media background for the respective concentrations, measurement values were calibrated against the control (0 mM SI). Data are presented as means + SD (n = 5-6). Statistical significance (*: $p < 0.05$) was determined with the Kruskal Wallis Test with post hoc Dunn's Multiple Comparison Test and multiple testing correction using the Benjamini-Hochberg method. (**B**) High risk (H) and low risk (L) hiPSC-RPE cell lines were compared in their cytotoxic response to acute oxidative stress with 0.5 mM and 3 mM SI using the data from experiments described in (A) by taking the means and SD of the individual means of the cell lines. Data are presented as means + SD (n = 3 for H, n = 4 for L). Statistical significance (*: $p < 0.05$) was determined with a two-tailed Student's T-Test.

4.1.3 Influence of 24 h Exposure to 0.5 mM SI on mRNA Expression of *CD46*, *VEGFA* and *HMOX1* in hiPSC-RPE Cells

For a general overview of the effects SI may have on mRNA expression in hiPSC-RPE cells, three genes, namely *CD46*, *VEGFA* and *HMOX1*, which are involved in distinct cellular mechanisms, were analyzed by qRT-PCR.

The expression of complement regulator membrane cofactor protein (CD46) in the RPE is known to be decreased in early stages of GA (Vogt et al., 2011) and early AMD (Ebrahimi et al., 2013), as demonstrated in CD46 immunostainings. Since it had previously been shown at the Institute that *CD46* expression is downregulated in hiPSC-RPE cells in response to oxidative stress with paraquat (PQ) (Dr. Karolina Plößl, unpublished results), it was obvious to examine whether exposure to oxidative stress with SI would lead to a similar regulation of gene expression. Treating hiPSC-RPE cells with 0.5 mM SI for 24 h in two independent experiments however failed to alter *CD46* mRNA expression as compared to untreated controls (**Figure 5 A**).

Oxidative stress is also known to cause an increased expression and secretion of *VEGFA* in RPE cells (Kannan et al., 2006; Byeon et al., 2010). This has been reported for various oxidants as well as *in vitro* RPE model systems (Kannan et al., 2006; Byeon et al., 2010; Cao et al., 2013). It has also been seen in the hiPSC-RPE cells studied in this thesis in response to PQ (Dr. Karolina Plößl, unpublished results). Therefore, we were interested to analyze *VEGFA* expression in hiPSC-RPE cells upon SI treatment. Two independent experiments showed that *VEGFA* mRNA expression in hiPSC-RPE cells was unaltered after exposure to 0.5 mM SI for 24 h in comparison to 0 mM SI (**Figure 5 B**). Most of the examined cell lines even demonstrated a slight decrease in *VEGFA* expression after SI treatment.

The antioxidant gene *HMOX1* was selected to represent a gene regulated by the NRF2 pathway in the qRT-PCR analysis after acute oxidative stress with SI. In two independent experiments, after incubation with 0.5 mM SI for 24 h, treated hiPSC-RPE cells exhibited an upregulation in *HMOX1* mRNA expression compared to the controls (0 mM SI) (**Figure 5 C**). *HMOX1* mRNA was increased to levels between 1.32 (± 0.36) and 2.95 (± 0.85) for SI-treated cells as compared to the controls.

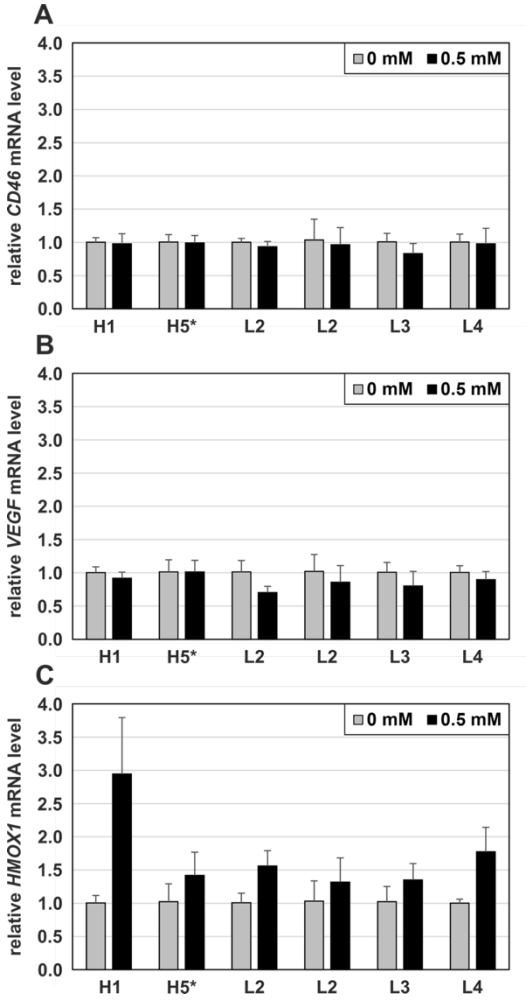

Figure 5: Influence of 24 h exposure to 0.5 mM SI on relative mRNA expression of *CD46*, *VEGFA* and *HMOX1* in hiPSC-RPE cells

Two high risk (H1, H5*) and three low risk (L2, L3, L4) hiPSC-RPE cell lines were treated with 0 mM and 0.5 mM SI for 24 h in two independent experiments. mRNA expression of *CD46* (**A**), *VEGFA* (**B**) and *HMOX1* (**C**) was determined via qRT-PCR. Expression was normalized to reference gene *HPRT1*, then calibrated against the control (0 mM SI). Data are presented as means + SD (n = 6).

4.2 Effects of Acute Chemical Oxidative Stress Induction with SI on hiPSC-RPE Cells

4.2.1 Verification of RPE Cell Morphology and Monolayer Integrity after 24 h SI Treatment

For the oxidative stress experiments of this thesis, the quality of the hiPSC-RPE cells before and after exposure to oxidative stress was crucial and was verified as follows: (1) RPE cell morphology was confirmed via immunocytochemistry next to regular microscopic controls and (2) barrier function was assessed via immunocytochemical stainings of tight junction protein ZO-1 (Stevenson et al., 1986) as well as TEER measurements.

The morphology and monolayer integrity of the hiPSC-RPE cells was not to be compromised upon induction of oxidative stress, otherwise oxidative stress responses between stressed and unstressed cells would not have been comparable. Immunocytochemical stainings of ZO-1 and DAPI were performed to visualize the hiPSC-RPE cells under the fluorescence microscope after incubation with 0 mM and 0.5 mM SI for 24 h. Being a structural protein of intercellular tight junctions, ZO-1 is essential in upholding the barrier function of the RPE monolayer as outer blood retina barrier (Obert et al., 2017). Nuclei were simultaneously stained with DAPI.

For every cell line and risk score, the hiPSC-RPE cells exhibited the characteristic hexagonal RPE cell shape, forming an even and uninterrupted monolayer, cell membrane to cell membrane, as marked by the continuous expression of ZO-1. Furthermore, cells were of similar size in all cell lines. In addition, it was verified that acute oxidative stress with 0.5 mM SI did not impact cell morphology or integrity of the monolayer (**Figure 6**).

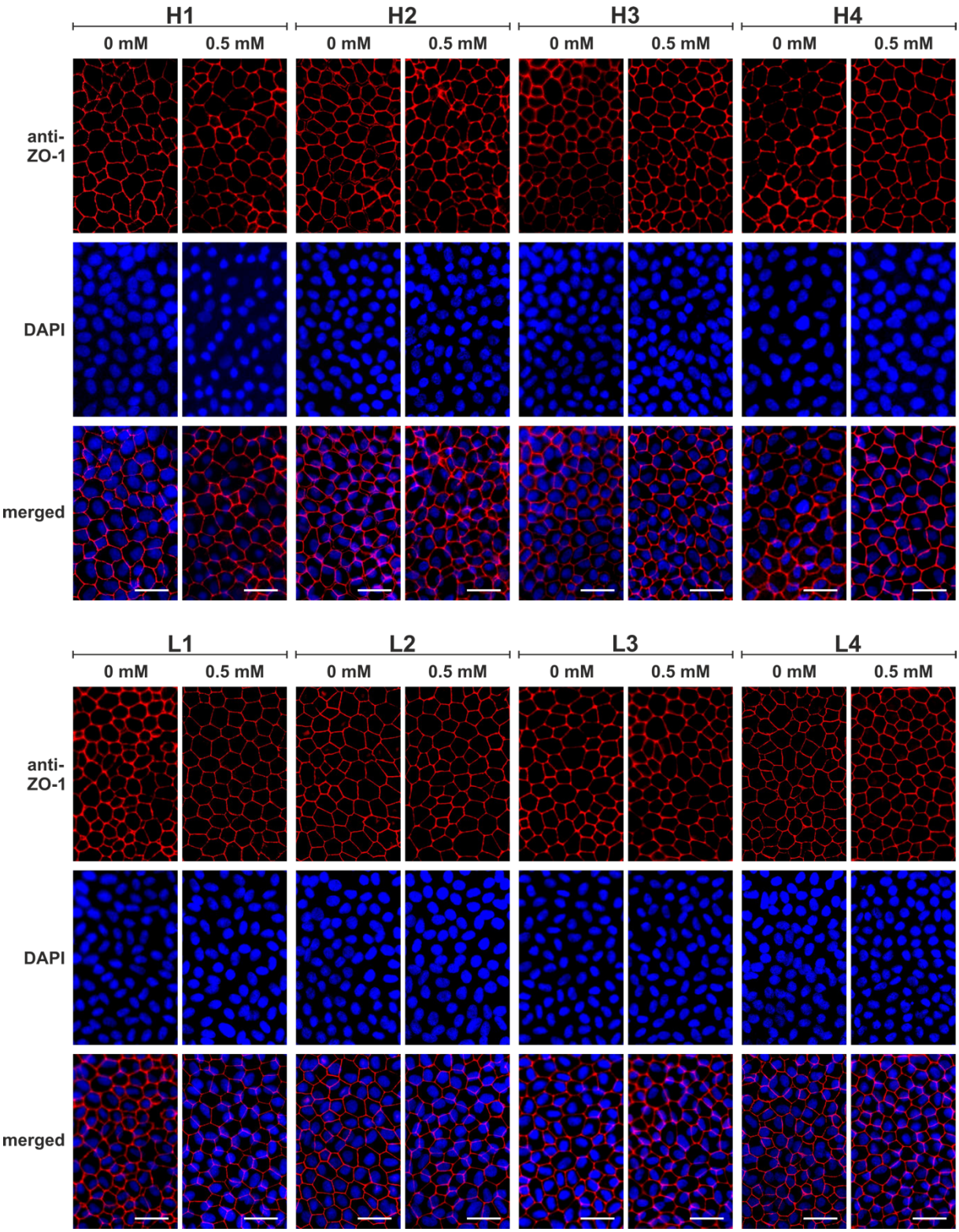

Figure 6: Verification of hiPSC-RPE cell quality regarding morphology and monolayer integrity after acute oxidative stress with SI

Four high risk (H1, H2, H3, H4) and four low risk (L1, L2, L3, L4) hiPSC-RPE cell lines were treated with 0 mM or 0.5 mM SI for 24 h. In subsequent immunocytochemical analysis, the tight junction marker ZO-1 (red) was labelled with an anti-ZO-1 antibody and nuclei were stained with DAPI (blue). Images were taken in 40x magnification under the fluorescence microscope. Scale bars: 25 µm.

4.2.2 TEER Measurements as Quality Control for RPE Monolayer Barrier Function

As a further quality measure to evaluate possible effects upon acute oxidative stress on RPE barrier function, TEER was determined in hiPSC-RPE cells after 24 h treatment with 0 mM and 0.5 mM SI. In three independent experiments, ambiguous results were obtained for treated and untreated conditions. Two cell lines (H4, L2) displayed significantly lower TEER values for SI-treated cells compared to controls, whereas the remaining cell lines demonstrated relatively constant TEER values in stressed and unstressed conditions, indicating that a concentration of 0.5 mM SI appears to not affect the RPE barrier. Cell line H4 exhibited noticeably higher TEER values for 0 mM SI than the other cell lines (**Figure 7 A**). Comparison of high and low risk cell lines did not reveal a significant difference in TEER, neither for treated nor for untreated cells (0 mM SI: $p = 0.34$, 0.5 mM SI: $p = 0.08$), but low risk cell lines seemed to have a slightly more permeable barrier due to lower TEER values under both conditions (**Figure 7 B**).

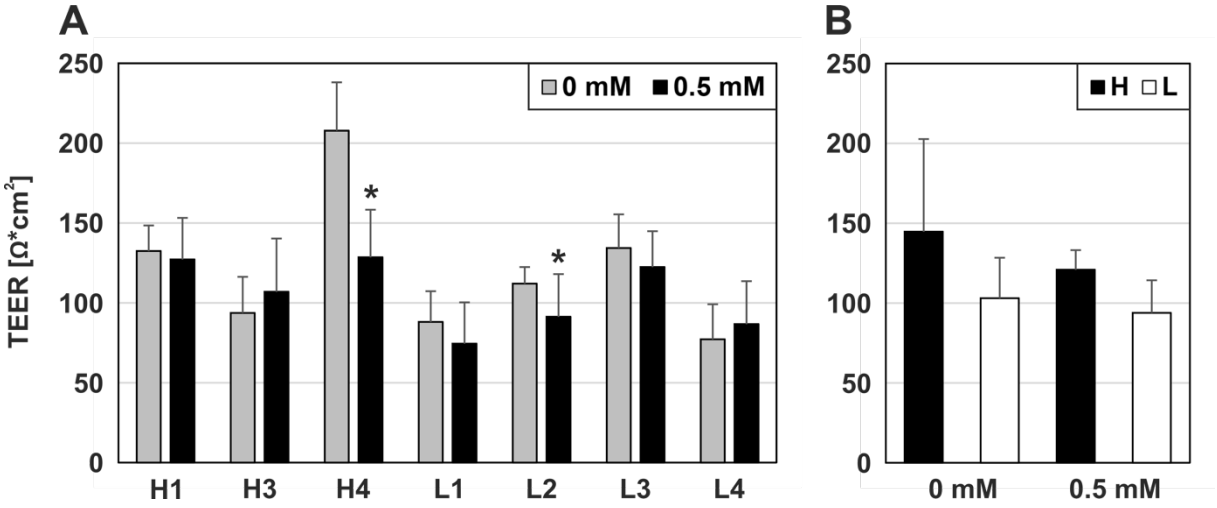

Figure 7: Influence of acute oxidative stress with SI on TEER of hiPSC-RPE cells
(**A**) Three high risk (H1, H3, H4) and four low risk (L1, L2, L3, L4) hiPSC-RPE cell lines were treated with 0 mM or 0.5 mM SI for 24 h in three independent experiments. After 24 h, TEER measurements were taken. After adjusting for blank resistance values for the respective concentrations, measurement values were multiplied with the surface area of the filter membrane, obtaining TEER values in the dimension $\Omega*cm^2$. Data are presented as means + SD (n = 12). Statistical significance (*: $p < 0.05$) was determined with a two-tailed Student's T-Test. (**B**) The TEER values of high risk (H) and low risk (L) hiPSC-RPE cell lines were compared in stressed (0.5 mM SI) and unstressed (0 mM SI) conditions. Means and SD of the individual means of the cell lines were taken from the data shown in (A). Data are presented as means + SD (n = 3 for H, n = 4 for L). Statistical significance (*: $p < 0.05$) was determined with a two-tailed Student's T-Test.

4.2.3 Increased mRNA Expression of Antioxidant Genes *HMOX1* and *NQO1* in hiPSC-RPE Cells upon 24 h SI Treatment

After showing that acute oxidative stress with SI does not affect the quality of the hiPSC-RPE cells and their monolayer in immunocytochemical analysis and TEER measurements, the influence of acute oxidative stress on mRNA expression of two NRF2 downstream target genes *HMOX1* and *NQO1* (Sachdeva et al., 2014; Zhao et al., 2019) was analyzed via qRT-

PCR. *NQO1* was chosen as a second antioxidant gene alongside *HMOX1*, which had revealed increased mRNA expression upon oxidative stress in preliminary experiments.

Subsequent to treatment with 0 mM and 0.5 mM SI for 24 h in two independent experiments, three high risk and four low risk hiPSC-RPE cell lines were analyzed regarding *HMOX1* and *NQO1* expression. Treatment with 0.5 mM SI induced transcription of both genes in all cell lines compared to control treatment (0 mM SI), of which all upregulations were statistically significant except for *HMOX1* mRNA expression in cell line H3. *HMOX1* mRNA expression was elevated to 2.97 (± 0.60) in H1, to 1.44 (± 0.47) in H3, to 3.35 (± 0.96) in H4, to 2.64 (± 0.91) in L1, to 2.20 (± 0.62) in L2, to 2.83 (± 0.77) in L3 and to 1.81 (± 0.66) in L4 (**Figure 8 A**). *NQO1* mRNA expression was increased to 12.20 (± 2.95) in H1, to 15.50 (± 4.18) in H3, to 13.13 (± 3.06) in H4, to 15.42 (± 2.89) in L1, to 9.80 (± 2.45) in L2, to 17.00 (± 5.67) in L3 and to 14.46 (± 4.95) in L4 (**Figure 8 B**). In conclusion, acute oxidative stress with SI evidently induced *NQO1* transcription more strongly than *HMOX1* transcription.

High risk and low risk cell lines did not show statistically significant differences, neither in *HMOX1* nor *NQO1* mRNA expression after treatment with 0.5 mM SI. *HMOX1* mRNA expression was increased to 2.59 (± 1.01) in high risk cell lines and to 2.37 (± 0.46) in low risk cell lines ($p = 0.63$) (**Figure 8 C**). *NQO1* mRNA expression was raised to 13.61 (± 1.7) in high risk cell lines and to 14.17 (± 3.10) in low risk cell lines ($p = 0.86$) (**Figure 8 D**).

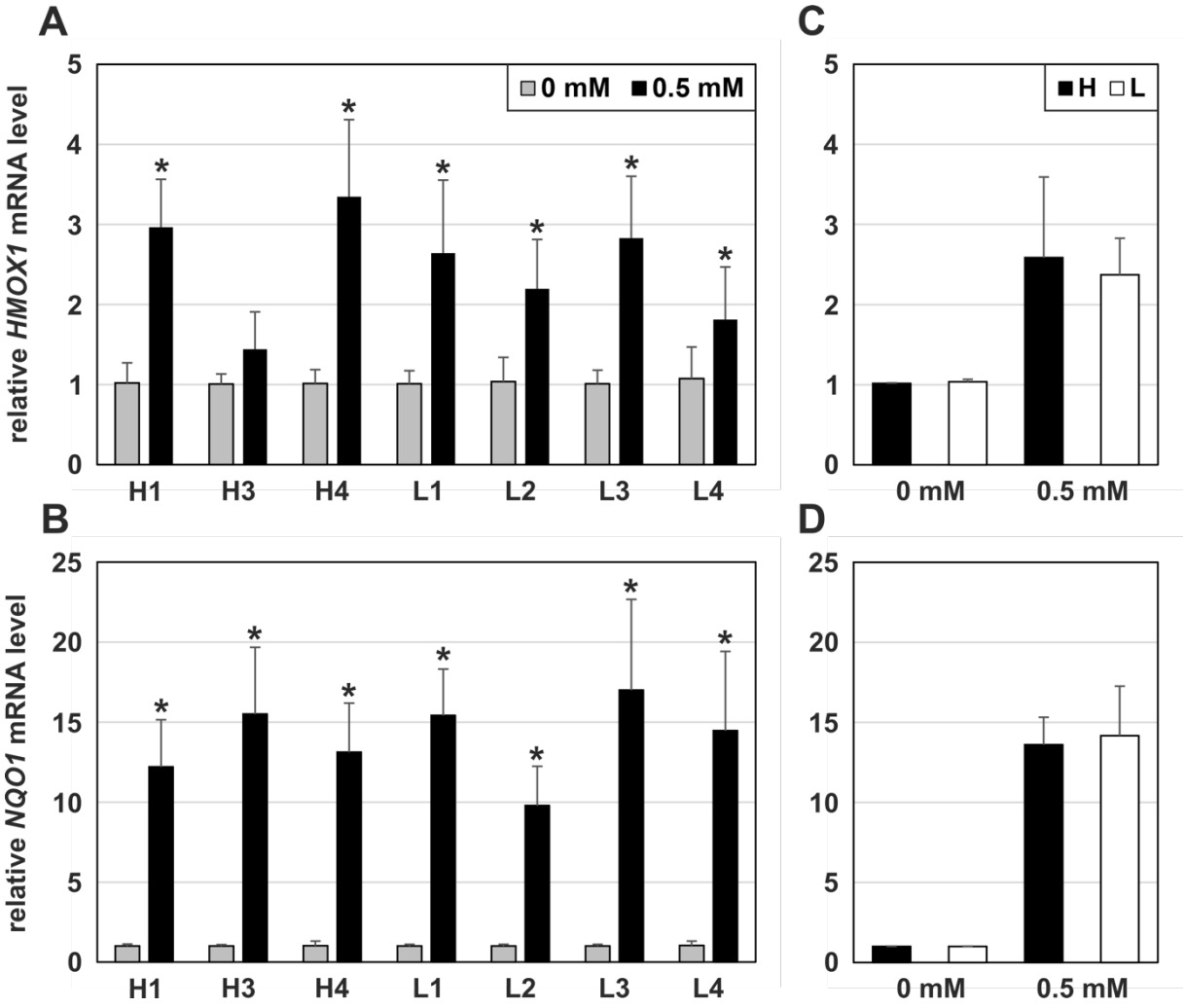

Figure 8: Influence of acute oxidative stress with SI on relative mRNA expression of *HMOX1* and *NQO1* in hiPSC-RPE cells

Three high risk (H1, H3, H4) and four low risk (L1, L2, L3, L4) hiPSC-RPE cell lines were treated with 0 mM or 0.5 mM SI for 24 h in two independent experiments. mRNA expression of *HMOX1* (**A**) and *NQO1* (**B**) was determined via qRT-PCR. Expression levels were normalized to reference gene *HPRT1*, then calibrated against the control (0 mM SI). Data are presented as means + SD (n = 8). Statistical significance (*: $p < 0.05$) was determined with a Wilcoxon Test.

High risk (H) and low risk (L) hiPSC-RPE cell lines were compared regarding their mRNA expression levels of *HMOX1* (**C**) and *NQO1* (**D**) under acute oxidative stress with SI (0.5 mM SI). Means and SD of the individual means of the cell lines were taken from the data shown in (A) or (B), respectively. Data are presented as means + SD (n = 3 for H, n = 4 for L). Statistical significance (*: $p < 0.05$) was determined with a Wilcoxon Test.

4.2.4 Increased HMOX1 and NQO1 Protein Expression in hiPSC-RPE Cells upon 24 h SI Treatment

After showing that hiPSC-RPE cells respond to acute oxidative stress with SI with increased *HMOX1* and *NQO1* mRNA expression, changes in expression also needed to be verified on the protein level. Four high risk and four low risk hiPSC-RPE cell lines were treated with 0.5 mM SI for 24 h in two independent experiments. Subsequently, proteins from cell lysates were analyzed via Western blot with antibodies against HMOX1 and NQO1 as well as ACTB as a loading control. As visualized in HMOX1 (28 kDa) and NQO1 (29 kDa) immunostainings, cells

incubated with 0.5 mM SI exhibited more intense staining than cells under control treatment (0 mM SI) (**Figure 9**). Densitometric quantification of signals from six replicates was performed in Image Studio. In all cell lines, HMOX1 as well as NQO1 protein expression was significantly increased in SI-treated cells compared to untreated controls. HMOX1 expression was increased to 3.81 (± 1.35) in H1, to 2.17 (± 1.25) in H2, to 1.87 (± 0.48) in H3, to 3.05 (±1.00) in H4, to 5.43 (± 4.45) in L1, to 4.41 (± 1.10) in L2, to 4.04 (± 2.75) in L3 and to 2.20 (± 1.06) in L4 (**Figure 9 A**). NQO1 expression values were raised to 14.42 (± 15.14) in H1, to 8.90 (± 7.48) in H2, to 11.52 (± 5.84) in H3, to 7.24 (± 3.13) in H4, to 7.26 (± 2.35) in L1, to 5.04 (± 1.05) in L2, to 11.28 (± 7.33) in L3 and to 6.52 (± 2.61) in L4 (**Figure 9 B**). Contrasting HMOX1 and NQO1 protein expression across all cell lines, the trend seen on mRNA level of NQO1 expression being upregulated more strongly than HMOX1 expression under acute SI treatment could be revealed on protein level as well.

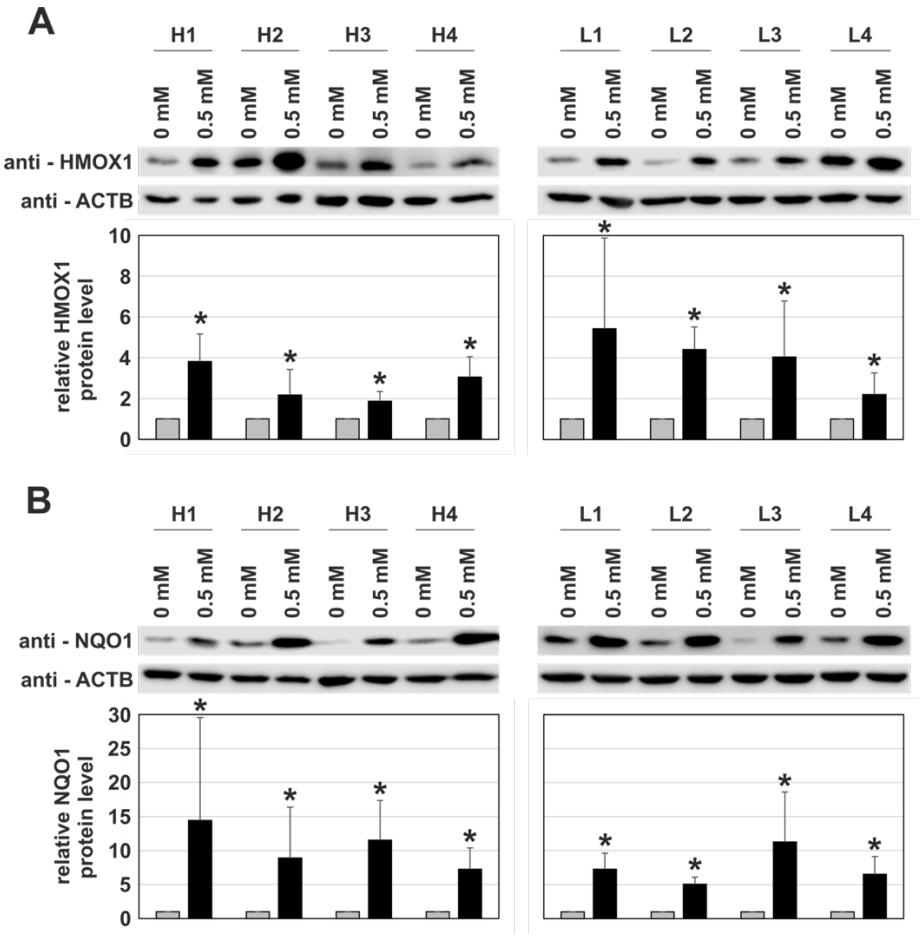

Figure 9: Influence of acute oxidative stress with SI on relative protein expression of HMOX1 and NQO1 in hiPSC-RPE cells

Four high risk (H1, H2, H3, H4) and four low risk (L1, L2, L3, L4) hiPSC-RPE cell lines were treated with 0 mM or 0.5 mM SI for 24 h in two independent experiments. Protein expression of HMOX1 (**A**) and NQO1 (**B**) was determined via Western blot analysis. ACTB was included as loading control. Representative immunoblots for 6 replicates are shown. For densitometric analysis of the bands, signal intensities were quantified in Image Studio. HMOX1 and NQO1 signal values were normalized to ACTB values and then calibrated against the control (0 mM SI). Data are presented as means + SD (n = 6). Statistical significance (*: $p < 0.05$) was determined with a Wilcoxon Test.

Comparing high and low risk cell lines in their responses to acute oxidative stress, HMOX1 expression was higher in low risk cell lines (4.02 (± 1.35)) than in high risk cell lines (2.73 (± 0.88)) (p = 0.17) (**Figure 10 A**), whereas NQO1 expression was higher in high risk cell lines (10.52 (± 3.14)) than in low risk cell lines (7.53 (± 2.67)) (p = 0.20) (**Figure 10 B**). However, these differences did not reach statistical significance.

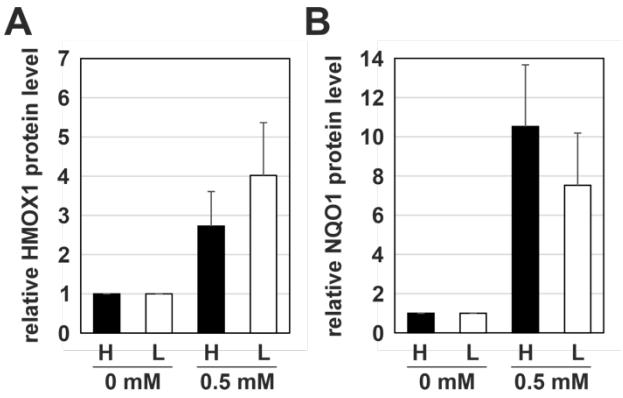

Figure 10: Comparison of relative HMOX1 and NQO1 protein expression in high and low risk cell lines in response to acute oxidative stress with SI

High risk (H) and low risk (L) hiPSC-RPE cell lines were compared regarding protein expression of HMOX1 (**A**) and NQO1 (**B**) under acute oxidative stress with SI (0.5 mM SI). Means and SD of the individual means of the cell lines were taken from the data shown in Figure 9 (A) or (B), respectively. Data are presented as means + SD (n = 4 for H, n = 4 for L). Statistical significance (*: $p < 0.05$) was determined with a two-tailed Student's T-Test.

4.3 Establishing Experimental Conditions for Chronic Chemical Oxidative Stress with SI

4.3.1 Influence of 72 h Exposure to 0.05 mM SI on mRNA Expression of *HMOX1* and *NQO1* in hiPSC-RPE Cells

To adopt a more physiological and therefore chronic exposure to oxidative stress, hiPSC-RPE cells were treated with SI for three days, replacing the media every 24 h. Based on the concentration of 0.5 mM SI employed in 24 h experiments, a concentration of 0.05 mM SI was selected for analyzing mRNA expression of *HMOX1* and *NQO1*. A media control with regular hiPSC-RPE cell culture medium was included to test whether change of media to cell culture medium without KOSR (0 mM), as used for SI solutions, would have an effect on mRNA expression in the examined genes due to KOSR deprivation for 72 h. KOSR depletion for three days left mRNA expression of both *HMOX1* and *NQO1* unaffected (**Figure 11**), which is a prerequisite for comparability with 24 h exposure to SI. As treatment with 0.05 mM SI hardly influenced *HMOX1* mRNA expression (**Figure 11 A**) and only slightly increased *NQO1* mRNA expression (**Figure 11 B**) in the first experiment, it could be concluded that higher concentrations of SI would be necessary to discover an effect resulting from the oxidative stress in the three day experiments.

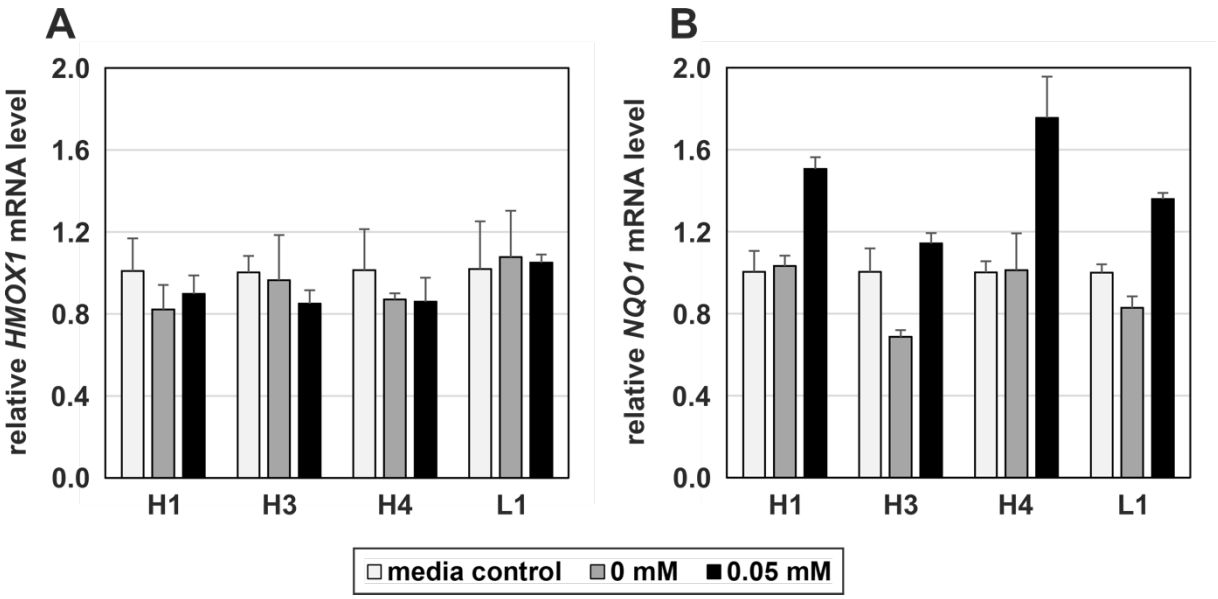

Figure 11: Influence of 72 h exposure to 0.05 mM SI on relative mRNA expression of *HMOX1* and *NQO1* in hiPSC-RPE cells

Three high risk (H1, H3, H4) and one low risk (L1) hiPSC-RPE cell line were treated with regular cell culture medium (media control), 0 mM or 0.05 mM SI for 72 h, replacing solutions every 24 h. mRNA expression of *HMOX1* (**A**) and *NQO1* (**B**) was determined via qRT-PCR. Expression levels were normalized to *HPRT1*, then calibrated against the media control. Data are presented as means + SD (n = 4).

4.3.2 Quantification of Cytotoxicity after Treatment with Higher Concentrations of SI

Since a rather low concentration of 0.05 mM SI did not influence *HMOX1* and *NQO1* mRNA expression after three days of treatment, the experimental conditions for a chronic stress setting needed to be reconsidered. It was necessary to explore higher concentrations, which ought to be high enough to cause detectable oxidative stress responses without causing measurable cytotoxicity in the hiPSC-RPE cells. Concentrations of 0.125 mM and 0.25 mM SI seemed natural to test for a 72 h period as 0.5 mM was the concentration utilized in 24 h experiments. Before using these higher concentrations in chronic oxidative stress experiments, their cytotoxic effect needed to be determined first. In two independent experiments, hiPSC-RPE cells were incubated with 0 mM, 0.125 mM and 0.25 mM SI for 72 h as well as 1.5 mM SI as positive control, changing solutions every 24 h. Subsequently, LDH assays were executed in the supernatants. Treatment with 0.125 mM and 0.25 mM SI showed no cytotoxic effects, but instead a slight decrease in cytotoxicity in all cell lines, which was even statistically significant for four cell lines (H2, L2, L3, L4) after exposure to 0.25 mM SI. In contrast, treatment with 1.5 mM SI caused a significant increase in cytotoxicity for two cell lines (H2, L2) as well as a clear upward trend for all other cell lines with an increase in cytotoxicity between 2.90 fold (± 1.12) and 10.10 fold (± 2.22) as compared to the controls (**Figure 12 A**). High and low risk cell lines did not display significant differences in their cytotoxic responses to treatment

with any of the examined concentrations (0.125 mM SI: p = 0.88, 0.25 mM SI: p = 0.47, 1.5 mM SI: p = 0.40) (**Figure 12 B**).

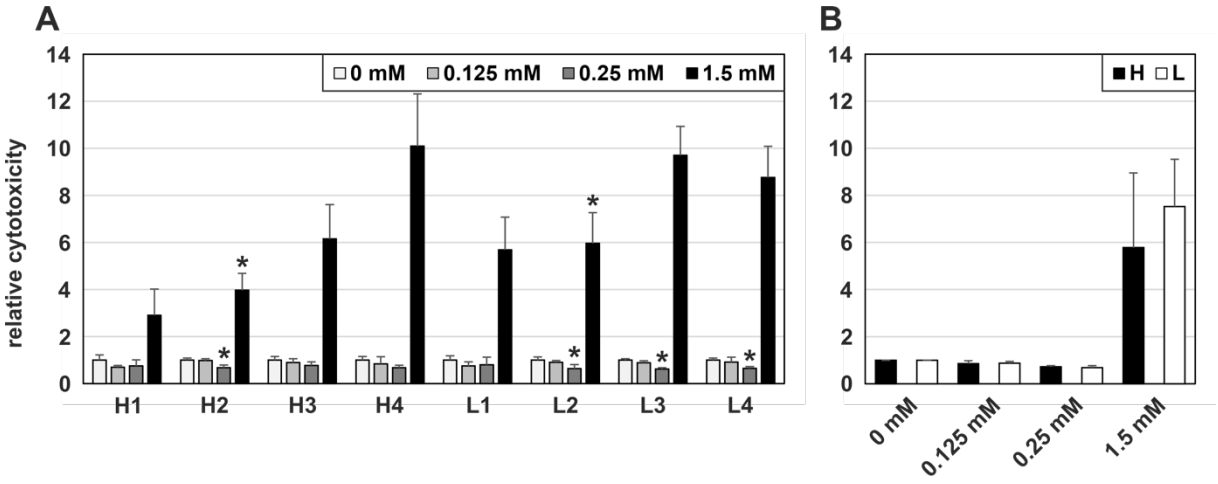

Figure 12: Effect of chronic oxidative stress with SI on cytotoxicity in hiPSC-RPE cells
(**A**) Four high risk (H1, H2, H3, H4) and four low risk (L1, L2, L3, L4) hiPSC-RPE cell lines were incubated with 0 mM, 0.125 mM, 0.25 mM and 1.5 mM SI for 72 h in two independent experiments, changing solutions every 24 h. After 72 h, cytotoxicity was quantified by measuring LDH release in the supernatants. After adjusting for media background controls for the respective concentrations, measurement values were calibrated against the control (0 mM SI). Data are presented as means + SD (n = 6-8). Statistical significance (*: $p < 0.05$) was determined with the Kruskal Wallis Test with post hoc Dunn's Multiple Comparison Test and multiple testing correction using the Benjamini-Hochberg method. (**B**) High risk (H) and low risk (L) hiPSC-RPE cell lines were compared in their cytotoxic response to chronic oxidative stress with 0.125 mM, 0.25 mM and 1.5 mM SI using the data from experiments described in (A) by taking the means and SD of the individual means of the cell lines. Data are presented as means + SD (n = 4 for H, n = 4 for L). Statistical significance (*: $p < 0.05$) was determined with a two-tailed Student's T-Test.

4.4 Effects of Chronic Chemical Oxidative Stress Induction with SI on hiPSC-RPE Cells

4.4.1 Verification of RPE Cell Morphology and Monolayer Integrity after 72 h SI Treatment

Immunocytochemical analysis of tight junction protein ZO-1 after exposure to 0 mM, 0.125 mM and 0.25 mM SI for 72 h served as quality control of the hiPSC-RPE cells under chronic oxidative stress conditions. For comparability, it was important to verify that all cell lines maintained their morphology and an intact monolayer after chronic treatment with given concentrations of SI. As visualized by continuous ZO-1 expression, all hiPSC-RPE cells were of similar size, exhibited the typical hexagonal RPE cell shape and formed an intact monolayer. No visible differences could be seen amongst cell lines or between high and low risk cell lines. Additionally, cell morphology and the monolayer were not impaired upon application of chronic oxidative stress with 0.125 mM and 0.25 mM SI (**Figure 13**). Minor changes in L1 were most likely handling artifacts.

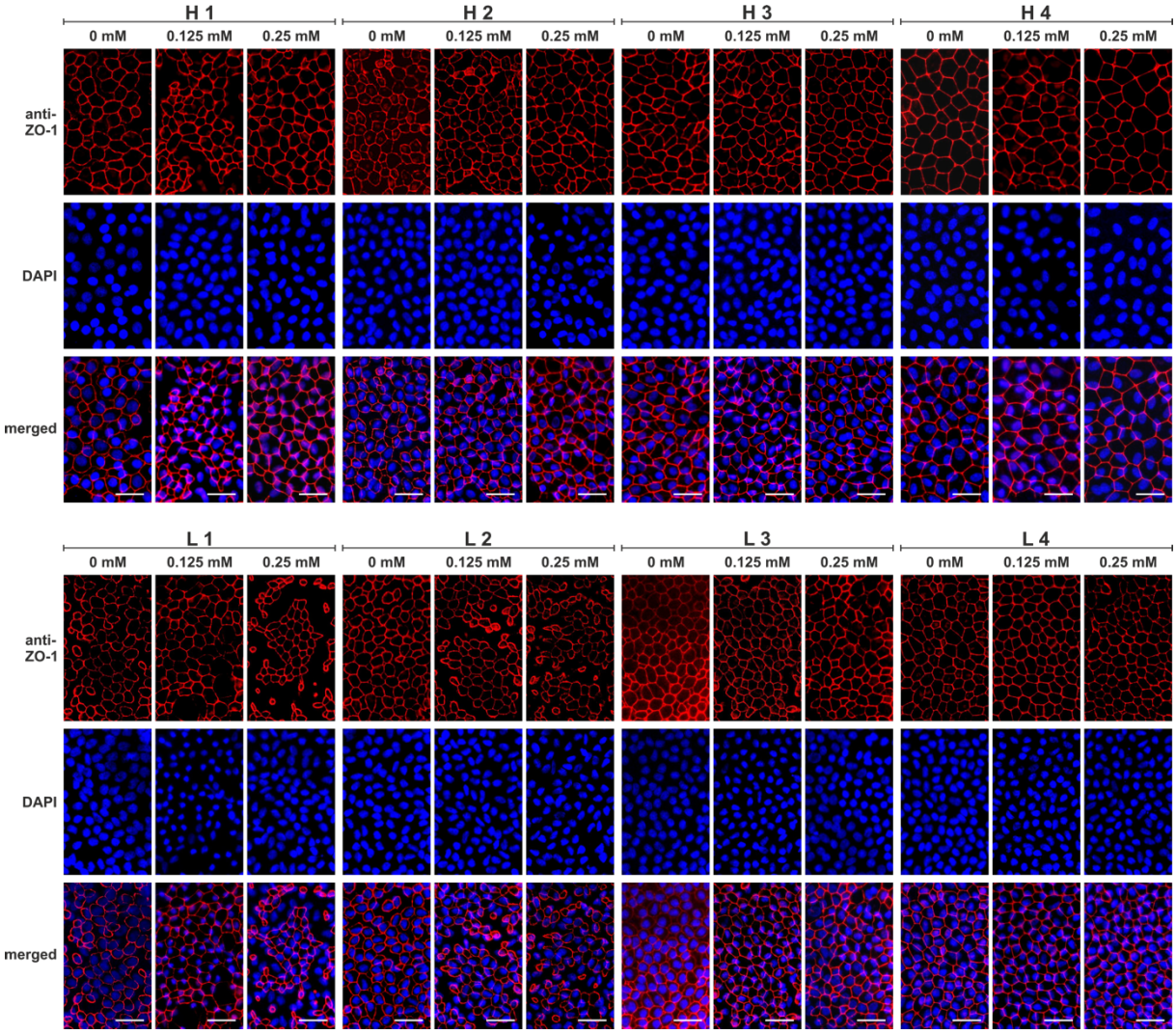

Figure 13: Verification of hiPSC-RPE cell quality regarding morphology and monolayer integrity after chronic oxidative stress with SI

Four high risk (H1, H2, H3, H4) and four low risk (L1, L2, L3, L4) hiPSC-RPE cell lines were treated with 0 mM, 0.125 mM or 0.25 mM SI for 72 h, replacing solutions every 24 h. In subsequent immunocytochemical analysis, the tight junction marker ZO-1 (red) was labelled with an anti-ZO-1 antibody and nuclei were stained with DAPI (blue). Images were taken in 40x magnification under the fluorescence microscope. Scale bars: 25 µm.

4.4.2 TEER Measurements as Quality Control for RPE Monolayer Barrier Function

To further investigate an influence of chronic oxidative stress with SI on the barrier function of hiPSC-RPE cells, TEER was measured after treatment with 0 mM, 0.125 mM and 0.25 mM SI for 72 h in two independent experiments. Three cell lines (H2, H3, L4) displayed significantly higher values for cells treated with 0.125 mM and 0.25 mM SI, whereas cell line L3 showed only significantly higher values after 0.125 mM SI treatment, which were decreased in 0.25 mM SI-treated cells. Cell line H4 had significantly lower values for 0.25 mM SI-treated cells. The remaining cell lines (H1, L1, L2) showed only insignificant TEER disparities, with values being slightly higher for 0.125 mM SI-treated cells than after treatment with 0 mM and 0.25 mM SI. Cell line H4 exhibited substantially higher values for all conditions in comparison to the

other cell lines (**Figure 14 A**). Overall, no general direction of change in TEER values between the individual cell lines was revealed, implying that treatment with 0.125 mM and 0.25 mM SI for 72 h does not affect RPE barrier function, as concluded for acute oxidative stress induction with 0.5 mM SI as well. There were no significant differences in TEER when contrasting high and low risk cell lines for each condition (0 mM SI: p = 0.45, 0.125 mM SI: p = 0.41, p = 0.25: p = 0.36). As in TEER measurements after acute oxidative stress with SI, low risk cell lines generally had lower TEER values than high risk cell lines, irrespective of treatment (**Figure 14 B**).

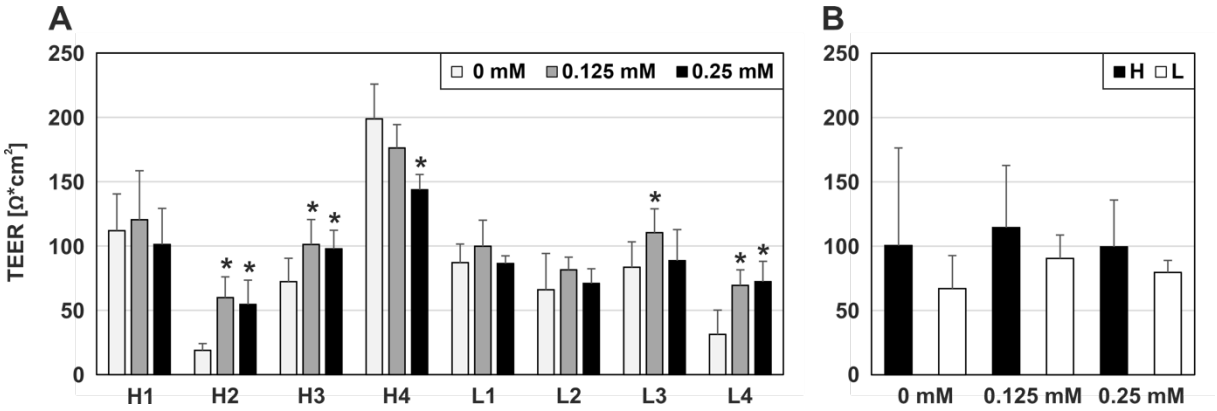

Figure 14: Influence of chronic oxidative stress with SI on TEER in hiPSC-RPE cells
(**A**) Four high risk (H1, H2, H3, H4) and four low risk (L1, L2, L3, L4) hiPSC-RPE cell lines were treated with 0 mM, 0.125 mM or 0.25 mM SI for 72 h in two independent experiments, replacing solutions every 24 h. After 72 h, TEER measurements were taken. After adjusting to blank resistance values, measurement values were multiplied with the surface area of the filter membrane, obtaining TEER values in the dimension Ω*cm^2. Data are presented as means + SD (n = 8). Statistical significance (*: $p < 0.05$) was determined with the Kruskal Wallis Test with post hoc Dunn's Multiple Comparison Test and multiple testing correction using the Benjamini-Hochberg method. (**B**) The TEER values of high risk (H) and low risk (L) hiPSC-RPE cell lines were compared in stressed (0.125 mM and 0.25 mM SI) and unstressed (0 mM SI) conditions. Means and SD of the individual means of the cell lines were taken from the data shown in (A). Data are presented as means + SD (n = 4 for H, n = 4 for L). Statistical significance (*: $p < 0.05$) was determined with a two-tailed Student's T-Test.

4.4.3 Increased mRNA Expression of Antioxidant Genes *HMOX1* and *NQO1* in hiPSC-RPE Cells upon 72 h SI Treatment

After ensuring that chronic oxidative stress with SI did not damage hiPSC-RPE cell morphology and their monolayer integrity, transcription of the antioxidant genes *HMOX1* and *NQO1* was investigated, since their expression was shown to be induced after acute oxidative stress with SI. In two independent experiments, four high risk and four low risk cell lines were exposed to 0 mM, 0.125 mM and 0.25 mM SI for 72 h, changing solutions every 24 h.

Subsequent qRT-PCR analysis revealed a dose-dependent increase in *HMOX1* and *NQO1* mRNA expression in all cell lines. *HMOX1* transcription was significantly upregulated in all cell lines after 0.25 mM SI treatment and in three cell lines (H2, H4, L1) after 0.125 mM SI treatment compared to controls (0 mM SI). 0.125 and 0.25 mM SI treatment increased *HMOX1* mRNA expression to 1.26 (± 0.26) and 1.76 (± 0.68) in H1, to 1.61 (± 0.29) and 1.99 (± 0.45) in H2, to

1.17 (± 0.20) and 1.43 (± 0.21) in H3, to 1.40 (± 0.22) and 1.99 (±0.38) in H4, to 1.53 (± 0.20) and 1.72 (± 0.20) in L1, to 1.46 (± 0.31) and 1.97 (± 0.34) in L2, to 1.25 (± 0.17) and 2.24 (± 0.39) in L3 and to 1.43 (± 0.34) and 2.28 (± 0.69) in L4, respectively (**Figure 15 A**). In all cell lines, *NQO1* transcription was statistically significantly increased in both 0.125 mM and 0.25 mM SI-treated cells compared to controls. 0.125 and 0.25 mM SI treatment increased *NQO1* mRNA expression to 4.21 (± 0.95) and 7.33 (± 0.85) in H1, to 2.98 (± 0.36) and 6.37 (± 0.38) in H2, to 4.97 (± 0.41) and 9.16 (± 0.94) in H3, to 5.77 (± 0.69) and 9.38 (± 0.95) in H4, to 6.71 (± 1.09) and 9.22 (± 1.53) in L1, to 4.43 (± 0.40) and 7.94 (± 0.50) in L2, to 4.89 (± 0.43) and 9.40 (± 0.71) in L3 and to 5.85 (± 0.89) and 9.80 (± 1.18) in L4, respectively (**Figure 15 B**). In summary, *NQO1* expression was higher than *HMOX1* expression after 0.125 mM and 0.25 mM SI treatment, which was in line with and in similar magnitudes as seen for 24 h treatment with 0.5 mM SI.

When comparing cell lines by risk score, low risk cell lines exhibited slightly higher values under chronic oxidative stress with SI for both *HMOX1* and *NQO1* mRNA expression as compared to high risk cell lines, but differences were not statistically significant. *HMOX1* mRNA was upregulated to 1.36 (± 0.19) in high risk cell lines and to 1.42 (± 0.12) in low risk cell lines after 0.125 mM SI treatment ($p = 0.69$), and increased to 1.79 (± 0.26) in high risk cell lines and to 2.05 (± 0.26) in low risk cell lines after 0.25 mM SI treatment ($p = 0.49$) (**Figure 15 C**). *NQO1* mRNA expression was increased to 4.48 (± 1.19) in high risk cell lines and to 5.47 (± 1.02) in low risk cell lines after 0.125 mM SI treatment ($p = 0.34$), and raised to 8.06 (± 1.45) in high risk cell lines and to 9.09 (± 0.80) in low risk cell lines after 0.25 mM SI treatment ($p = 0.20$) (**Figure 15 D**).

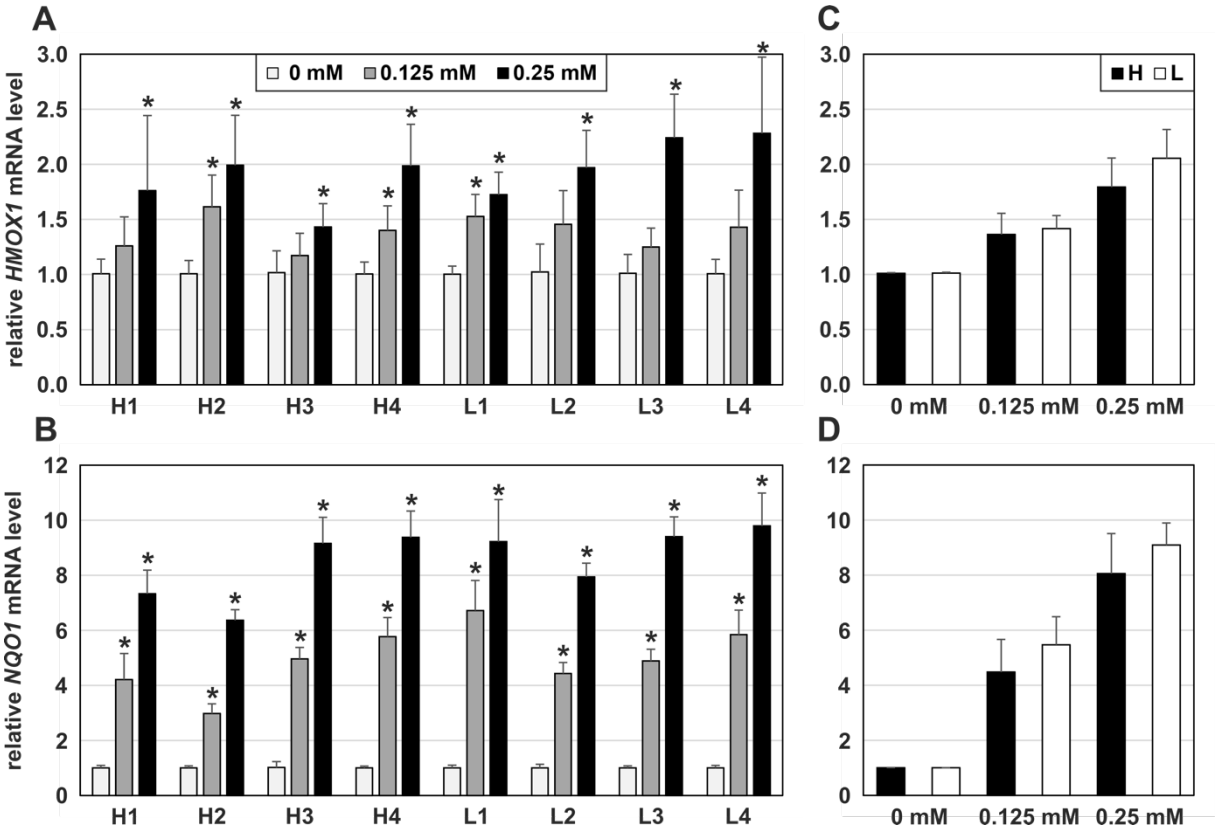

Figure 15: Influence of chronic oxidative stress with SI on relative mRNA expression of *HMOX1* and *NQO1* in hiPSC-RPE cells

Four high risk (H1, H2, H3, H4) and four low risk (L1, L2, L3, L4) hiPSC-RPE cell lines were treated with 0 mM, 0.125 mM or 0.25 mM SI for 72 h in two independent experiments, changing solutions every 24 h. mRNA expression of *HMOX1* (**A**) and *NQO1* (**B**) was determined via qRT-PCR. Expression levels were normalized to reference gene *HPRT1*, then calibrated against the control (0 mM SI). Data are presented as means + SD (n = 8). Statistical significance (*: $p < 0.05$) was determined with the Kruskal Wallis Test with post hoc Dunn's Multiple Comparison Test and multiple testing correction using the Benjamini-Hochberg method.

High risk (H) and low risk (L) hiPSC-RPE cell lines were compared regarding their mRNA expression levels of *HMOX1* (**C**) and *NQO1* (**D**) under chronic oxidative stress with SI (0.125 mM and 0.25 mM SI). Means and SD of the individual means of the cell lines were taken from the data shown in (A) or (B), respectively. Data are presented as means + SD (n = 4 for H, n = 4 for L). Statistical significance (*: $p < 0.05$) was determined with a Wilcoxon Test.

4.4.4 Increased HMOX1 and NQO1 Protein Expression in hiPSC-RPE Cells upon 72 h SI Treatment

Since *HMOX1* and *NQO1* mRNA were upregulated in hiPSC-RPE cells under chronic oxidative stress with SI, this effect was to be confirmed for protein expression. After treating four high and four low risk cell lines with 0 mM, 0.125 mM and 0.25 mM SI for 72 h in two independent experiments, protein samples were subjected to Western blot analysis to examine protein expression of HMOX1 and NQO1. ACTB was stained as a loading control. Intensities of both HMOX1 (28 kDa) and NQO1 (29 kDa) molecular weight species were noticeably increased for increasing concentrations of SI (**Figure 16**). Signals of four replicates were quantified by densitometric analysis executed in Image Studio. In the majority of cell lines, protein expression was dose-dependent and elevated compared to controls (0 mM SI). Statistically significant upregulation in HMOX1 protein expression was detected for 0.25 mM SI treatment

in four cell lines (H3, H4, L2, L3) (**Figure 16 A**), but a clear trend was visible for the other cell lines as well. NQO1 protein expression was significantly increased in 0.25 mM SI-treated cells in six cell lines (H1, H2, H3, H4, L1, L3) as well as in cell line L1 upon 0.125 mM SI treatment (**Figure 16 B**). Across all cell lines, levels of protein of NQO1 were higher than those of HMOX1 under both 0.125 mM and 0.25 mM SI treatment, which is consistent with and in a similar magnitude to the differences detected between *NQO1* and *HMOX1* mRNA expression. Additionally, the differences in upregulation of NQO1 and HMOX1 protein were in line with the differences in protein expression previously observed after 24 h SI treatment.

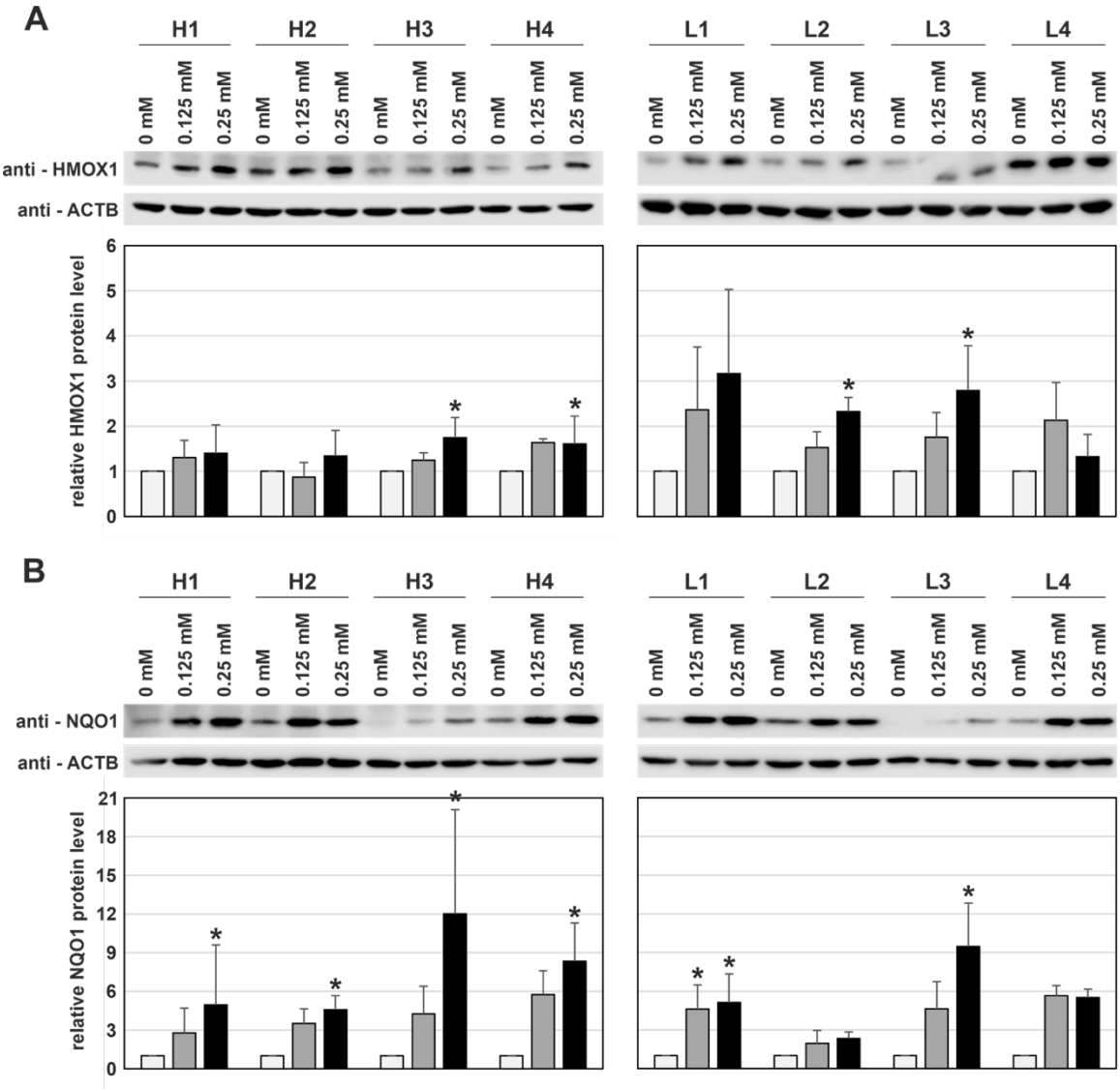

Figure 16: Influence of chronic oxidative stress with SI on relative protein expression of HMOX1 and NQO1 in hiPSC-RPE cells

Four high risk (H1, H2, H3, H4) and four low risk (L1, L2, L3, L4) hiPSC-RPE cell lines were treated with 0 mM, 0.125 mM or 0.25 mM SI for 72 h in two independent experiments, replacing solutions every 24 h. Protein expression of HMOX1 (**A**) and NQO1 (**B**) was determined via Western blot analysis. ACTB was included as loading control. Representative immunoblots for 4 replicates are shown. For densitometric analysis of the bands, signal intensities were quantified in Image Studio. HMOX1 and NQO1 signal values were normalized to ACTB values and then calibrated against the control (0 mM SI). Data are presented as means + SD (n = 4). Statistical significance (*: $p < 0.05$) was determined with the Kruskal Wallis Test with post hoc Dunn's Multiple Comparison Test and multiple testing correction using the Benjamini-Hochberg method.

Between high and low risk cell lines, similar trends in protein expression were observed as already seen in protein analysis after acute oxidative stress induction. Chronic oxidative stress with both 0.125 mM and 0.25 mM SI induced higher HMOX1 protein expression in low risk cell lines (1.94 (± 0.37) and 2.40 (± 0.80)) than in high risk cell lines (1.26 (± 0.31) and 1.52 (± 0.19)) (**Figure 17 A**), consistent with the trends observed previously for acute oxidative stress with SI. The difference between high and low risk cell lines under 0.125 mM SI treatment was statistically significant (p = 0.03), but not under treatment with 0.25 mM SI (p = 0.11). NQO1 protein expression in 0.125 mM SI-treated cells was slightly higher in low risk cell lines (4.22 (± 1.58) than in high risk cell lines (4.07 (± 1.28)) (p = 0.89). Treatment with 0.25 mM SI led to higher NQO1 protein expression in high risk cell lines (7.47 (± 3.47)) than in low risk cell lines (5.61 (± 2.93)) (p = 0.44) (**Figure 17 B**), indicating the same tendency as seen after acute oxidative stress with 0.5 mM SI.

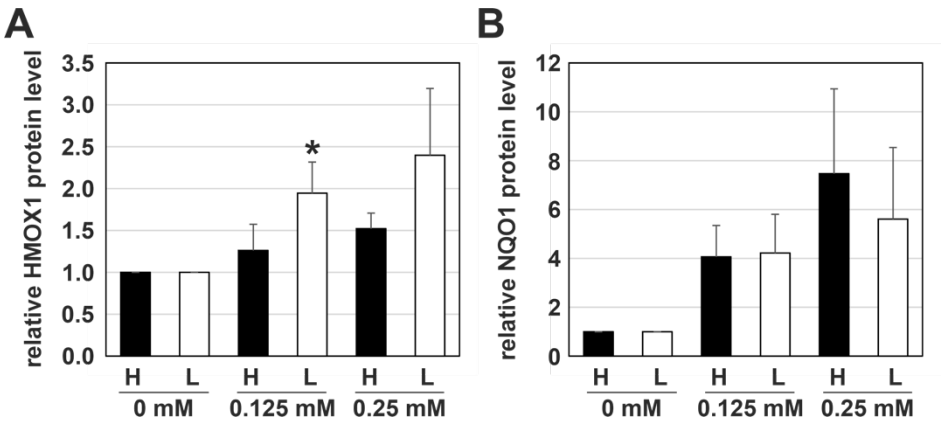

Figure 17: Comparison of relative HMOX1 and NQO1 protein expression in high and low risk cell lines in response to chronic oxidative stress with SI

High risk (H) and low risk (L) hiPSC-RPE cell lines were compared regarding their protein expression levels of HMOX1 (**A**) and NQO1 (**B**) under chronic oxidative stress with SI (0.125 mM and 0.25 mM SI). Means and SD of the individual means of the cell lines were taken from the data shown in Figure 16 (A) or (B), respectively. Data are presented as means + SD (n = 4 for H, n = 4 for L). Statistical significance (*: $p < 0.05$) was determined with a two-tailed Student's T-Test.

4.5 Establishing Experimental Conditions for Acute Physical Oxidative Stress by BL Irradiation

Like SI, BL irradiation was used as a stressor the hiPSC-RPE cell lines studied in this thesis had never been exposed to before. Therefore, the experimental conditions for BL treatment experiments needed to be established. Studying and quantifying the oxidative effect of BL, a physical stressor, on the hiPSC-RPE cells required careful planning in advance and fine-tuning of the experimental setup to keep it reproducible across the experiments. After installing the Blue Light LED Light Source into an incubator, hiPSC-RPE cells were exposed to various irradiation doses to work out the optimal duration of BL exposure for oxidative stress experiments.

4.5.1 Determining an Optimal Irradiation Duration for BL Experiments by Cell Viability Analysis

MTT assays for cell viability analysis were implemented to determine the optimal irradiation duration for BL exposure, which needed to be long enough to induce a detectable oxidative stress response in the hiPSC-RPE cells while not or little affecting cell viability.

In a first set of experiments, eight time points (1.5 h, 3 h, 6 h, 7.5 h, 9 h, 12 h, 18 h, 24 h) were tested based on cytotoxicity studies performed by Brandstetter and colleagues (Brandstetter et al., 2015) with the Blue Light LED Light Source, where 24 h of irradiation reportedly induced almost complete cytotoxicity in lipofuscin-loaded ARPE-19 cells. To this end, the regular cell culture medium was replaced with irradiation medium in irradiation as well as non-irradiation (control) plates to prevent phenol red from interfering with irradiation affecting the cells. Each 96-well plate contained three high risk (H1, H3, H4) and four low risk (L1, L2, L3, L4) cell lines, so they were in close proximity to one another. The eight irradiation plates were placed in the BL incubator at the same time, while control plates remained in a regular incubator. After the respective time periods, MTT assays were performed simultaneously in the irradiated plate and its corresponding non-irradiated control plate. In the evaluation, measurement values were calibrated against the respective non-irradiated controls. The combined measurements for all cell lines together are shown in **Figure 18**. The increase in cell viability after 3 h of irradiation is most likely due to measurement variability. Cell viability was significantly decreased after exposure to BL for 7.5 h and above. A strong reduction in cell viability was observed after exposure to 18 h and 24 h of BL, which reduced cell viability to 58.91 % and 19.07 %, respectively, compared to the corresponding non-irradiated control plates.

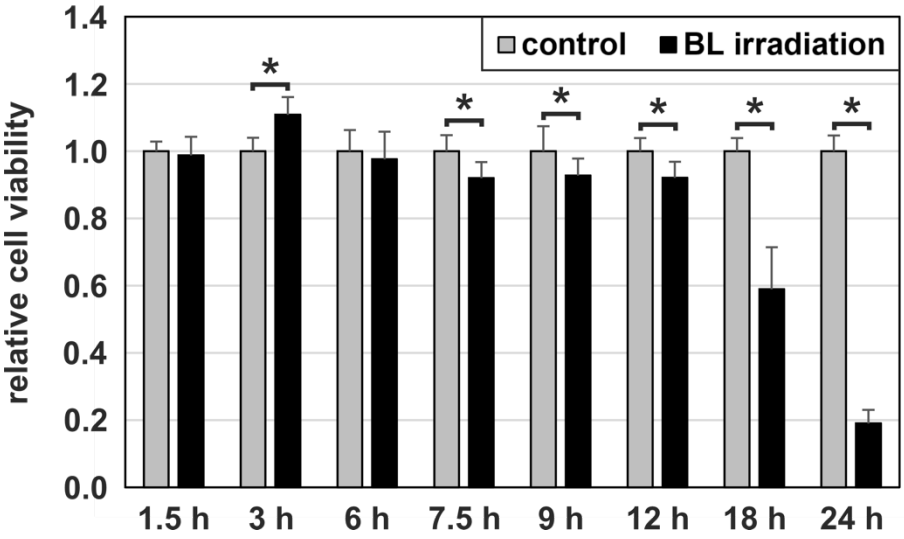

Figure 18: Influence of BL irradiation (1.5 h to 24 h) on cell viability in hiPSC-RPE cells
Three high risk (H1, H3, H4) and four low risk (L1, L2, L3, L4) hiPSC-RPE cell lines plated on 96-well plates were irradiated with BL for 1.5 h, 3 h, 6 h, 7.5 h, 9 h, 12 h, 18 h or 24 h. After the respective times of irradiation, cell viability was assessed in parallel in the irradiated plate and the corresponding non-irradiated plate (control) via MTT assay. Measurements were calibrated against the respective non-irradiated controls. Depicted are combined values

of the seven cell lines. Data are presented as means + SD (n = 28). Statistical significance (*: $p < 0.05$) was determined with the Kruskal Wallis Test with post hoc Dunn's Multiple Comparison Test and multiple testing correction using the Benjamini-Hochberg method.

In the next set of experiments, the experimental procedure for BL irradiation was reversed, aiming to exclude discrepancies resulting from performing the MTT assays at different time points. By adding the cell culture plates into the BL incubator one by one, the MTT assays and absorbance measurements after all irradiation times (12 h, 14 h, 16 h and 18 h) could take place at the same time. Measurements of the irradiated cells were calibrated against non-irradiated cells (0 h), for which the MTT assay was performed along with the others. Contrary to expectation, cell viability did not decrease dose-dependently in any of the eight cell lines examined (**Figure 19**). In all cell lines, exposure durations of 12 h and 16 h significantly reduced cell viability to approximately 45 to 65 %, whereas exposure durations of 14 h and 18 h reduced cell viability to approximately 65 to 85 %, which was not significant. This curious trend was confirmed in an identical independent experiment and led to the conclusion, that irradiance may vary between different positions inside the incubator, even with plates positioned as centrally under the LEDs as possible.

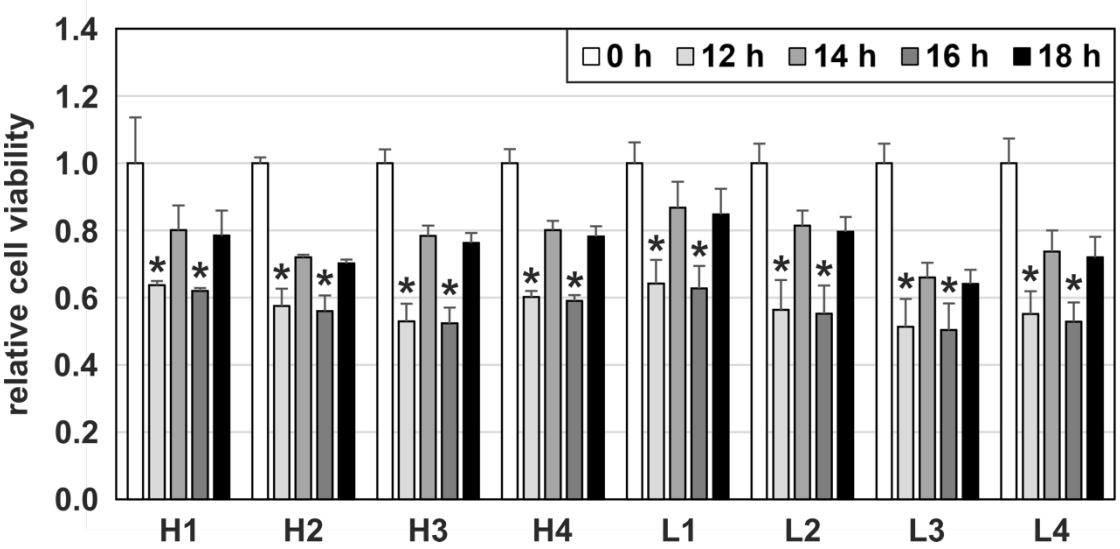

Figure 19: Influence of BL irradiation (12 h to 18 h) on cell viability in hiPSC-RPE cells
Four high risk (H1, H2, H3, H4) and four low risk (L1, L2, L3, L4) hiPSC-RPE cell lines plated on 96-well plates were irradiated with BL for 12 h, 14 h, 16 h or 18 h. After the respective times of irradiation, cell viability was assessed in all plates at the same time via MTT assay. Measurements were calibrated against a non-irradiated control (0 h). Data are presented as means + SD (n = 4). Statistical significance (*: $p < 0.05$) was determined with the Kruskal Wallis Test with post hoc Dunn's Multiple Comparison Test and multiple testing correction using the Benjamini-Hochberg method.

To test this hypothesis, cell viability was compared for plates irradiated for the same durations in different positions inside the incubator. Firstly, three plates, two of which were positioned to the left and right adjacent to a central plate directly below the LEDs were irradiated for 6 h. A

duration of 6 h was too low to affect cell viability for any of the positions compared to a non-irradiated control. Next, the same plate positions were tested for 9 h exposure in two independent experiments. A 9 h time period was considered to be worth testing, because 6 h of irradiation were too short to cause any effect on cell viability and 12 h of irradiation and above were shown to reduce cell viability in a previous experiment (**Figure 19**). All cell lines irradiated on the central plate displayed significantly reduced cell viability to between 31.68 to 52.64 % compared to the non-irradiated controls (0 h). Cells irradiated on the left and right from the central position showed a decrease in relative cell viability to approximately 80 to 95 %. Therefore, the hypothesis of inconsistent irradiation across the area of the incubator was confirmed and the radius for consistent irradiation was smaller than expected.

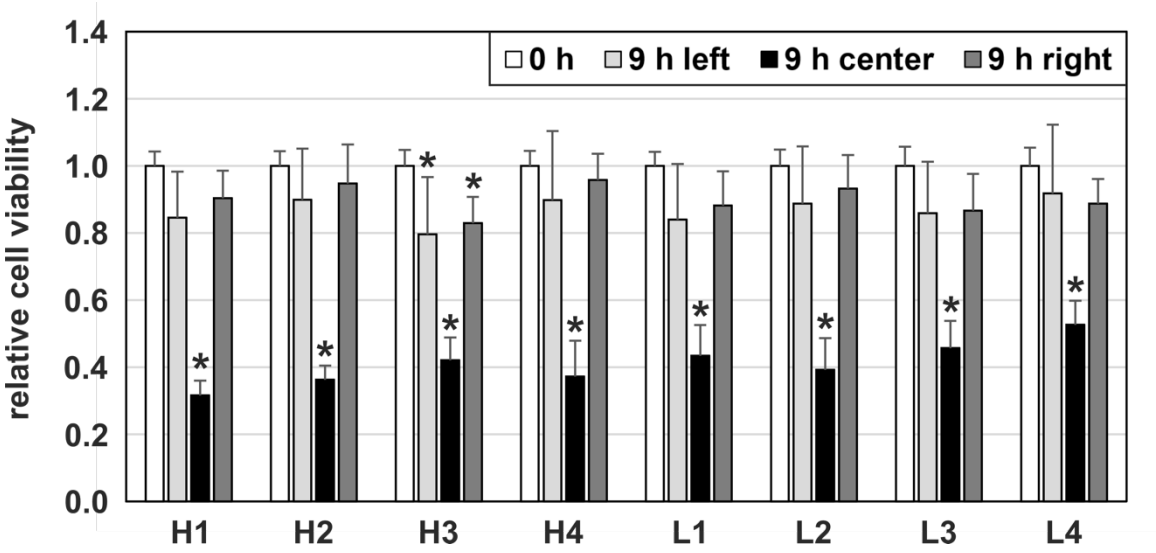

Figure 20: Influence of 9 h BL irradiation on cell viability in hiPSC-RPE cells in different positions to the LEDs

Four high risk (H1, H2, H3, H4) and four low risk (L1, L2, L3, L4) hiPSC-RPE cell lines plated on 96-well plates were irradiated with BL for 9 h in two independent experiments. One plate was positioned centrally under the LEDs and two plates were adjacently positioned to the left and right. After 9 h of irradiation, cell viability was assessed in the three plates at the same time via MTT assay. Measurements were calibrated against a non-irradiated control (0 h). Data are presented as means + SD (n = 8). Statistical significance (*: $p < 0.05$) was determined with the Kruskal Wallis Test with post hoc Dunn's Multiple Comparison Test and multiple testing correction using the Benjamini-Hochberg method.

4.5.2 Confirmation of Selected Irradiation Duration by Quantification of Cytotoxicity

After refining the irradiation time to 9 h, LDH assays were performed to confirm that this was the optimal duration for inducing an oxidative stress response in the hiPSC-RPE cells without causing cell death. After switching cell culture medium to irradiation medium, four high and four low risk hiPSC-RPE cell lines were treated with BL for 9 h in three independent experiments. Non-irradiated cells (0 h) were included as controls. After the 9 h time period, LDH released into the supernatant was measured. In all cell lines examined, treatment with 9 h BL irradiation did not lead to a significant increase in cytotoxicity compared to controls. A

statistically significant decrease to 0.71 (± 0.33) in cytotoxicity could be detected in cell line L4, while LDH release in all other cell lines was not affected by BL (**Figure 21 A**). No significant difference in cytotoxic response to treatment with 9 h BL irradiation was observed between high and low risk cell lines (p = 0.06) (**Figure 21 B**).

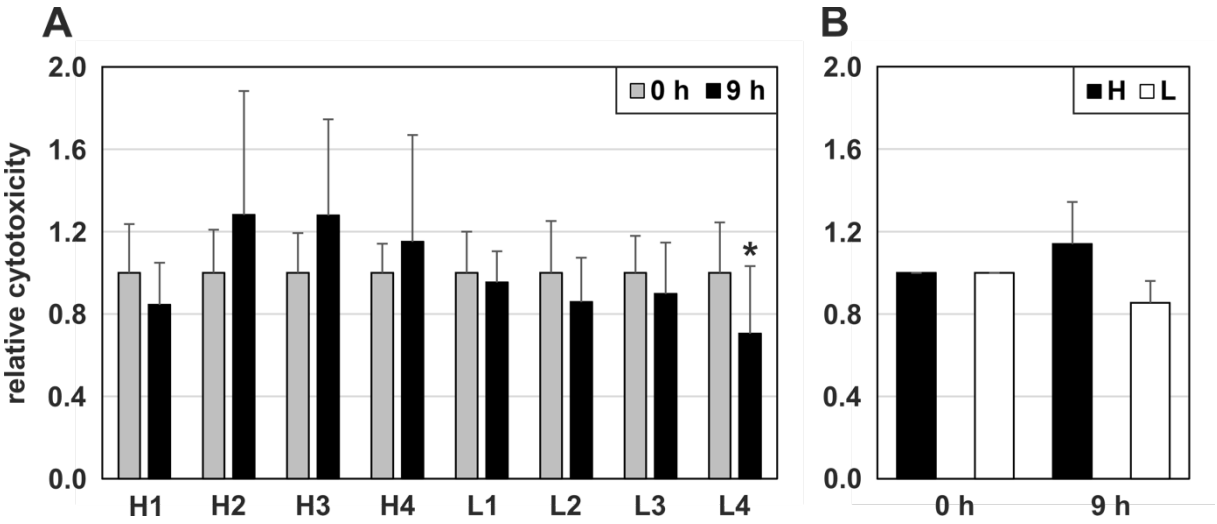

Figure 21: Effect of acute oxidative stress by BL irradiation on cytotoxicity in hiPSC-RPE cells
(**A**) Four high risk (H1, H2, H3, H4) and four low risk (L1, L2, L3, L4) hiPSC-RPE cell lines were irradiated with BL for 9 h in three independent experiments. Non-irradiated cells (0 h) served as controls. After 9 h, cytotoxicity was quantified by measuring LDH release in the supernatants. After adjusting for irradiation medium background controls, measurements were calibrated against the non-irradiated controls. Data are presented as means + SD (n = 9-11). Statistical significance (*: $p < 0.05$) was determined with a Wilcoxon Test. (**B**) High risk (H) and low risk (L) hiPSC-RPE cell lines were compared in their cytotoxic response to acute physical oxidative stress by 9 h of BL irradiation using the data from experiments described in (A) by taking the means and SD of the individual means of the cell lines. Data are presented as means + SD (n = 4 for H, n = 4 for L). Statistical significance (*: $p < 0.05$) was determined with a two-tailed Student's T-Test.

4.6 Effects of Acute Physical Oxidative Stress Induction by BL Irradiation on hiPSC-RPE Cells

4.6.1 Verification of RPE Cell Morphology and Monolayer Integrity after 9 h BL Irradiation

Immunocytochemical immunostaining of tight junction protein ZO-1 and DAPI Hoechst staining were performed as quality control of the hiPSC-RPE cell lines after treatment with the selected time of 9 h BL exposure as well as no BL exposure (0 h) for comparison. Potential alterations in cell shape or damage to the monolayer would influence comparability in further experiments and therefore would need to be revealed beforehand. In all cell lines analyzed and regardless of risk score, continuous ZO-1 expression marking the cell membranes revealed cells of characteristic cobblestone RPE cell morphology forming an uninterrupted single cell layer. In addition, it could be confirmed that 9 h BL exposure did not impact the RPE cell shape and monolayer integrity (**Figure 22**).

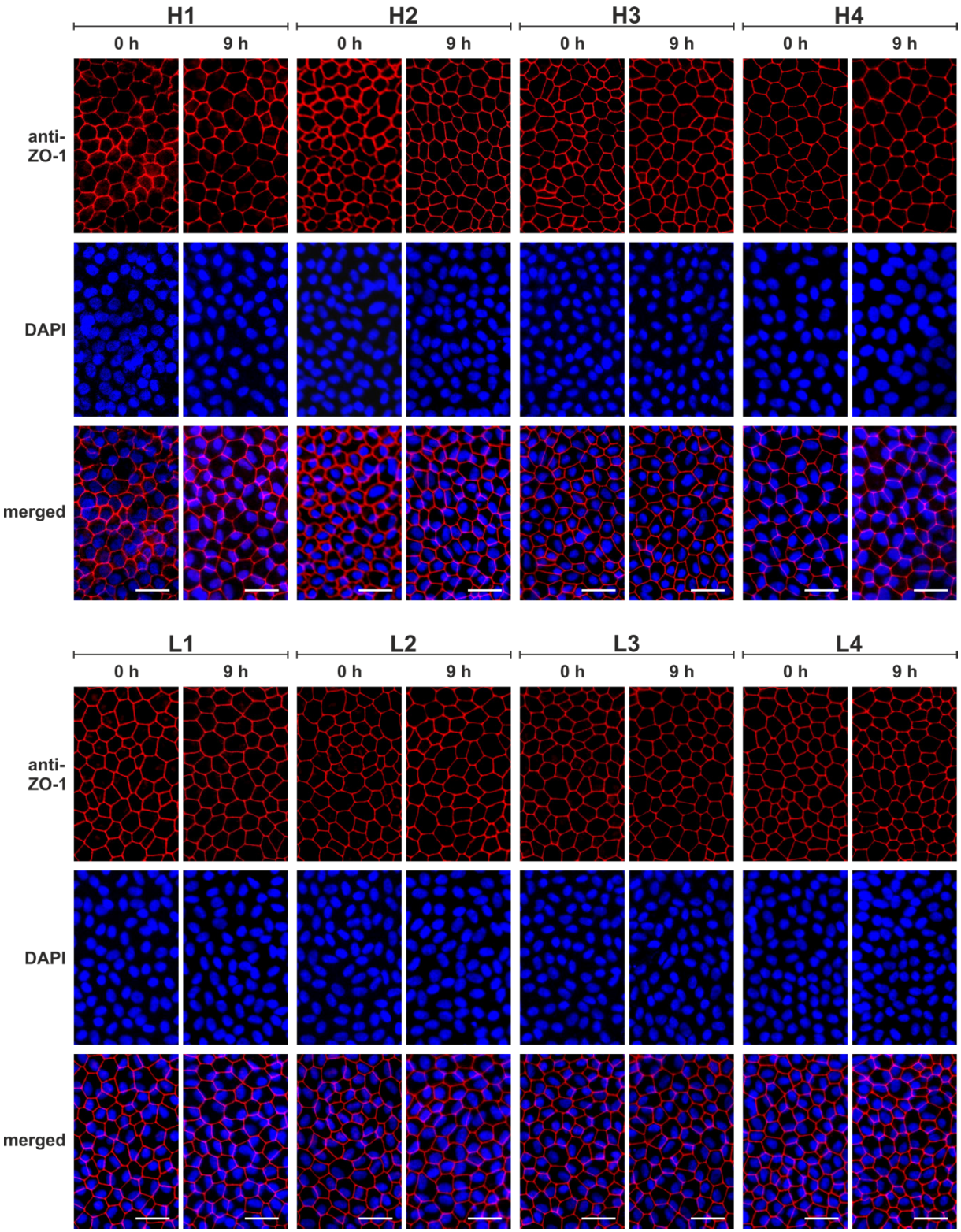

Figure 22: Verification of hiPSC-RPE cell quality regarding morphology and monolayer integrity after acute physical oxidative stress

Four high risk (H1, H2, H3, H4) and four low risk (L1, L2, L3, L4) hiPSC-RPE cell lines were irradiated with BL for 9 h. Non-irradiated cells (0 h) served as controls. In subsequent immunocytochemical analysis, the tight junction marker ZO-1 (red) was labelled with an anti-ZO-1 antibody and nuclei were stained with DAPI (blue). Images were taken in 40x magnification under the fluorescence microscope. Scale bars: 25 µm.

4.6.2 Increased mRNA Expression of Antioxidant Genes *HMOX1* and *NQO1* in hiPSC-RPE Cells after 9 h BL Irradiation

After validating cell morphology and monolayer integrity of hiPSC-RPE cell lines after 9 h of BL irradiation, mRNA expression of the antioxidant genes *HMOX1* and *NQO1* was studied via qRT-PCR analysis. Four high risk and four low risk cell lines were irradiated with BL for 9 h in two independent experiments. Non-irradiated cells were used as controls (0 h). Irradiation with BL for 9 h induced statistically significant upregulations in both *HMOX1* and *NQO1* mRNA expression compared to controls in all cell lines tested. *HMOX1* mRNA expression was increased to 14.32 (± 5.42) in H1, to 26.81 (± 14.88) in H2, to 83.56 (± 27.61) in H3, to 36.38 (± 13.04) in H4, to 52.04 (± 7.84) in L1, to 43.97 (± 14.90) in L2, to 24.01 (± 5.45) in L3 and to 8.71 (± 5.77) in L4 (**Figure 23 A**). *NQO1* mRNA expression was raised to 2.98 (± 0.21) in H1, to 2.94 (± 0.43) in H2, to 5.29 (± 2.00) in H3, to 3.40 (± 0.18) in H4, to 3.72 (± 0.40) in L1, to 2.58 (± 0.26) in L2, to 5.97 (± 1.92) in L3 and to 7.32 (± 2.27) in L4 (**Figure 23 B**). In summary, *HMOX1* expression was upregulated more strongly than *NQO1* expression after exposure to 9 h BL irradiation. This is opposite to the trends seen after acute or chronic SI treatment, which had both led to higher *NQO1* mRNA expression compared to *HMOX1* expression.

There were no statistically significant differences between high and low risk cell lines in neither *HMOX1* nor *NQO1* transcription after exposure to BL irradiation for 9 h. *HMOX1* mRNA expression was raised to 40.27 (± 30.24) in high risk cell lines and to 32.18 (± 19.59) in low risk cell lines ($p = 0.67$) (**Figure 23 C**). *NQO1* mRNA expression was increased to 3.65 (± 1.11) in high risk cell lines and to 4.90 (± 2.15) in low risk cell lines ($p = 0.36$) (**Figure 23 D**).

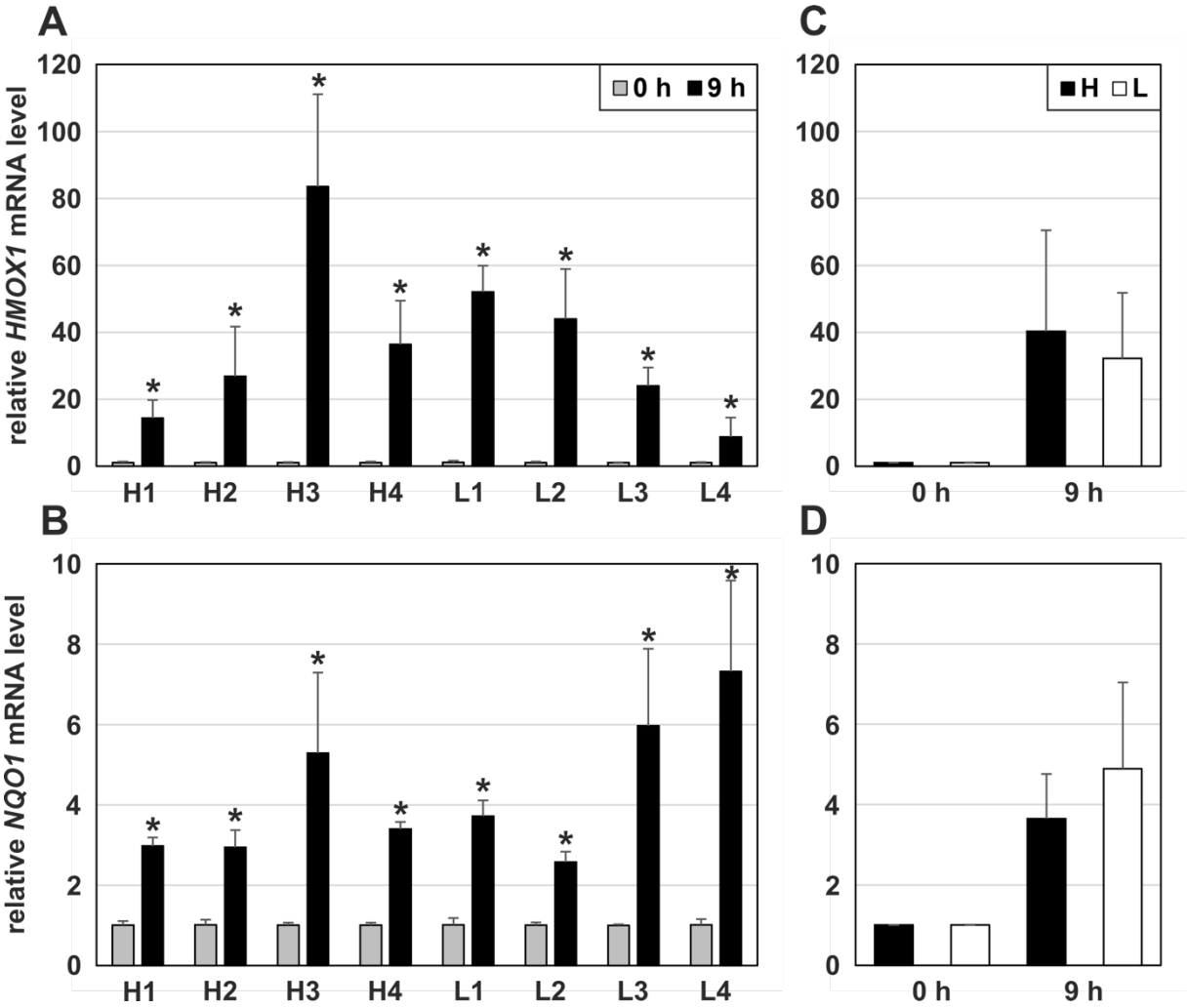

Figure 23: Influence of acute oxidative stress by BL irradiation on relative mRNA expression of *HMOX1* and *NQO1* in hiPSC-RPE cells

Four high risk (H1, H2, H3, H4) and four low risk (L1, L2, L3, L4) hiPSC-RPE cell lines were irradiated with BL for 9 h in two independent experiments. Non-irradiated cells (0 h) served as controls. mRNA expression of *HMOX1* (**A**) and *NQO1* (**B**) was determined via qRT-PCR. Expression was normalized to reference gene *HPRT1*, then calibrated against the control (0 h). Data are presented as means + SD (n = 6). Statistical significance (*: $p < 0.05$) was determined with a Wilcoxon Test.

High risk (H) and low risk (L) hiPSC-RPE cell lines were compared regarding their mRNA expression levels of *HMOX1* (**C**) and *NQO1* (**D**) after induction of acute physical oxidative stress by 9 h BL. Means and SD of the individual means of the cell lines were taken from the data shown in (A) or (B), respectively. Data are presented as means + SD (n = 4 for H, n = 4 for L). Statistical significance (*: $p < 0.05$) was determined with a two-tailed Student's T-Test.

4.6.3 Increased HMOX1 and NQO1 Protein Expression in hiPSC-RPE Cells after 9 h BL Irradiation

Since 9 h BL irradiation induced *HMOX1* and *NQO1* mRNA expression, its effect on protein expression needed to be examined as well. After changing cell culture medium to irradiation medium, four high and three low risk cell lines were irradiated with BL for 9 h. Corresponding non-irradiated plates served as controls (0 h). HMOX1 and NQO1 protein expression in the cell lysates was explored via Western blot analysis. ACTB was stained as a loading control. HMOX1 (28 kDa), NQO1 (29 kDa) and ACTB immunostainings are depicted representatively

for three replicates (**Figure 24**). In all cell lines, HMOX1 stainings were visibly more intense after irradiation compared to controls. Differences in intensity were not as prominent in NQO1 stainings when compared to HMOX1 stainings. Densitometric quantification in Image Studio could not disclose statistically significant differences in HMOX1 or NQO1 expression between irradiated and non-irradiated cells, although under visual inspection stainings were evidently more intense after irradiation. Although not significant, HMOX1 protein expression after BL exposure was increased in all cell lines in a broad bandwidth compared to controls. BL irradiation increased relative HMOX1 protein expression to 7.14 (± 4.49) in H1, to 6.56 (± 1.99) in H2, to 1.52 (± 0.95) in H3, to 1.65 (± 0.14) in H4, to 32.38 (± 16.10) in L1, to 13.42 (± 1.65) in L2 and to 3.63 (± 3.06) in L3 (**Figure 24 A**). Relative NQO1 protein expression was insignificantly upregulated to 2.14 (± 2.17) in H1, to 2.06 (± 1.33) in H2 and to 1.42 (± 0.80) in H4, downregulated to 0.28 (± 0.39) in L3 and hardly regulated in H3, L1 and L2 (**Figure 24 B**). Contrasting HMOX1 and NQO1 protein expression for the seven cell lines combined, HMOX1 protein quantities were higher than those of NQO1 under BL irradiation, confirming regulation differences seen for mRNA expression and contrasting the trends observed under SI treatment.

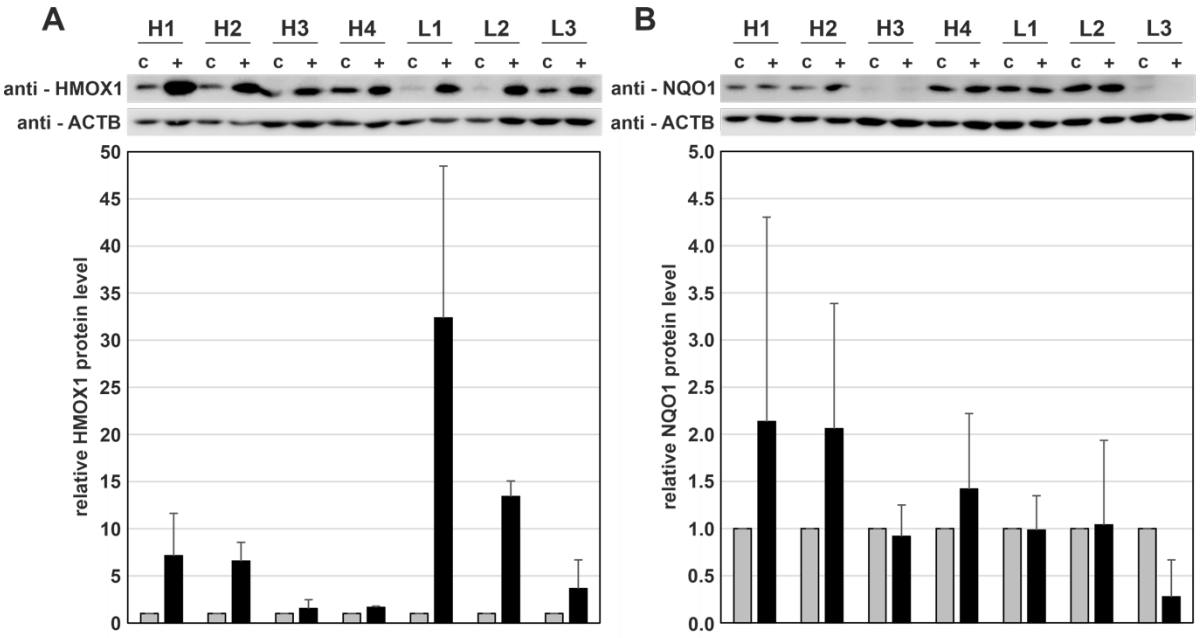

Figure 24: Influence of acute oxidative stress by BL irradiation on relative protein expression of HMOX1 and NQO1 in hiPSC-RPE cells

Four high risk (H1, H2, H3, H4) and three low risk (L1, L2, L3) hiPSC-RPE cell lines were irradiated with BL for 9 h in two independent experiments. Non-irradiated cells (0 h) served as controls. Protein expression of HMOX1 (**A**) and NQO1 (**B**) was determined via Western blot analysis. ACTB was included as loading control. Representative immunoblots for 3 replicates are shown. For densitometric analysis of the bands, signal intensities were quantified in Image Studio. HMOX1 and NQO1 signal values were normalized to ACTB values and then calibrated against the control (0 h). Data are presented as means + SD (n = 3). Statistical significance (*: $p < 0.05$) was determined with a Wilcoxon Test.

Comparing protein expression by AMD risk profile after acute physical oxidative stress exposure, HMOX1 protein quantities were higher in low risk cell lines (16.48 (± 14.62)) than in high risk cell lines (4.22 (± 3.05)) (p = 0.23) (**Figure 25 A**), and NQO1 protein was higher in high risk cell lines (1.63 (± 0.58)) than in low risk cell lines (0.77 (± 0.43)) (p = 0.23) (**Figure 25 B**). Differences were not statistically significant, but interestingly these were the same trends as already seen after acute and chronic chemical oxidative stress exposure to SI in **Figure 10** and **Figure 17**.

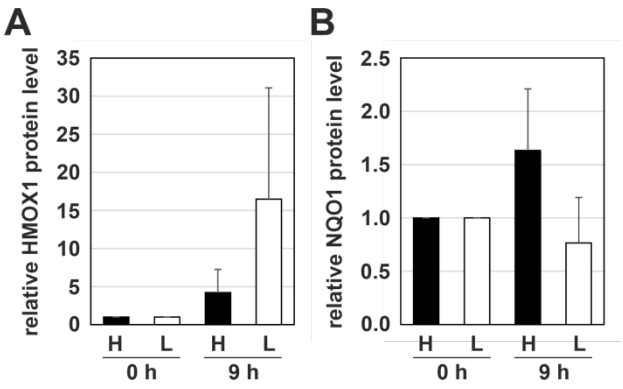

Figure 25: Comparison of relative HMOX1 and NQO1 protein expression in high and low risk cell lines in response to acute oxidative stress by BL irradiation
High risk (H) and low risk (L) hiPSC-RPE cell lines were compared regarding protein expression of HMOX1 (**A**) and NQO1 (**B**) under acute physical oxidative stress by 9 h BL irradiation. Means and SD of the individual means of the cell lines were taken from the data shown in Figure 24 (A) or (B), respectively. Data are presented as means + SD (n = 4 for H, n = 3 for L). Statistical significance (*: $p < 0.05$) was determined with a Wilcoxon Test.

4.7 Effects of Physiological Oxidative Stress Following Phagocytosis of POS and HNE-modified POS

After investigating the effects of the artificial chemical stressor SI and the physical stressor BL on the hiPSC-RPE cells, POS phagocytosis was introduced into the model system as a physiological stressor. For assessment of phagocytotic ability, the hiPSC-RPE cells were fed with POS, which were isolated from porcine retinae, as well as with HNE-modified POS. Lastly, combining POS feeding and the exposure to BL allows the analysis of whether the additional stress of phagocytotic activity modifies the oxidative stress response in hiPSC-RPE cells induced by BL irradiation. This should help to evaluate to which extent POS feeding is worth integrating into NRF2 pathway analysis in this model system.

4.7.1 Confirmation of POS Uptake and Degradation in hiPSC-RPE Cell Lines

Firstly, successful POS uptake and degradation needed to be confirmed for the hiPSC-RPE cell lines. Cells were fed with POS in a concentration of 4 µg/cm^2 based on previous studies (Krohne et al., 2010a; Westenskow et al., 2012) and were incubated for 2 h. The 2 h feeding period for POS uptake into the cells had been tested in previous experiments at the Institute of Human Genetics as well as in hiPSC-RPE cells in multiple other research groups (Singh et al., 2013a; Singh et al., 2015; Hazim et al., 2017; Dalvi et al., 2019). After 2 h, the cells were washed with cell culture medium without KOSR and fresh cell culture medium was added.

POS uptake including bound and internalized POS (0 h post feeding) and degradation (4 h, 6 h, 8 h post feeding) was visualized by Western blot analysis of the POS-specific protein rhodopsin (Singh et al., 2015; Dalvi et al., 2019). ACTB was included as a loading control. Rhodopsin stainings confirmed that all examined cell lines were able to phagocytose porcine POS, with stainings being most intense at 0 h post feeding and decreasing with continuous POS degradation (**Figure 26**). For visual inspection the approximately 47 kDa rhodopsin molecular weight was analyzed which represents most likely glycosylated rhodopsin monomers. No general differences were observed between high and low risk cell lines although cell lines H4 and L4 showed smaller amounts of rhodopsin compared to the other cell lines due to staining artifacts.

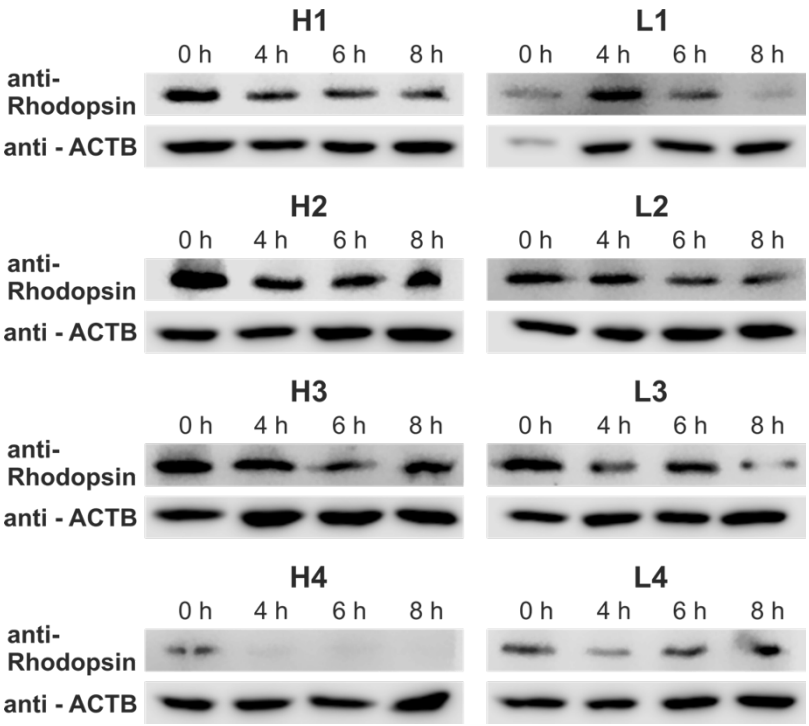

Figure 26: Analysis of POS phagocytosis in hiPSC-RPE cell lines
Four high risk (H1, H2, H3, H4) and four low risk (L1, L2, L3, L4) hiPSC-RPE cell lines were incubated with POS in a concentration of 4 µg/cm^2 for two hours. After two hours, cells were washed and new cell culture medium was added (0 h). Rhodopsin protein expression was determined via Western blot analysis to assess POS uptake at 0 h post feeding and degradation 4 h, 6 h and 8 h later. ACTB was included as loading control. Representative immunoblots for 3 replicates are shown.

4.7.2 Rhodopsin Degradation after Feeding of POS or HNE-Modified POS in hiPSC-RPE Cells

HNE is a lipid peroxidation product which has been shown to cause damage to lipofuscin-associated proteins in human RPE cells by aberrant covalent modification (Schutt et al., 2003). Furthermore, POS proteins modified with HNE have been shown to be stabilized against lysosomal proteolysis compared to non-modified POS (Kaemmerer et al., 2007).

To test the effect of HNE-modification in our model system, hiPSC-RPE cells were fed with POS or HNE-modified POS for 6 consecutive days. POS and HNE-POS solutions were prepared fresh daily and were replaced after every 24 h of incubation. In each cell line, unfed cells were included as controls. Cells were harvested for protein samples 2 h after the sixth POS-feeding and subjected to Western blot analysis with anti-Rhodopsin antibodies. ACTB

was stained as a loading control. In all cell lines examined, rhodopsin was evidently more intense after feeding of HNE-modified POS than after feeding of regular POS, confirming HNE-mediated stabilization of POS against lysosomal degradation as described by Kaemmerer et al., 2007. Staining intensities were similar between high and low risk cell lines. As expected, cells without feeding POS failed to display rhodopsin staining.

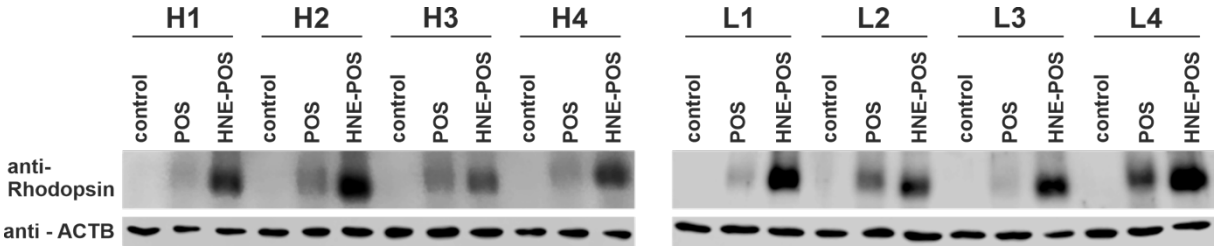

Figure 27: Comparison of POS and HNE-POS phagocytosis in hiPSC-RPE cell lines after 6 days of feeding

Four high risk (H1, H2, H3, H4) and four low risk (L1, L2, L3, L4) hiPSC-RPE cell lines were incubated with POS or HNE-modified POS for 6 days, replacing solutions every 24 h. Unfed cells were included as controls. Rhodopsin protein expression was determined via Western blot analysis in cells harvested 2 h after the sixth POS-feeding. ACTB was included as loading control. Representative immunoblots for 2 replicates are shown.

4.7.3 Combinatory Effect of Physiological and Physical Oxidative Stress on mRNA Expression of Antioxidant Genes *HMOX1* and *NQO1*

In this experiment, incubation with HNE-POS was combined with subsequent BL irradiation to elucidate whether phagocytosis of the HNE-modified POS affects *HMOX1* and *NQO1* mRNA expression induced by BL irradiation in hiPSC-RPE cells. The experimental setup was chosen on the basis of the setup described in Brandstetter et al., 2015. Four high and four low risk cell lines were incubated with 4 µg/cm^2 HNE-POS for 7 consecutive days in order to induce lipofuscinogenesis (Krohne et al., 2010a). The POS solution applied above the transwell filter inserts and the regular cell culture medium below the filters were renewed daily. The day after the seventh POS-feeding, the hiPSC-RPE cells were exposed to BL irradiation for 9 h. To discriminate between the individual treatments, hiPSC-RPE cells of each cell line which had only been exposed to the 7 d HNE-POS incubation or the 9 h BL irradiation were included in the experiment, as well as untreated controls. *HMOX1* and *NQO1* mRNA expression were investigated via qRT-PCR analysis. As revealed in previous experiments, 9 h BL irradiation induced both *HMOX1* and *NQO1* mRNA expression, with higher *HMOX1* than *NQO1* expression. Interestingly, *HMOX1* mRNA expression in BL-irradiated cells in H3 was much lower than in the previous experiments. HNE-POS treatment did not affect *HMOX1* or *NQO1* mRNA expression in irradiated or non-irradiated cells (**Figure 28 A** and **B**). With more replicates or less stringent statistics, statistical significance in expression between irradiated and non-irradiated cells with or without HNE-POS incubation would most certainly be reached. There were no significant differences between high and low risk cell lines in neither *HMOX1* nor *NQO1* mRNA expression in any of the examined conditions (*HMOX1*: BL: $p = 0.89$, POS:

p = 0.49, POS+BL: p = 1; *NQO1*: BL: p = 0.69, POS: p = 0.34, POS+BL: p = 0.69) (**Figure 28 C** and **D**).

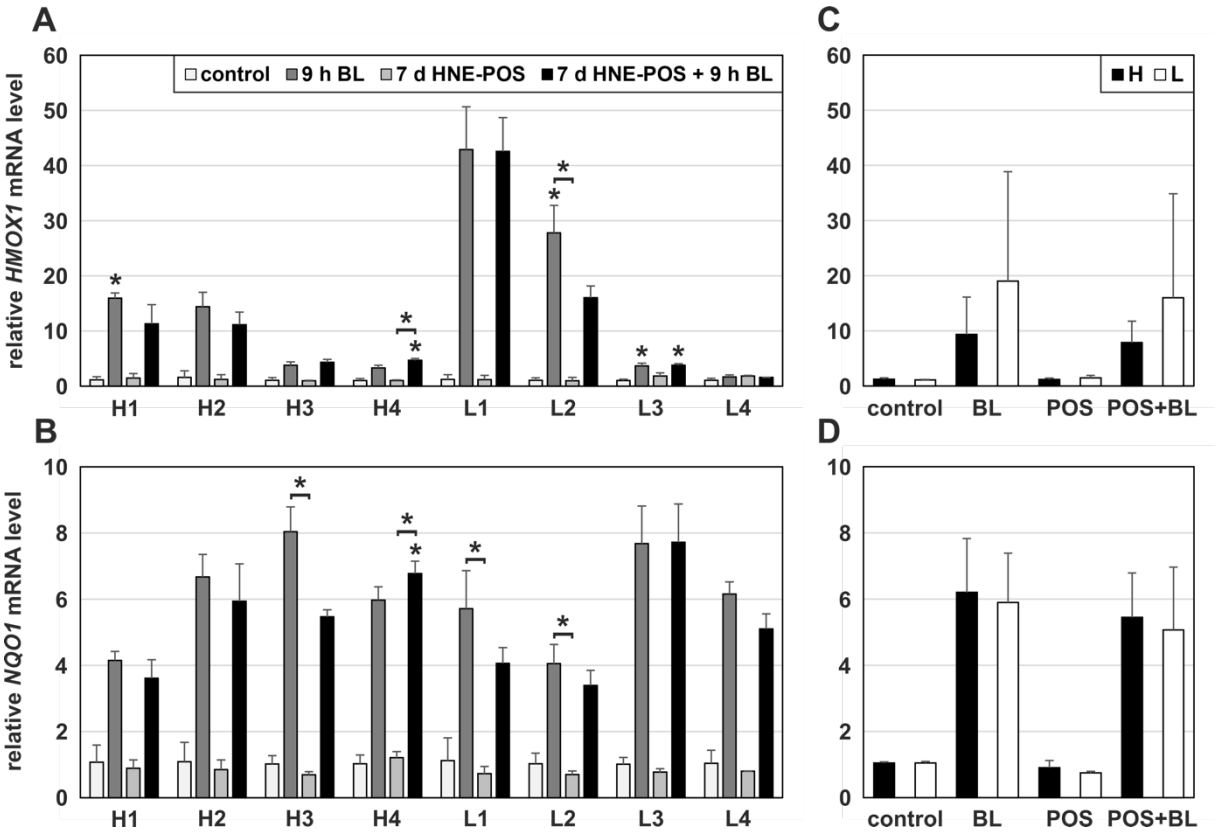

Figure 28: Influence of physiological oxidative stress by HNE-POS phagocytosis and acute physical oxidative stress by BL irradiation on relative mRNA expression of *HMOX1* and *NQO1* in hiPSC-RPE cells

Four high risk (H1, H2, H3, H4) and four low risk (L1, L2, L3, L4) hiPSC-RPE cell lines were incubated with HNE-modified POS for 7 days, replacing solutions every 24 h, and were subsequently irradiated with BL for 9 h. For each cell line, cells which had only been incubated with HNE-POS or irradiated with BL as well as untreated cells serving as controls were included in the experiment. mRNA expression of *HMOX1* (**A**) and *NQO1* (**B**) was determined via qRT-PCR. Expression levels were normalized to reference gene *HPRT1*, then calibrated against the control. Data are presented as means + SD (n = 3). Statistical significance (*: $p < 0.05$) was determined with the Kruskal Wallis Test with post hoc Dunn's Multiple Comparison Test and multiple testing correction using the Benjamini-Hochberg method.

High risk (H) and low risk (L) hiPSC-RPE cell lines were compared regarding their mRNA expression levels of *HMOX1* (**C**) and *NQO1* (**D**) after exposure to HNE-POS, BL irradiation or both. Means and SD of the individual means of the cell lines were taken from the data shown in (A) or (B), respectively. Data are presented as means + SD (n = 4 for H, n = 4 for L). Statistical significance (*: $p < 0.05$) was determined with a Wilcoxon Test.

5 Discussion

Oxidative stress is widely accepted to contribute to AMD development, but its pathobiological implication in AMD pathogenesis and interaction with other disease mechanisms, specifically genetic susceptibility, are still to be elucidated. Thus, in this thesis, a unique cellular model was developed to examine the two risk factors oxidative stress and genetic predisposition in combination, providing a further step in unraveling disease mechanisms leading to AMD.

Specifically, oxidative stress was induced with the chemical stressor SI and the physical stressor BL irradiation in patient-derived hiPSC-RPE cell lines carrying a known genetic risk for AMD. The oxidative stress response of the hiPSC-RPE cells was analyzed in the NRF2 signaling pathway and compared between high and low risk cell lines. The results demonstrated that mRNA and protein expression of the NRF2 target genes *HMOX1* and *NQO1* were upregulated in all cell lines for all oxidative stress conditions tested. It should be noted that the two stressors SI and BL induced opposite trends with different degrees in increase of gene expression. Comparing high and low risk cell lines, the *in vitro* data did not show a significant difference in their oxidative stress response in any of the tested conditions, which led us to the conclusion that genetic AMD susceptibility did not affect the NRF2-dependent oxidative stress response.

In a further study, the hiPSC-RPE cells were fed with POS to replicate a purely physiological stressor in the cellular model next to the external oxidative stressors SI and BL. Phagocytotic ability could be confirmed for all hiPSC-RPE cell lines included in the project. Further investigations showed that HNE-modified POS were stabilized against lysosomal degradation (described in Kaemmerer et al., 2007). HNE-POS feeding and phagocytotic activity for 7 days previous to BL irradiation failed to impact *HMOX1* and *NQO1* mRNA expression in response to BL treatment in the hiPSC-RPE cells.

5.1 Cell Culture Model to Best Replicate AMD Pathologies

A first and crucial question to ask when studying molecular pathomechanisms involved in AMD is which kind of model to use. It should best replicate the complex physiological and importantly pathophysiological conditions involved in the development and advancement of disease the human retina undergoes *in vivo*. Various animal models and cell model systems have been reported and implemented for the study of AMD pathogenesis. Animal models of a variety of species including drosophila, mice, rats, rabbits, guinea pigs, pigs and monkeys have helped unravel several AMD pathomechanisms, but no model has yet been able to fully mimic the many characteristics and interplaying factors of AMD (Pennesi et al., 2012; Chen et al., 2014; Kannan & Hinton, 2014; Abokyi et al., 2020). Mice are the animal of choice in AMD research due to structural similarities to the human retina, cost-effectiveness, relatively rapid disease

progression and the possibility of genetic engineering to investigate the many polymorphisms associated with AMD (Zeiss, 2010; Pennesi et al., 2012; Chen et al., 2014; Volland et al., 2015; Abokyi et al., 2020; Ratnayaka & Lotery, 2020). However, mice do not develop a macula, the retinal region centrally involved in AMD, and some murine models used for studying AMD show phenotypes or genetic alterations that don't correspond with the polymorphisms actually associated with the disease (Zeiss, 2010; Pennesi et al., 2012; Ratnayaka & Lotery, 2020). Regarding antioxidant gene expression studies, it needs to be kept in mind that mice and humans are known to show differences in regulation of *HMOX1* expression (reviewed in Sikorski et al., 2004; Lever et al., 2016).

A general advantage of working with cell culture models is that they comprise a controlled, defined system which can be targeted by specific interventions, with effects allowing direct inferences to the respective parameter alteration or manipulation (Hornof et al., 2005; Forest et al., 2015). Consequently, reproducibility of experimental conditions and results is commonly higher than in animal tissue (Hornof et al., 2005). Furthermore, using human cell lines instead of tissues extracted from study animals rules out issues regarding possible genetic/ physiological differences between species (Hornof et al., 2005). Since the RPE is of central importance in AMD pathogenesis (reviewed in Somasundaran et al., 2020), numerous human RPE cell culture models have been developed to study various aspects of the disease. Such human RPE cell cultures include primary human (fetal) RPE, the immortalized human cell line ARPE-19, which arose spontaneously from primary RPE cell culture and was characterized by Dunn et al. in 1996, as well as hiPSC-RPE cells (reviewed in Hornof et al., 2005; Forest et al., 2015). The generation of iPSC was first described by Takahashi and Yamanaka in 2006. By retroviral transduction of only four defined TFs, mouse fibroblasts as well as adult human dermal fibroblasts could be reprogrammed into pluripotent stem cells, which were termed iPSC (Takahashi & Yamanaka, 2006; Takahashi et al., 2007). By obtaining and reprogramming somatic cells, for instance from blood samples and skin biopsies, which were the sources of the hiPSC-RPE cells used in this thesis, the extraction of primary cells like RPE cells, which are difficult to access, can easily be bypassed (reviewed in Grassmann et al., 2015a). The hiPSC technology is considered a breakthrough in personalized medicine, as it makes the generation of individual, patient-derived cell lines possible (Brandl et al., 2015; Grassmann et al., 2015a). As is the case for other cell types derived from iPSC implemented to model various degenerative diseases, the hiPSC-RPE cells present not only an advance in laboratory research on disease pathomechanisms, but also in a clinical context for screening of drug candidates and even therapeutic autologous transplantation without immune rejection into eyes affected by AMD, which is especially urgent for the currently untreatable dry form of the disease (Jin et al., 2011; reviewed in Yamanaka, 2012; Kim, 2014, Mack et al., 2014; Brandl et al., 2015; Forest et al., 2015; Hazim et al., 2017; Mandai et al., 2017).

It has to be considered that by using RPE cells as the only cell type for disease modeling, the systemic effects and interactions of AMD are disregarded and excluded from the model system (Forest et al., 2015). Furthermore, the differentiation period of hiPSC-RPE cells is naturally much shorter than a lifetime of RPE cells *in vivo* with all its physiological and pathophysiological implications (Gong et al., 2020). However, since the hiPSC-RPE cells are cultivated for many weeks, they may be regarded as “aged” RPE cells (Dalvi et al., 2019) and therefore somewhat may mimic the role of aged RPE in AMD pathogenesis in a shorter time frame. Previous studies have compared hiPSC-RPE cell lines derived from AMD patients to those derived from healthy controls and have found the first to display disease phenotypes associated with AMD such as upregulation of complement genes, increased susceptibility to oxidative stress and higher ROS levels upon induction of oxidative stress (Chang et al., 2014; Golestaneh et al., 2016; Saini et al., 2017; Voisin et al., 2019; Gong et al., 2020).

The generation of the hiPSC-RPE cells studied at the Institute of Human Genetics, their resemblance to native RPE regarding structural and functional properties as well as their cryostorability are described in the protocol published in Brandl et al., 2014. In the present study, the quality of the examined hiPSC-RPE cell lines was verified in immunocytochemical stainings of tight junction protein ZO-1 (Stevenson et al., 1986) as well as TEER measurements before and after exposure to oxidative stress. Although TEER measurements provide a simple and non-invasive method to determine barrier integrity of monolayers, many variables including positioning of the electrodes, cell passage number and cell culture period (exemplified for hiPSC-RPE cells in Brandl et al., 2014), media composition and temperature during measurement can influence TEER values, making them examiner- and laboratory-dependent (Srinivasan et al., 2015). The value of TEER measurements is therefore limited to an orienting quality control of monolayers and is not sufficient to allow for quantitative statements. By cultivating and treating four high risk and four low risk hiPSC-RPE cell lines simultaneously biological variability (Dalvi et al., 2019) could be replicated in the model system. The number of cell lines was ideal, as comparisons across cell lines and between risk scores could be made and reliable conclusions regarding the general reaction of the hiPSC-RPE cells to different forms of oxidative stress could be drawn, yet without causing inevitable plating restrictions and critically extended time lengths in experiments.

5.2 Experimental Treatment Conditions for the Oxidative Stressors SI and BL

By selecting the chemical stressor SI and the physical stressor BL as sources of oxidative stress for the hiPSC-RPE cell experiments in this dissertation, two different qualities of oxidative stress could be investigated and compared. SI is a retinotoxin known to induce oxidative stress and damage the RPE and has been applied in many retinal degeneration

models due to its reproducibility and simple variation in concentration and treatment duration (summarized in Kiuchi et al., 2002; Enzmann et al., 2006; Machalińska et al., 2010; Wang et al., 2014b; Zhou et al., 2014; Du et al., 2018; Moriguchi et al., 2018; Chan et al., 2019). BL is the wavelength most injurious to RPE cells (reviewed in Strauss, 2005; Wu et al., 2006). The widespread use of LEDs as lamps and in displays has raised concerns regarding retinal damage caused by the BL component. It needs to be noted that the damaging effects found under extreme exposure conditions in *in vitro* models and animal studies cannot be directly translated to a person's normal LED exposure (International Commission on Non-Ionizing Radiation Protection (ICNIRP), 2020).

Publications examining the effect of SI on ARPE-19 cells served as a first point of reference for the concentration range to test in MTT assays in order to determine cell viability (Juel et al., 2013; Hanus et al., 2016; Zhang et al., 2016). MTT assay results for 24 h SI-induced oxidative stress in ARPE-19 cells vary between published reports. In Juel et al., 2013, cell viability in ARPE-19 cells is described to be significantly reduced at 1 mM SI, whereas Hanus et al., 2016 reported a half maximal effective concentration (EC50) of 10.5 mM SI and Zhang et al., 2016 published a non-significant reduction in cell viability for concentrations up to 10 mM SI. The differences in significant concentrations of SI can stem from varying cell treatment and assay protocols. The maximum concentration of 10 mM SI chosen for MTT assays in the present study reduced cell viability by 90-100 % in all hiPSC-RPE cell lines examined, whereas 0.5 mM SI did not significantly reduce cell viability. It is common that different RPE cell model systems show different reactions in similar situations due to varying cellular origins, development and genetic, morphological and molecular characteristics (e.g. Mazzoni et al., 2014; Srinivasan et al., 2015; Garcia et al., 2015; Takayama et al., 2016). Quantification of cytotoxicity via LDH assay confirmed that the concentration of 0.5 mM was not cytotoxic to the hiPSC-RPE cells and therefore suitable to use in oxidative stress experiments.

To better replicate the physiological, more chronic oxidative stress that the RPE is subjected to in *vivo*, the hiPSC-RPE cells were also exposed to SI for three days mimicking a more chronic exposure. As 0.125 mM SI and 0.25 mM SI treatment for three days did not appear to be toxic to the cells, these concentrations were deemed suitable for oxidative stress experiments. In the study published by Zhang et al., 2016, one of the first investigations of the effect of chronic SI treatment on RPE cells *in vitro*, 5 day treatment with 1, 2 or 5 mM SI reportedly increased ARPE-19 cell viability while on the other hand 10 and 20 mM SI decreased cell viability (Zhang et al., 2016). The lower concentrations are approximately 10 times higher than the concentrations chosen for the 72 h SI experiments with the hiPSC-RPE cells in the present study. This discrepancy may be attributable to the fact that ARPE-19 cells constitute more immature RPE cells than hiPSC-RPE cells and therefore show a strikingly different stress response, as suggested by Garcia et al., 2015.

Brandstetter and colleagues reported a dose-dependent increase in cytotoxicity in lipofuscin-loaded ARPE-19 cells upon BL irradiation with a Blue Light LED Light Source, which was almost complete after 24 h of irradiation (Brandstetter et al., 2015). For my experiments, an almost identical copy of the light source used by Brandstetter et al., 2015 was installed in a 37°C incubator, which however, due to the height of the incubator, reduced the LED-cell distance to 26 cm compared to the 35 cm distance reported by Brandstetter et al., 2015. Over multiple sets of MTT assays determining cell viability for various time intervals of BL exposure of up to 24 h and subsequent LDH assays for cytotoxicity analysis, an exposure for 9 h was decided upon as optimal irradiation duration for oxidative stress experiments with BL, as it caused a detectable oxidative stress response but no cytotoxicity in the hiPSC-RPE cells. The established irradiation duration of 9 h would be in line with results from Brandstetter et al., 2015 for control cells, however they selected durations of 3 h and 6 h, since previous lipofuscin-loading made the cells more susceptible to photooxidative damage (Brandstetter et al., 2015). Varying cell viability between cells in different positions of the incubator revealed inconsistent irradiation effects across the incubator area and a smaller than expected radius for consistent irradiation, possibly due to the reduced LED cell distance. Regarding oxidative stress experiments, it needs to be taken into consideration that intense, acute 9 h BL treatment of directly exposed hiPSC-RPE cells can partly mimic the induced oxidative stress mechanisms but does not represent lifelong exposure to lower doses of BL.

5.3 Upregulation of *HMOX1* and *NQO1* Expression in hiPSC-RPE Cells upon SI Treatment and BL Irradiation

Although the focus of this project was on the NRF2-associated oxidative stress response, mRNA expression of the genes *CD46*, *VEGFA* was determined additionally to receive an initial overview of which mechanism could be affected by induction of acute oxidative stress with SI in the hiPSC-RPE cells. As complement factor and C3 regulator *CD46* is thought to be the only membrane-bound complement regulator localized in the basolateral RPE membrane and its immunolabeling has been reported to be decreased in early stages of GA and early AMD, it is an obvious protein to investigate in studies concerning AMD and the RPE (Vogt et al., 2011; Ebrahimi et al., 2013; Datta et al., 2017). In contrast to the downregulation of *CD46* expression in the hiPSC-RPE cells observed at the Institute in response to acute PQ exposure (Dr. Karolina Plößl, unpublished results), acute oxidative stress induction with 0.5 mM SI for 24 h did not affect *CD46* mRNA expression.

Increased *VEGFA* expression and secretion has been reported in response to multiple oxidative stressors, treatment durations and different *in vitro* RPE cell models (Kannan et al., 2006; Byeon et al., 2010; Cao et al., 2013) as well as in response to PQ treatment in the hiPSC-RPE cells studied at the Institute (Dr. Karolina Plößl, unpublished results). In present study,

VEGFA mRNA expression was not increased after treating the hiPSC-RPE cells with 0.5 mM SI for 24 h. Most cell lines even exhibiting a slight decrease in mRNA expression. Interestingly and in contrast to the research listed above, Zhang and colleagues found a decrease in *VEGFA* expression in ARPE-19 cells after continuous treatment with SI for 5 days and proposed that stress responses could vary between different oxidative stressors and durations of exposure (Zhang et al., 2016). This would explain the lack of a major stress response reflected in the *VEGFA* signaling pathway observed in the hiPSC-RPE cells upon acute SI treatment.

HMOX1 and *NQO1*, the genes of focus in this project, are two of the main NRF2-responsive antioxidant target genes that have been studied in various oxidative stress settings using cell and mouse model systems for the RPE (Sachdeva et al., 2014; Wang et al., 2014a; Wang et al., 2014b; Garcia et al., 2015; Hanus et al., 2015; Xie et al., 2017; Zhao et al., 2019; Jadeja et al., 2020; Suárez-Barrio et al., 2020). However, prior to this study, the effect of the stressors SI and BL on these target genes had not yet been investigated in hiPSC-RPE cells.

Comparing cell lines by risk score, a clear trend prevailed for protein expression after acute and chronic SI treatment as well as BL irradiation with higher HMOX1 expression in low risk cell lines and reversely higher NQO1 expression in high risk cell lines, with only NQO1 expression after 0.125 mM SI treatment falling out of line. Nevertheless, the *in vitro* data failed to reveal a significant difference in the oxidative stress response to SI and BL between high and low risk cell lines, with the exception of HMOX1 protein expression after 0.125 mM SI for 72 h. Therefore, it was concluded that genetic susceptibility to AMD is unlikely to affect the antioxidant stress response regarding *HMOX1* and *NQO1*. This thesis was backed by later studies exposing the hiPSC-RPE cells to extended chronic SI treatment periods of 7 d and 30 d and different treatment durations for PQ stress (Dr. Karolina Plößl, unpublished results). Consequently, it could be plausible that genetic AMD predisposition alone without pathological changes and/ or adjacent structures of the retina present isn't sufficient to alter the antioxidant stress response of the RPE cells, a least regarding the two studied genes.

Some of the experiments were repeated with hiPSC-RPE cells cultivated without the cell culture differentiation component Nicotinamide (Dr. Karolina Plößl, unpublished results), as it has been shown that Nicotinamide ameliorates AMD phenotypes (Saini et al., 2017) and therefore could perhaps conceal differences between the high and low risk hiPSC-RPE cell lines upon oxidative stress induction. However, only even more elevated expression of *HMOX1* and *NQO1* upon SI exposure was observed, but not significant disparities between high and low risk cell lines. Being able to simultaneously study the effects of oxidative stress on hiPSC-RPE cell lines with a known genetic high or low AMD risk and perhaps reveal differences in their response to an oxidative stressor is of high value for finding new therapeutic targets as well as exploring preventative measures for protecting at-risk patients from developing AMD

features. At this point a related study design including the factor “age” by cultivating the hiPSC-RPE cells for shorter and longer time periods, reflecting young and old RPE cells, might be worth considering to discern differences in the oxidative stress response between cell lines of high and low risk. Sachdeva and colleagues discovered that the aging mouse RPE exhibited higher levels of the NRF2-downstream genes *HMOX1*, *NQO1* and Glutamate-cysteine ligase regulatory subunit (*GCLM*) in unstressed conditions compared to RPE of young mice. This indicated an increase in basal oxidative stress with age which is counteracted by adaptive upregulation of the antioxidants. The aging mouse RPE also showed impaired induction of the NRF2-regulated antioxidant response upon oxidative stress with SI (Sachdeva et al., 2014).

Regarding protein expression after BL irradiation, densitometric quantification did not distinctly reflect the visual differences observed in staining intensities between irradiated and non-irradiated cells, contrary to the clear results of protein quantification after acute and chronic SI treatment. The densitometric analysis disclosed largely varying and non-significant changes in expression between the cell lines, partly with relatively large standard deviations. This can be explained by variations in staining intensities between the individual samples due to a relatively small sample size of three replicates. The here described issue with the applied densitometric methodology, where differences in quantification and subsequent statistical analysis must not have been robust enough to reveal significant results, would assumably be mitigated by including more samples into the analysis to achieve clearer and more stable results.

Generally speaking, cells adjust their response to varying situations by using multiple signaling pathways and TFs (Alam & Cook, 2007). As reviewed by Alam and Cook, *HMOX1* expression can be induced by numerous stimuli and is thought to be uniquely regulated by all four of the most important stress-responsive TFs, which next to NRF2 include the activator protein-1 (AP-1), nuclear factor-κB (NF-κB) and the heat shock factor (HSF), each of which activate different elements of the cell’s response to stress. Functional overlaps of these pathways can be either explained by a stimulus inducing numerous types of stress or by a gene with binding sites for more than one TF (Alam & Cook, 2007). Therefore, *HMOX1* expression could be activated by an alternative pathway to or additional stress pathway alongside NRF2, explaining the expression differences compared to *NQO1*. This has previously been demonstrated for ethanol-induced oxidative stress in Kupffer cells (Yeligar et al., 2010) and has been hypothesized in a further related study with RPE cells (Hanus et al., 2015). Furthermore, SI and BL are different types of oxidative stressors of different qualities, chemical and physical, and thus could lead to different fine-tuning of the response mechanisms of the RPE cells to the oxidative stress with activation of a different combination of TFs. This could explain the disparities between *HMOX1* and *NQO1* expression in response to SI and BL observed in this study.

Alternatively, some research has implied that antioxidant gene expression may be exposure time dependent, e.g. *HMOX1* expression upon BL exposure (Suárez-Barrio et al., 2020). A study on more chronic oxidative stress with PQ for three weeks investigated the dynamics of NRF2 effector responses to PQ across the stress period and found *HMOX1* and *NQO1* to be the main NRF2 effectors in the early stress phases, additionally *NQO1* and *GCLC* expression was significantly further increased at week 3 (Garcia et al., 2015). Therefore, upregulation of *NQO1* could occur before that of *HMOX1* upon SI treatment, and the opposite could be conceivable for BL exposure. This question could be resolved by analyzing the dynamics of gene expression across extended treatment periods, as performed by Garcia and colleagues (Garcia et al., 2015). It has furthermore been reported that *HMOX1* activation induced by low levels of arsenite is regulated by NRF2 early on, but that long-term *HMOX1* expression is induced by NRF2-independent pathways, most likely the AP-1 signaling pathway (Harada et al., 2008). To explicitly prove NRF2 signaling pathway activation, NRF2 translocation to the nucleus would need to be confirmed (Kensler et al., 2007; Chen et al., 2017; Xie et al., 2017). Therefore, mRNA and protein expression of NRF2 as well as the effect of NRF2 knockdown or siNRF2 on the antioxidant genes in the hiPSC-RPE cells would be interesting to pursue.

Research regarding NRF2 signaling and deficiency models have aided in the understanding of the implication of NRF2 in AMD pathology (e.g. Zhao et al., 2011; Sachdeva et al., 2014; Wang et al., 2014a; Chen et al., 2017; Zhao et al., 2019). It has been demonstrated that Nrf2-deficient mice develop age-dependent retinal pathology with typical AMD features (Zhao et al., 2011). A further finding revealed alterations of NRF2 in human eyes affected by AMD, with decreased NRF2 immunolabeling in degenerated RPE overlying drusen (Wang et al., 2014a). Since the aging RPE is susceptible to oxidative stress due to an impaired NRF2-mediated antioxidant response (Sachdeva et al., 2014), multiple NRF2 activators/ stabilizers promoting NRF2 signaling and boosting antioxidant gene expression have been proposed as potential therapeutic agents in AMD therapy by providing protection against oxidative stress (e.g. Zhang et al., 2014; Garcia et al., 2015; Hanus et al., 2015; Xie et al., 2017; Zhao et al., 2019). Furthermore, as suggested for various other diseases, the antioxidant genes themselves, such as *HMOX1* could be targeted therapeutically (Immenschuh & Ramadori, 2000; Chen & Kunsch, 2004). Although targeting just this one pathway may not be sufficient to stop disease progression due to the complexity of AMD (van Lookeren Campagne et al., 2014), every possible novel therapeutic option provides a further step in understanding the involvement of oxidative stress mechanisms in AMD pathology and could be distributed in combination with other agents in the future.

5.4 Inclusion of POS Phagocytosis into the Model System

In the last part of the thesis, the hiPSC-RPE cells were challenged with POS isolated from porcine retinae in order to include a physiological stressor into the *in vitro* model next to the external oxidative stressors SI and BL. As visualized in rhodopsin stainings, there were no large differences in POS uptake and degradation between high and low risk cell lines. Accordingly, a recent study reported the capacity of POS phagocytosis to be similar among hiPSC-RPE cell lines derived from AMD patients and unaffected controls (Gong et al., 2020). In contrast, POS degradation in hiPSC-RPE cells from patients with Best Disease, a monogenic degenerative disease of the macula, has been observed to be delayed compared to respective controls (Singh et al., 2013b; Singh et al., 2015).

Results from a previous study have shown that a large part of lipofuscin protein components in the human RPE are modified by the lipid peroxidation product HNE (Schutt et al., 2003). Before combining HNE-modified POS treatment with BL irradiation, the HNE-mediated stabilization of POS against lysosomal degradation demonstrated by Kaemmerer et al., 2007 was verified in the hiPSC-RPE cell lines investigated in this thesis. It is further known, that phagocytosis of modified POS leads to accumulation and storage of undegraded modified proteins and dysfunction of lysosomal degradation and hence induces lipofuscinogenesis in RPE cells (Kaemmerer et al., 2007; Krohne et al., 2010a; Krohne et al., 2010b). Consequently, the phototoxic lipofuscin (Davies et al., 2001) can contribute to RPE damage and AMD pathogenesis.

HNE has been shown to induce NRF2 activation, increase *HMOX1* expression in various cell types and protect them against cytotoxicity induced by oxidative stress (Chen et al., 2005; Ishikado et al., 2010; Huang et al., 2012). Furthermore, photooxidative damage upon BL exposure and subsequent NLRP3 inflammasome activation have been reported to be increased in RPE cells containing accumulated lipofuscin induced by feeding of modified POS (Brandstetter et al., 2015). Hence, the current work investigated whether, in a similar experimental setup, the NRF2-associated oxidative stress response to BL treatment was altered in hiPSC-RPE cells which had previously been incubated with modified POS. Results revealed that pre-treatment with HNE-modified POS for 7 consecutive days did not significantly affect *HMOX1* and *NQO1* mRNA expression in irradiated nor non-irradiated hiPSC-RPE cells in any of the cell lines. Thus, in this case, the additional physiological challenge of POS phagocytosis did not alter the oxidative stress response to the external stressor BL in the hiPSC-RPE cells. Nevertheless, including POS exposure into the analysis further increased the value of the *in vivo* representation of the physiological oxidative stress situation, but of course in a reduced time span. More replicates of the experiment and combinations of POS

feeding and exposure to oxidative stressors would be necessary before making a definitive statement.

5.5 Conclusion

In this study, the effect of the oxidative stressors SI and BL on the NRF2 signaling pathway in hiPSC-RPE cell lines with known genetic susceptibility to AMD was investigated. The *in vitro* data revealed opposite trends with different degrees in *HMOX1* and *NQO1* expression upon SI and BL exposure, indicating that these stressors induce a variable fine-tuning of pathway activation with slightly varying response mechanisms. As high and low risk cell lines did not significantly differ in *HMOX1* and *NQO1* expression, it was concluded that genetic predisposition to AMD does not measurably influence the oxidative stress response associated with the NRF2 signaling pathway. These findings provide a valuable contribution to resolving the implications of oxidative stress in AMD, especially with genetic AMD susceptibility taken into consideration. Furthermore, the reproducible experimental protocols established in the scope of this thesis are available for further research on oxidative stress induction in the hiPSC-RPE cell lines.

6 References

Abokyi, S., To, C. H., Lam, T. T., & Tse, D. Y. (2020). Central Role of Oxidative Stress in Age-Related Macular Degeneration: Evidence from a Review of the Molecular Mechanisms and Animal Models. *Oxidative Medicine and Cellular Longevity*, *2020*, 7901270. https://doi.org/10.1155/2020/7901270

Agrón, E., Mares, J., Clemons, T. E., Swaroop, A., Chew, E. Y., Keenan, T. D. L., & AREDS and AREDS2 Research Groups (2021). Dietary Nutrient Intake and Progression to Late Age-Related Macular Degeneration in the Age-Related Eye Disease Studies 1 and 2. *Ophthalmology*, *128*(3), 425–442. https://doi.org/10.1016/j.ophtha.2020.08.018

Albanes, D., Heinonen, O. P., Huttunen, J. K., Taylor, P. R., Virtamo, J., Edwards, B. K., Haapakoski, J., Rautalahti, M., Hartman, A. M., & Palmgren, J. (1995). Effects of alpha-tocopherol and beta-carotene supplements on cancer incidence in the Alpha-Tocopherol Beta-Carotene Cancer Prevention Study. *The American Journal of Clinical Nutrition*, *62*(6 Suppl), 1427S–1430S. https://doi.org/10.1093/ajcn/62.6.1427S

Al-Zamil, W. M., & Yassin, S. A. (2017). Recent developments in age-related macular degeneration: a review. *Clinical Interventions in Aging*, *12*, 1313–1330. https://doi.org/10.2147/CIA.S143508

Alam, J., & Cook, J. L. (2007). How many transcription factors does it take to turn on the heme oxygenase-1 gene? *American Journal of Respiratory Cell and Molecular Biology*, *36*(2), 166–174. https://doi.org/10.1165/rcmb.2006-0340TR

Ambati, J., Atkinson, J. P., & Gelfand, B. D. (2013). Immunology of age-related macular degeneration. *Nature Reviews. Immunology*, *13*(6), 438–451. https://doi.org/10.1038/nri3459

Ammar, M. J., Hsu, J., Chiang, A., Ho, A. C., & Regillo, C. D. (2020). Age-related macular degeneration therapy: A review. *Current Opinion in Ophthalmology*, *31*(3), 215–221. https://doi.org/10.1097/ICU.0000000000000657

Anderson, D. H., Mullins, R. F., Hageman, G. S., & Johnson, L. V. (2002). A role for local inflammation in the formation of drusen in the aging eye. *American Journal of Ophthalmology*, *134*(3), 411–431. https://doi.org/10.1016/s0002-9394(02)01624-0

Age-Related Eye Disease Study Research Group (2001). A Randomized, Placebo-Controlled, Clinical Trial of High-Dose Supplementation With Vitamins C and E, Beta Carotene, and Zinc for Age-Related Macular Degeneration and Vision Loss: AREDS Report No. 8. *Arch Ophthalmol.*, *119*(10):1417-1436. https://doi.org/10.1001/archopht.119.10.1417

Age-Related Eye Disease Study 2 (AREDS2) Research Group, Chew, E. Y., Clemons, T. E., Sangiovanni, J. P., Danis, R. P., Ferris, F. L., 3rd, Elman, M. J., Antoszyk, A. N., Ruby, A. J., Orth, D., Bressler, S. B., Fish, G. E., Hubbard, G. B., Klein, M. L., Chandra, S. R., Blodi, B. A., Domalpally, A., Friberg, T., Wong, W. T., Rosenfeld, P. J., … Sperduto, R. D. (2014). Secondary analyses of the effects of lutein/zeaxanthin on age-related macular degeneration progression: AREDS2 report No. 3. *JAMA Ophthalmology*, *132*(2), 142–149. https://doi.org/10.1001/jamaophthalmol.2013.7376

Beatty, S., Koh, H., Phil, M., Henson, D., & Boulton, M. (2000). The role of oxidative stress in the pathogenesis of age-related macular degeneration. *Survey of Ophthalmology*, *45*(2), 115–134. https://doi.org/10.1016/s0039-6257(00)00140-5

Benjamini, Y., & Hochberg, Y. (1995). Controlling the false discovery rate: a practical and powerful approach to multiple testing. *Journal of the Royal Statistical Society: Series B (Methodolical)*, *57*(1), 289–300. https://doi.org/10.1111/j.2517-6161.1995.tb02031.x

Bhutto, I. A., Baba, T., Merges, C., Juriasinghani, V., McLeod, D. S., & Lutty, G. A. (2011). C-reactive protein and complement factor H in aged human eyes and eyes with age-related macular degeneration. *The British Journal of Ophthalmology*, *95*(9), 1323–1330. https://doi.org/10.1136/bjo.2010.199216

Bhutto, I., & Lutty, G. (2012). Understanding age-related macular degeneration (AMD): Relationships between the photoreceptor/retinal pigment epithelium/Bruch's membrane/choriocapillaris complex. *Molecular Aspects of Medicine*, *33*(4), 295–317. https://doi.org/https://doi.org/10.1016/j.mam.2012.04.005

Bonilha, V. L. (2014). Retinal pigment epithelium (RPE) cytoskeleton in vivo and in vitro. *Experimental Eye Research*, *126*, 38–45. https://doi.org/10.1016/J.EXER.2013.09.015

Boulton, M., & Dayhaw-Barker, P. (2001). The role of the retinal pigment epithelium: topographical variation and ageing changes. *Eye (London, England)*, *15*(Pt 3), 384–389. https://doi.org/10.1038/eye.2001.141

Brandl, C., Zimmermann, S. J., Milenkovic, V. M., Rosendahl, S. M., Grassmann, F., Milenkovic, A., Hehr, U., Federlin, M., Wetzel, C. H., Helbig, H., & Weber, B. H. F. (2014). In-depth characterisation of Retinal Pigment Epithelium (RPE) cells derived from human induced pluripotent stem cells (hiPSC). *Neuromolecular Medicine*, *16*(3), 551–564. https://doi.org/10.1007/s12017-014-8308-8

Brandl, C., Grassmann, F., Riolfi, J., & Weber, B. H. F. (2015). Tapping Stem Cells to Target AMD: Challenges and Prospects. *Journal of Clinical Medicine*, *4*(2), 282–303. https://doi.org/10.3390/jcm4020282

Brandl, C., Breinlich, V., Stark, K. J., Enzinger, S., Aßenmacher, M., Olden, M., Grassmann, F., Graw, J., Heier, M., Peters, A., Helbig, H., Küchenhoff, H., Weber, B. H. F., & Heid, I. M. (2016). Features of Age-Related Macular Degeneration in the General Adults and Their Dependency on Age, Sex, and Smoking: Results from the German KORA Study. *PloS ONE*, *11*(11), e0167181. https://doi.org/10.1371/journal.pone.0167181

Brandl, C., Zimmermann, M. E., Günther, F., Barth, T., Olden, M., Schelter, S. C., Kronenberg, F., Loss, J., Küchenhoff, H., Helbig, H., Weber, B. H. F., Stark, K. J., & Heid, I. M. (2018). On the impact of different approaches to classify age-related macular degeneration: Results from the German AugUR study. *Scientific Reports*, *8*(1), 8675. https://doi.org/10.1038/s41598-018-26629-5

Brandl, C., Brücklmayer, C., Günther, F., Zimmermann, M. E., Küchenhoff, H., Helbig, H., Weber, B. H. F., Heid, I. M., & Stark, K. J. (2019). Retinal Layer Thicknesses in Early Age-Related Macular Degeneration: Results From the German AugUR Study. *Investigative Ophthalmology & Visual Science*, *60*(5), 1581–1594. https://doi.org/10.1167/iovs.18-25332

Brandl, C., Günther, F., Zimmermann, M. E., Hartmann, K. I., Eberlein, G., Barth, T., Winkler, T. W., Linkohr, B., Heier, M., Peters, A., Li, J. Q., Finger, R. P., Helbig, H., Weber, B. H. F., Küchenhoff, H., Mueller, A., Stark, K. J., & Heid, I. M. (2022). Incidence, progression and risk factors of age-related macular degeneration in 35-95-year-old individuals from three jointly designed German cohort studies. *BMJ open Ophthalmology*, *7*(1), e000912. https://doi.org/10.1136/bmjophth-2021-000912

Brandstetter, C., Mohr, L. K., Latz, E., Holz, F. G., & Krohne, T. U. (2015). Light induces NLRP3 inflammasome activation in retinal pigment epithelial cells via lipofuscin-mediated photooxidative damage. *Journal of Molecular Medicine (Berlin, Germany)*, *93*(8), 905–916. https://doi.org/10.1007/s00109-015-1275-1

Bressler, S. B., Muñoz, B., Solomon, S. D., & West, S. K. (2008). Racial Differences in the Prevalence of Age-Related Macular Degeneration. *Archives of Ophthalmology*, *126*(2), 241. https://doi.org/10.1001/archophthalmol.2007.53

Brown, G. C., Brown, M. M., Sharma, S., Stein, J. D., Roth, Z., Campanella, J., & Beauchamp, G. R. (2005). The burden of age-related macular degeneration: a value-based medicine analysis. *Transactions of the American Ophthalmological Society*, *103,* 173–186.

Byeon, S. H., Lee, S. C., Choi, S. H., Lee, H. K., Lee, J. H., Chu, Y. K., & Kwon, O. W. (2010). Vascular endothelial growth factor as an autocrine survival factor for retinal pigment epithelial cells under oxidative stress via the VEGF-R2/PI3K/Akt. *Investigative Ophthalmology & Visual Science*, *51*(2), 1190–1197. https://doi.org/10.1167/iovs.09-4144

Cai, X., & McGinnis, J. F. (2012). Oxidative stress: the achilles' heel of neurodegenerative diseases of the retina. *Frontiers in Bioscience (Landmark edition), 17*(5), 1976–1995. https://doi.org/10.2741/4033

Campochiaro, P. A., Soloway, P., Ryan, S. J., & Miller, J. W. (1999). The pathogenesis of choroidal neovascularization in patients with age-related macular degeneration. *Molecular Vision*, *5*, 34.

Cano, M., Thimmalappula, R., Fujihara, M., Nagai, N., Sporn, M., Wang, A. L., Neufeld, A. H., Biswal, S., & Handa, J. T. (2010). Cigarette smoking, oxidative stress, the anti-oxidant response through Nrf2 signaling, and Age-related Macular Degeneration. *Vision Research*, *50*(7), 652–664. https://doi.org/10.1016/j.visres.2009.08.018

Cao, S., Walker, G. B., Wang, X., Cui, J. Z., & Matsubara, J. A. (2013). Altered cytokine profiles of human retinal pigment epithelium: oxidant injury and replicative senescence. *Molecular Vision*, *19*, 718–728.

Carrasco, J., Pietsch, G. A., Nicolas, M. P., Koerber, C., Bennison, C., & Yoon, J. (2020). Real-World Effectiveness and Real-World Cost-Effectiveness of Intravitreal Aflibercept and Intravitreal Ranibizumab in Neovascular Age-Related Macular Degeneration: Systematic Review and Meta-Analysis of Real-World Studies. *Advances in Therapy*, *37*(1), 300–315. https://doi.org/10.1007/s12325-019-01147-6

Chan, C. M., Huang, D. Y., Sekar, P., Hsu, S. H., & Lin, W. W. (2019). Reactive oxygen species-dependent mitochondrial dynamics and autophagy confer protective effects in retinal pigment epithelial cells against sodium iodate-induced cell death. *Journal of Biomedical Science*, *26*(1), 40. https://doi.org/10.1186/s12929-019-0531-z

Chang, Y. C., Chang, W. C., Hung, K. H., Yang, D. M., Cheng, Y. H., Liao, Y. W., Woung, L. C., Tsai, C. Y., Hsu, C. C., Lin, T. C., Liu, J. H., Chiou, S. H., Peng, C. H., & Chen, S. J. (2014). The generation of induced pluripotent stem cells for macular degeneration as a drug screening platform: identification of curcumin as a protective agent for retinal pigment epithelial cells against oxidative stress. *Frontiers in Aging Neuroscience*, *6*, 191. https://doi.org/10.3389/fnagi.2014.00191

Chappelow, A. V., & Kaiser, P. K. (2008). Neovascular age-related macular degeneration: Potential therapies. *Drugs*, *68*(8), 1029–1036. https://doi.org/10.2165/00003495-200868080-00002

Chen, X. L., & Kunsch, C. (2004). Induction of Cytoprotective Genes Through Nrf2 / Antioxidant Response Element Pathway: A New Therapeutic Approach for the Treatment of Inflammatory Diseases. *Current Pharmaceutical Design*, *10*(8), 879–891. https://doi.org/10.2174/1381612043452901

Chen, Z. H., Saito, Y., Yoshida, Y., Sekine, A., Noguchi, N., & Niki, E. (2005). 4-Hydroxynonenal induces adaptive response and enhances PC12 cell tolerance primarily through induction of thioredoxin reductase 1 via activation of Nrf2. *Journal of Biological Chemistry*, *280*(51), 41921–41927. https://doi.org/10.1074/jbc.M508556200

Chen, Y., Bedell, M., & Zhang, K. (2010). Age-related macular degeneration: genetic and environmental factors of disease. *Molecular Interventions*, *10*(5), 271–281. https://doi.org/10.1124/mi.10.5.4

Chen, S., Popp, N. A., & Chan, C. C. (2014). Animal models of age-related macular degeneration and their translatability into the clinic. *Expert Review of Ophthalmology*, *9*(4), 285–295. https://doi.org/10.1586/17469899.2014.939171

Chen, S., Einspanier, R., & Schoen, J. (2015). Transepithelial electrical resistance (TEER): a functional parameter to monitor the quality of oviduct epithelial cells cultured on filter supports. *Histochemistry and Cell Biology*, *144*(5), 509–515. https://doi.org/10.1007/s00418-015-1351-1

Chen, W. J., Wu, C., Xu, Z., Kuse, Y., Hara, H., & Duh, E. J. (2017). Nrf2 protects photoreceptor cells from photo-oxidative stress induced by blue light. *Experimental Eye Research*, *154*, 151–158. https://doi.org/10.1016/j.exer.2016.12.001

Chen, P., Lai, Z., Wu, Y., Xu, L., Cai, X., Qiu, J., Yang, P., Yang, M., Zhou, P., Zhuang, J., Ge, J., Yu, K., & Zhuang, J. (2019). Retinal Neuron Is More Sensitive to Blue Light-Induced Damage than Glia Cell Due to DNA Double-Strand Breaks. *Cells*, *8*(1), 68. https://doi.org/10.3390/cells8010068

Chew, E. Y., Clemons, T. E., Agrón, E., Domalpally, A., Keenan, T. D. L., Vitale, S., Weber, C., Smith, D. C., Christen, W., & AREDS2 Research Group (2022). Long-term Outcomes of Adding Lutein/Zeaxanthin and ω-3 Fatty Acids to the AREDS Supplements on Age-Related Macular Degeneration Progression: AREDS2 Report 28. *JAMA Ophthalmology*, *140*(7), 692–698. https://doi.org/10.1001/jamaophthalmol.2022.1640

Cimarolli, V. R., Casten, R. J., Rovner, B. W., Heyl, V., Sörensen, S., & Horowitz, A. (2016). Anxiety and depression in patients with advanced macular degeneration: Current perspectives. *Clinical Ophthalmology*, *10*, 55–63. https://doi.org/10.2147/OPTH.S80489

Crabb, J. W., Miyagi, M., Gu, X., Shadrach, K., West, K. A., Sakaguchi, H., Kamei, M., Hasan, A., Yan, L., Rayborn, M. E., Salomon, R. G., & Hollyfield, J. G. (2002). Drusen proteome analysis: An approach to the etiology of age-related macular degeneration. *Proceedings of the National Academy of Sciences of the United States of America*, *99*(23), 14682–14687. https://doi.org/10.1073/pnas.222551899

Cruess, A. F., Zlateva, G., Xu, X., Soubrane, G., Pauleikhoff, D., Lotery, A., Mones, J., Buggage, R., Schaefer, C., Knight, T., & Goss, T. F. (2008). Economic burden of bilateral neovascular age-related macular degeneration: Multi-country observational study. *PharmacoEconomics*, *26*(1), 57–73. https://doi.org/10.2165/00019053-200826010-00006

Curcio, C. A., Presley, J. B., Malek, G., Medeiros, N. E., Avery, D. V., & Kruth, H. S. (2005). Esterified and unesterified cholesterol in drusen and basal deposits of eyes with age-related maculopathy. *Experimental Eye Research*, *81*(6), 731–741. https://doi.org/10.1016/j.exer.2005.04.012

Dalvi, S., Galloway, C. A., Winschel, L., Hashim, A., Soto, C., Tang, C., MacDonald, L. A., & Singh, R. (2019). Environmental stress impairs photoreceptor outer segment (POS) phagocytosis and degradation and induces autofluorescent material accumulation in hiPSC-RPE cells. *Cell Death Discovery*, *5*, 96. https://doi.org/10.1038/s41420-019-0171-9

Datta, S., Cano, M., Ebrahimi, K., Wang, L., & Handa, J. T. (2017). The impact of oxidative stress and inflammation on RPE degeneration in non-neovascular AMD. *Progress in Retinal and Eye Research*, *60*, 201–218. https://doi.org/10.1016/j.preteyeres.2017.03.002

Davies, S., Elliott, M. H., Floor, E., Truscott, T. G., Zareba, M., Sarna, T., Shamsi, F. A., & Boulton, M. E. (2001). Photocytotoxicity of lipofuscin in human retinal pigment epithelial cells. *Free Radical Biology & Medicine*, *31*(2), 256–265. https://doi.org/10.1016/s0891-5849(01)00582-2

Di Carlo, E., & Augustin, A. J. (2021). Prevention of the Onset of Age-Related Macular Degeneration. *Journal of Clinical Medicine*, *10*(15), 3297. https://doi.org/10.3390/jcm10153297

Doyle, S. L., Campbell, M., Ozaki, E., Salomon, R. G., Mori, A., Kenna, P. F., Farrar, G. J., Kiang, A. S., Humphries, M. M., Lavelle, E. C., O'Neill, L. A., Hollyfield, J. G., & Humphries, P. (2012). NLRP3 has a protective role in age-related macular degeneration through the induction of IL-18 by drusen components. *Nature Medicine*, *18*(5), 791–798. https://doi.org/10.1038/nm.2717

Du, W., An, Y., He, X., Zhang, D., & He, W. (2018). Protection of Kaempferol on Oxidative Stress-Induced Retinal Pigment Epithelial Cell Damage. *Oxidative Medicine and Cellular Longevity, 2018*, 1610751. https://doi.org/10.1155/2018/1610751

Dunn, K. C., Aotaki-Keen, A. E., Putkey, F. R., & Hjelmeland, L. M. (1996). ARPE-19, a human retinal pigment epithelial cell line with differentiated properties. *Experimental Eye Research*, *62*(2), 155–170. https://doi.org/10.1006/exer.1996.0020

Ebrahimi, K. B., Fijalkowski, N., Cano, M., & Handa, J. T. (2013). Decreased membrane complement regulators in the retinal pigmented epithelium contributes to age-related macular degeneration. *The Journal of Pathology*, *229*(5), 729–742. https://doi.org/10.1002/path.4128

Enzmann, V., Row, B. W., Yamauchi, Y., Kheirandish, L., Gozal, D., Kaplan, H. J., & McCall, M. A. (2006). Behavioral and anatomical abnormalities in a sodium iodate-induced model of retinal pigment epithelium degeneration. *Experimental Eye Research*, *82*(3), 441–448. https://doi.org/10.1016/j.exer.2005.08.002

Fabre, M., Mateo, L., Lamaa, D., Baillif, S., Pagès, G., Demange, L., Ronco, C., & Benhida, R. (2022). Recent Advances in Age-Related Macular Degeneration Therapies. *Molecules (Basel, Switzerland)*, *27*(16), 5089. https://doi.org/10.3390/molecules27165089

Feeney-Burns, L., Hilderbrand, E. S., & Eldridge, S. (1984). Aging human RPE: morphometric analysis of macular, equatorial, and peripheral cells. *Investigative Ophthalmology & Visual Science*, *25*(2), 195–200.

Ferris, F. L., 3rd, Fine, S. L., & Hyman, L. (1984). Age-related macular degeneration and blindness due to neovascular maculopathy. *Archives of Ophthalmology (Chicago, Ill. : 1960)*, *102*(11), 1640–1642. https://doi.org/10.1001/archopht.1984.01040031330019

Ferris, F. L., 3rd, Wilkinson, C. P., Bird, A., Chakravarthy, U., Chew, E., Csaky, K., Sadda, S. R., & Beckman Initiative for Macular Research Classification Committee (2013). Clinical classification of age-related macular degeneration. *Ophthalmology*, *120*(4), 844–851. https://doi.org/10.1016/j.ophtha.2012.10.036

Fleckenstein, M., Keenan, T. D. L., Guymer, R. H., Chakravarthy, U., Schmitz-Valckenberg, S., Klaver, C. C., Wong, W. T., & Chew, E. Y. (2021). Age-related macular degeneration. *Nature reviews. Disease primers*, *7*(1), 31. https://doi.org/10.1038/s41572-021-00265-2

Forest, D. L., Johnson, L. V., & Clegg, D. O. (2015). Cellular models and therapies for age-related macular degeneration. *DMM Disease Models and Mechanisms*, *8*(5), 421–427. https://doi.org/10.1242/dmm.017236

Frampton, J. E. (2013). Ranibizumab: A review of its use in the treatment of neovascular age-related macular degeneration. *Drugs and Aging*, *30*(5), 331–358. https://doi.org/10.1007/s40266-013-0077-9

Fritsche, L. G., Chen, W., Schu, M., Yaspan, B. L., Yu, Y., Thorleifsson, G., Zack, D. J., Arakawa, S., Cipriani, V., Ripke, S., Igo, R. P., Jr, Buitendijk, G. H., Sim, X., Weeks, D. E., Guymer, R. H., Merriam, J. E., Francis, P. J., Hannum, G., Agarwal, A., Armbrecht, A. M., … AMD Gene Consortium (2013). Seven new loci associated with age-related macular degeneration. *Nature Genetics*, *45*(4), 433–439e4392. https://doi.org/10.1038/ng.2578

Fritsche, L. G., Fariss, R. N., Stambolian, D., Abecasis, G. R., Curcio, C. A., & Swaroop, A. (2014). Age-related macular degeneration: genetics and biology coming together. *Annual Review of Genomics and Human Genetics, 15*, 151–171. https://doi.org/10.1146/annurev-genom-090413-025610

Fritsche, L. G., Igl, W., Bailey, J. N. C., Grassmann, F., Sengupta, S., Bragg-Gresham, J. L., … Heid, I. M. (2016). A large genome-wide association study of age-related macular degeneration highlights contributions of rare and common variants. *Nature Genetics*, *48*(2), 134–143. https://doi.org/10.1038/ng.3448

Gao, J., Liu, R. T., Cao, S., Cui, J. Z., Wang, A., To, E., & Matsubara, J. A. (2015). NLRP3 inflammasome: activation and regulation in age-related macular degeneration. *Mediators of Inflammation*, *2015*, 690243. https://doi.org/10.1155/2015/690243

Garcia, T. Y., Gutierrez, M., Reynolds, J., & Lamba, D. A. (2015). Modeling the Dynamic AMD-Associated Chronic Oxidative Stress Changes in Human ESC and iPSC-Derived RPE Cells. *Investigative Opthalmology & Visual Science*, *56*(12), 7480. https://doi.org/10.1167/iovs.15-17251

Gass J. D. (1972). Drusen and disciform macular detachment and degeneration. *Transactions of the American Ophthalmological Society*, *70*, 409–436.

GBD 2019 Blindness and Vision Impairment Collaborators, & Vision Loss Expert Group of the Global Burden of Disease Study (2021). Causes of blindness and vision impairment in 2020 and trends over 30 years, and prevalence of avoidable blindness in relation to VISION 2020: the Right to Sight: an analysis for the Global Burden of Disease Study. *The Lancet. Global health*, *9*(2), e144–e160. https://doi.org/10.1016/S2214-109X(20)30489-7

Golestaneh, N., Chu, Y., Cheng, S. K., Cao, H., Poliakov, E., & Berinstein, D. M. (2016). Repressed sirt1/pgc-1α pathway and mitochondrial disintegration in ipsc-derived rpe disease model of age-related macular degeneration. *Journal of Translational Medicine*, *14*(1), 1–17. https://doi.org/10.1186/s12967-016-1101-8

Gong, J., Cai, H., Noggle, S., Paull, D., Rizzolo, L. J., Del Priore, L. V., & Fields, M. A. (2020). Stem cell-derived retinal pigment epithelium from patients with age-related macular degeneration exhibit reduced metabolism and matrix interactions. *Stem Cells Translational Medicine*, *9*(3), 364–376. https://doi.org/10.1002/sctm.19-0321

Gorusupudi, A., Nelson, K., & Bernstein, P. S. (2017). The age-related eye disease 2 study: Micronutrients in the treatment of macular degeneration. *Advances in Nutrition*, *8*(1), 40–53. https://doi.org/10.3945/an.116.013177

Grassmann, F., Fritsche, L. G., Keilhauer, C. N., Heid, I. M., & Weber, B. H. F. (2012). Modelling the genetic risk in age-related macular degeneration. *PloS ONE*, *7*(5), e37979. https://doi.org/10.1371/journal.pone.0037979

Grassmann, F., Ach, T., Brandl, C., Heid, I. M., & Weber, B. H. F. (2015). What Does Genetics Tell Us About Age-Related Macular Degeneration? *Annual Review of Vision Science*, *1*(1), 73–96. https://doi.org/10.1146/annurev-vision-082114-035609 (a)

Grassmann, F., Fauser, S., & Weber, B. H. F. (2015). The genetics of age-related macular degeneration (AMD) - Novel targets for designing treatment options? *European Journal of Pharmaceutics and Biopharmaceutics*, *95*, 194–202. https://doi.org/10.1016/j.ejpb.2015.04.039 (b)

Green, W. R., McDonnell, P. J., & Yeo, J. H. (1985). Pathologic features of senile macular degeneration. *Ophthalmology*, *92*(5), 615–627. https://doi.org/10.1016/S0161-6420(85)33993-3

Grossniklaus, H. E., & Green, W. R. (2004). Choroidal neovascularization. *American Journal of Ophthalmology*, *137*(3), 496–503. https://doi.org/10.1016/j.ajo.2003.09.042

Guimaraes, T. A. C., Georgiou, M., Bainbridge, J. W. B., & Michaelides, M. (2021). Gene therapy for neovascular age-related macular degeneration: rationale, clinical trials and future directions. *The British Journal of Ophthalmology*, *105*(2), 151–157. https://doi.org/10.1136/bjophthalmol-2020-316195

Hageman, G. S., Luthert, P. J., Victor Chong, N. H., Johnson, L. V., Anderson, D. H., & Mullins, R. F. (2001). An integrated hypothesis that considers drusen as biomarkers of immune-mediated processes at the RPE-Bruch's membrane interface in aging and age-related macular degeneration. *Progress in Retinal and Eye Research*, *20*(6), 705–732. https://doi.org/10.1016/S1350-9462(01)00010-6

Hanus, J., Kolkin, A., Chimienti, J., Botsay, S., & Wang, S. (2015). 4-Acetoxyphenol Prevents RPE Oxidative Stress-Induced Necrosis by Functioning as an NRF2 Stabilizer. *Investigative Ophthalmology & Visual Science*, *56*(9), 5048–5059. https://doi.org/10.1167/iovs.15-16401

Hanus, J., Anderson, C., Sarraf, D., Ma, J., & Wang, S. (2016). Retinal pigment epithelial cell necroptosis in response to sodium iodate. *Cell Death Discovery*, *2*, 16054. https://doi.org/10.1038/cddiscovery.2016.54

Harada, H., Sugimoto, R., Watanabe, A., Taketani, S., Okada, K., Warabi, E., Siow, R., Itoh, K., Yamamoto, M., & Ishii, T. (2008). Differential roles for Nrf2 and AP-1 in upregulation of HO-1 expression by arsenite in murine embryonic fibroblasts. *Free Radical Research*, *42*(4), 297–304. https://doi.org/10.1080/10715760801975735

Hazim, R. A., Karumbayaram, S., Jiang, M., Dimashkie, A., Lopes, V. S., Li, D., Burgess, B. L., Vijayaraj, P., Alva-Ornelas, J. A., Zack, J. A., Kohn, D. B., Gomperts, B. N., Pyle, A. D., Lowry, W. E., & Williams, D. S. (2017). Differentiation of RPE cells from integration-free iPS cells and their cell biological characterization. *Stem Cell Research & Therapy*, *8*(1), 217. https://doi.org/10.1186/s13287-017-0652-9

Heier, J. S., Khanani, A. M., Quezada Ruiz, C., Basu, K., Ferrone, P. J., Brittain, C., Figueroa, M. S., Lin, H., Holz, F. G., Patel, V., Lai, T. Y. Y., Silverman, D., Regillo, C., Swaminathan, B., Viola, F., Cheung, C. M. G., Wong, T. Y., & TENAYA and LUCERNE Investigators (2022). Efficacy, durability, and safety of intravitreal faricimab up to every 16 weeks for neovascular age-related macular degeneration (TENAYA and LUCERNE): two randomised, double-masked, phase 3, non-inferiority trials. *Lancet (London, England)*, *399*(10326), 729–740. https://doi.org/10.1016/S0140-6736(22)00010-1

Holekamp, N. M., Campochiaro, P. A., Chang, M. A., Miller, D., Pieramici, D., Adamis, A. P., Brittain, C., Evans, E., Kaufman, D., Maass, K. F., Patel, S., Ranade, S., Singh, N., Barteselli, G., Regillo, C., & all Archway Investigators (2022). Archway Randomized Phase 3 Trial of the Port Delivery System with Ranibizumab for Neovascular Age-Related Macular Degeneration. *Ophthalmology*, *129*(3), 295–307. https://doi.org/10.1016/j.ophtha.2021.09.016

Holz, F. G., Strauss, E. C., Schmitz-Valckenberg, S., & Van Lookeren Campagne, M. (2014). Geographic atrophy: Clinical features and potential therapeutic approaches. *Ophthalmology*, *121*(5), 1079–1091. https://doi.org/10.1016/j.ophtha.2013.11.023

Hornof, M., Toropainen, E., & Urtti, A. (2005). Cell culture models of the ocular barriers. *European Journal of Pharmaceutics and Biopharmaceutics*, *60*(2), 207–225. https://doi.org/10.1016/j.ejpb.2005.01.009

Huang, H. C., Nguyen, T., & Pickett, C. B. (2002). Phosphorylation of Nrf2 at Ser-40 by protein kinase C regulates antioxidant response element-mediated transcription. The *Journal of Biological Chemistry*, *277*(45), 42769–42774. https://doi.org/10.1074/jbc.M206911200

Huang, Y., Li, W., & Kong, A. N. (2012). Anti-oxidative stress regulator NF-E2-related factor 2 mediates the adaptive induction of antioxidant and detoxifying enzymes by lipid peroxidation metabolite 4-hydroxynonenal. *Cell & Bioscience*, *2*(1), 40. https://doi.org/10.1186/2045-3701-2-40

Huang, Y., Li, W., Su, Z. Y., & Kong, A. N. (2015). The complexity of the Nrf2 pathway: Beyond the antioxidant response. *The Journal of Nutritional Biochemistry*, *26*(12), 1401–1413. https://doi.org/10.1016/j.jnutbio.2015.08.001

Ildefonso, C. J., Biswal, M. R., Ahmed, C. M., & Lewin, A. S. (2016). The NLRP3 Inflammasome and its Role in Age-Related Macular Degeneration. *Advances in Experimental Medicine and Biology*, *854*, 59–65. https://doi.org/10.1007/978-3-319-17121-0_9

Immenschuh, S., & Ramadori, G. (2000). Gene regulation of heme oxygenase-1 as a therapeutic target. *Biochemical Pharmacology*, *60*(8), 1121–1128. https://doi.org/10.1016/S0006-2952(00)00443-3

International Commission on Non-Ionizing Radiation Protection (ICNIRP) (2020). Light-Emitting Diodes (LEDS): Implications for Safety. *Health Physics*, *118*(5), 549–561. https://doi.org/10.1097/HP.0000000000001259

Ishikado, A., Nishio, Y., Morino, K., Ugi, S., Kondo, H., Makino, T., Kashiwagi, A., & Maegawa, H. (2010). Low concentration of 4-hydroxy hexenal increases heme oxygenase-1 expression through activation of Nrf2 and antioxidative activity in vascular endothelial cells. *Biochemical and Biophysical Research Communications*, *402*(1), 99–104. https://doi.org/10.1016/j.bbrc.2010.09.124

Itoh, K., Chiba, T., Takahashi, S., Ishii, T., Igarashi, K., Katoh, Y., Oyake, T., Hayashi, N., Satoh, K., Hatayama, I., Yamamoto, M., & Nabeshima, Y. (1997). An Nrf2/small Maf heterodimer mediates the induction of phase II detoxifying enzyme genes through antioxidant response elements. *Biochemical and Biophysical Research Communications*, *236*(2), 313–322. https://doi.org/10.1006/bbrc.1997.6943

Jadeja, R. N., Jones, M. A., Abdelrahman, A. A., Powell, F. L., Thounaojam, M. C., Gutsaeva, D., Bartoli, M., & Martin, P. M. (2020). Inhibiting microRNA-144 potentiates Nrf2-dependent antioxidant signaling in RPE and protects against oxidative stress-induced outer retinal degeneration. *Redox Biology*, *28*, 101336. https://doi.org/10.1016/j.redox.2019.101336

Jager, R. D., Mieler, W. F., & Miller, J. W. (2008). Age-related macular degeneration. *New England Journal of Medicine*, *358*(24), 2606. https://doi.org/10.1056/NEJMra0801537

Jakobsdottir, J., Conley, Y. P., Weeks, D. E., Mah, T. S., Ferrell, R. E., & Gorin, M. B. (2005). Susceptibility genes for age-related maculopathy on chromosome 10q26. *American Journal of Human Genetics*, *77*(3), 389–407. https://doi.org/10.1086/444437

Jarrett, S. G., & Boulton, M. E. (2012). Consequences of oxidative stress in age-related macular degeneration. *Molecular Aspects of Medicine*, *33*(4), 399–417. https://doi.org/10.1016/j.mam.2012.03.009

Jin, Z. B., Okamoto, S., Osakada, F., Homma, K., Assawachananont, J., Hirami, Y., Iwata, T., & Takahashi, M. (2011). Modeling retinal degeneration using patient-specific induced pluripotent stem cells. *PloS ONE*, *6*(2), e17084. https://doi.org/10.1371/journal.pone.0017084

Johnson, L. V., Leitner, W. P., Rivest, A. J., Staples, M. K., Radeke, M. J., & Anderson, D. H. (2002). The Alzheimer's Aβ-peptide is deposited at sites of complement activation in pathologic deposits associated with aging and age-related macular degeneration. *Proceedings of the National Academy of Sciences of the United States of America*, *99*(18), 11830–11835. https://doi.org/10.1073/pnas.192203399

Juel, H. B., Faber, C., Svendsen, S. G., Vallejo, A. N., & Nissen, M. H. (2013). Inflammatory cytokines protect retinal pigment epithelial cells from oxidative stress-induced death. *PloS ONE*, *8*(5), e64619. https://doi.org/10.1371/journal.pone.0064619

Kaemmerer, E., Schutt, F., Krohne, T. U., Holz, F. G., & Kopitz, J. (2007). Effects of Lipid Peroxidation-Related Protein Modifications on RPE Lysosomal Functions and POS Phagocytosis. *Investigative Opthalmology & Visual Science*, *48*(3), 1342. https://doi.org/10.1167/iovs.06-0549

Kaiser, P. K., Schmitz-Valckenberg, M. S., & Holz, F. G. (2022). ANTI-VASCULAR ENDOTHELIAL GROWTH FACTOR BIOSIMILARS IN OPHTHALMOLOGY. *Retina (Philadelphia, Pa.)*, *42*(12), 2243–2250. https://doi.org/10.1097/IAE.0000000000003626

Kannan, R., Zhang, N., Sreekumar, P. G., Spee, C. K., Rodriguez, A., Barron, E., & Hinton, D. R. (2006). Stimulation of apical and basolateral vascular endothelial growth factor-A and vascular endothelial growth factor-C secretion by oxidative stress in polarized retinal pigment epithelial cells. *Molecular Vision*, *12*, 1649–1659.

Kannan, R., & Hinton, D. R. (2014). Sodium iodate induced retinal degeneration: New insights from an old model. *Neural Regeneration Research*, *9*(23), 2044–2045. https://doi.org/10.4103/1673-5374.147927

Kauppinen, A., Niskanen, H., Suuronen, T., Kinnunen, K., Salminen, A., & Kaarniranta, K. (2012). Oxidative stress activates NLRP3 inflammasomes in ARPE-19 cells—Implications for age-related macular degeneration (AMD). *Immunology Letters*, *147*(1–2), 29–33. https://doi.org/10.1016/J.IMLET.2012.05.005

Kensler, T. W., Wakabayashi, N., & Biswal, S. (2007). Cell survival responses to environmental stresses via the Keap1-Nrf2-ARE pathway. *Annual Review of Pharmacology and Toxicology*, *47*, 89–116. https://doi.org/10.1146/annurev.pharmtox.46.120604.141046

Kevany, B. M., & Palczewski, K. (2010). Phagocytosis of retinal rod and cone photoreceptors. *Physiology (Bethesda, Md.)*, *25*(1), 8–15. https://doi.org/10.1152/physiol.00038.2009

Khanna, S., Komati, R., Eichenbaum, D. A., Hariprasad, I., Ciulla, T. A., & Hariprasad, S. M. (2019). Current and upcoming anti-VEGF therapies and dosing strategies for the

treatment of neovascular AMD: A comparative review. *BMJ Open Ophthalmology*, *4*(1), 1–8. https://doi.org/10.1136/bmjophth-2019-000398

Kiel, C., Nebauer, C. A., Strunz, T., Stelzl, S., & Weber, B. H. F. (2021). Epistatic interactions of genetic loci associated with age-related macular degeneration. *Scientific Reports*, *11*(1), 13114. https://doi.org/10.1038/s41598-021-92351-4

Kim, C. (2014). Disease modeling and cell based therapy with iPSC: Future therapeutic option with fast and safe application. *Blood Research*, *49*(1), 7–14. https://doi.org/10.5045/br.2014.49.1.7

Kim, S., Kim, Y. J., Kim, N. R., & Chin, H. S. (2015). Effects of Bevacizumab on Bcl-2 Expression and Apoptosis in Retinal Pigment Epithelial Cells under Oxidative Stress. *Korean Journal of Ophthalmology : KJO*, *29*(6), 424–432. https://doi.org/10.3341/kjo.2015.29.6.424

Kiuchi, K., Yoshizawa, K., Shikata, N., Moriguchi, K., & Tsubura, A. (2002). Morphologic characteristics of retinal degeneration induced by sodium iodate in mice. *Current Eye Research*, *25*(6), 373–379. https://doi.org/10.1076/ceyr.25.6.373.14227

Klein, R. J., Zeiss, C., Chew, E. Y., Tsai, J. Y., Sackler, R. S., Haynes, C., Henning, A. K., SanGiovanni, J. P., Mane, S. M., Mayne, S. T., Bracken, M. B., Ferris, F. L., Ott, J., Barnstable, C., & Hoh, J. (2005). Complement factor H polymorphism in age-related macular degeneration. *Science (New York, N.Y.)*, *308*(5720), 385–389. https://doi.org/10.1126/science.1109557

Krohne, T. U., Stratmann, N. K., Kopitz, J., & Holz, F. G. (2010). Effects of lipid peroxidation products on lipofuscinogenesis and autophagy in human retinal pigment epithelial cells. *Experimental Eye Research*, *90*(3), 465–471. https://doi.org/10.1016/J.EXER.2009.12.011 (a)

Krohne, T. U., Kaemmerer, E., Holz, F. G., & Kopitz, J. (2010). Lipid peroxidation products reduce lysosomal protease activities in human retinal pigment epithelial cells via two different mechanisms of action. *Experimental Eye Research*, *90*(2), 261–266. https://doi.org/10.1016/j.exer.2009.10.014 (b)

Lambert, N. G., ElShelmani, H., Singh, M. K., Mansergh, F. C., Wride, M. A., Padilla, M., Keegan, D., Hogg, R. E., & Ambati, B. K. (2016). Risk factors and biomarkers of age-related macular degeneration. *Progress in Retinal and Eye Research*, *54*, 64–102. https://doi.org/10.1016/j.preteyeres.2016.04.003

Lambros, M. L., & Plafker, S. M. (2016). Oxidative Stress and the Nrf2 Anti-Oxidant Transcription Factor in Age-Related Macular Degeneration. *Advances in Experimental Medicine and Biology*, *854*, 67–72. https://doi.org/10.1007/978-3-319-17121-0_10

Lever, J. M., Boddu, R., George, J. F., & Agarwal, A. (2016). Heme oxygenase-1 in kidney health and disease. *Antioxidants and Redox Signaling*, *25*(3), 165–183. https://doi.org/10.1089/ars.2016.6659

Li, J. Q., Welchowski, T., Schmid, M., Mauschitz, M. M., Holz, F. G., & Finger, R. P. (2020). Prevalence and incidence of age-related macular degeneration in Europe: a systematic review and meta-analysis. *The British Journal of Ophthalmology*, *104*(8), 1077–1084. https://doi.org/10.1136/bjophthalmol-2019-314422

Lim, L. S., Mitchell, P., Seddon, J. M., Holz, F. G., & Wong, T. Y. (2012). Age-related macular degeneration. *Lancet (London, England), 379*(9827), 1728–1738. https://doi.org/10.1016/S0140-6736(12)60282-7

Liu, R. T., Gao, J., Cao, S., Sandhu, N., Cui, J. Z., Chou, C. L., Fang, E., & Matsubara, J. A. (2013). Inflammatory mediators induced by amyloid-beta in the retina and RPE in vivo: implications for inflammasome activation in age-related macular degeneration. *Investigative Ophthalmology & Visual Science*, *54*(3), 2225–2237. https://doi.org/10.1167/iovs.12-10849

Livak, K. J., & Schmittgen, T. D. (2001). Analysis of relative gene expression data using real-time quantitative PCR and the 2(-Delta Delta C(T)) Method. *Methods (San Diego, Calif.)*, *25*(4), 402–408. https://doi.org/10.1006/meth.2001.1262

van Leeuwen, R., Klaver, C. C. W., Vingerling, J. R., Hofman, A., & de Jong, P. T. V. M. (2003). Epidemiology of age-related maculopathy: A review. *European Journal of Epidemiology*, *18*(9), 845–854. https://doi.org/10.1023/a:1025643303914

van Lookeren Campagne, M., LeCouter, J., Yaspan, B. L., & Ye, W. (2014). Mechanisms of age-related macular degeneration and therapeutic opportunities. *The Journal of Pathology*, *232*(2), 151–164. https://doi.org/10.1002/path.4266

Machalińska, A., Lubiński, W., Kłos, P., Kawa, M., Baumert, B., Penkala, K., Grzegrzółka, R., Karczewicz, D., Wiszniewska, B., & Machaliński, B. (2010). Sodium iodate selectively injuries the posterior pole of the retina in a dose-dependent manner: Morphological and electrophysiological study. *Neurochemical Research*, *35*(11), 1819–1827. https://doi.org/10.1007/s11064-010-0248-6

Mack, D. L., Guan, X., Wagoner, A., Walker, S. J., & Childers, M. K. (2014). Disease-in-A-dish: The contribution of patient-specific induced pluripotent stem cell technology to regenerative rehabilitation. *American Journal of Physical Medicine and Rehabilitation*, *93*(11), S155–S168. https://doi.org/10.1097/PHM.0000000000000141

Mandai, M., Watanabe, A., Kurimoto, Y., Hirami, Y., Morinaga, C., Daimon, T., … Takahashi, M. (2017). Autologous induced stem-cell-derived retinal cells for macular degeneration. *New England Journal of Medicine*, *376*(11), 1038–1046. https://doi.org/10.1056/NEJMoa1608368

Mazzoni, F., Safa, H., & Finnemann, S. C. (2014). Understanding photoreceptor outer segment phagocytosis: Use and utility of RPE cells in culture. *Experimental Eye Research*, *126*, 51–60. https://doi.org/10.1016/j.exer.2014.01.010

McLeod, D. S., Grebe, R., Bhutto, I., Merges, C., Baba, T., & Lutty, G. A. (2009). Relationship between RPE and choriocapillaris in age-related macular degeneration. *Investigative Ophthalmology & Visual Science*, *50*(10), 4982–4991. https://doi.org/10.1167/iovs.09-3639

Moriguchi, M., Nakamura, S., Inoue, Y., Nishinaka, A., Nakamura, M., Shimazawa, M., & Hara, H. (2018). Irreversible Photoreceptors and RPE Cells Damage by Intravenous Sodium Iodate in Mice Is Related to Macrophage Accumulation. *Investigative Ophthalmology & Visual Science*, 59(8), 3476–3487. https://doi.org/10.1167/iovs.17-23532

Nachtigal, A. L., Milenkovic, A., Brandl, C., Schulz, H. L., Duerr, L. M. J., Lang, G. E., Reiff, C., Herrmann, P., Kellner, U., & Weber, B. H. F. (2020). Mutation-Dependent Pathomechanisms Determine the Phenotype in the Bestrophinopathies. *International Journal of Molecular Sciences*, *21*(5), 1597. https://doi.org/10.3390/ijms21051597

Obert, E., Strauss, R., Brandon, C., Grek, C., Ghatnekar, G., Gourdie, R., & Rohrer, B. (2017). Targeting the tight junction protein, zonula occludens-1, with the connexin43 mimetic peptide, αCT1, reduces VEGF-dependent RPE pathophysiology. *Journal of Molecular Medicine (Berlin, Germany)*, *95*(5), 535–552. https://doi.org/10.1007/s00109-017-1506-8

Ogle, D.H.; Wheeler, P.; Dinno, A. (2019). FSA: Fisheries Stock Analysis. R package version 0.8.25.

Oh, Y. S., & Jun, H. S. (2018). Effects of Glucagon-Like Peptide-1 on Oxidative Stress and Nrf2 Signaling. *International Journal of Molecular Sciences, 19(1), 26.* https://doi.org/10.3390/ijms19010026

Omenn, G. S., Goodman, G. E., Thornquist, M. D., Balmes, J., Cullen, M. R., Glass, A., … Hammar, S. (1996). Risk factors for lung cancer and for intervention effects in CARET, the beta-carotene and retinol efficacy trial. *Journal of the National Cancer Institute*, *88*(21), 1550–1559. https://doi.org/10.1093/jnci/88.21.1550

Pennesi, M. E., Neuringer, M., & Courtney, R. J. (2012). Animal models of age related macular degeneration. *Molecular Aspects of Medicine*, *33*(4), 487–509. https://doi.org/10.1016/j.mam.2012.06.003

Pollard, K. S., Dudoit, S., & van der Laan, M. J. (2005). *Multiple Testing Procedures: the multtest Package and Applications to Genomics*. https://doi.org/10.1007/0-387-29362-0_15

R Development Core Team, R. (2011). R: A Language and Environment for Statistical Computing. In *R Foundation for Statistical Computing*. https://doi.org/10.1007/978-3-540-74686-7

Ranade, S. V., Wieland, M. R., Tam, T., Rea, J. C., Horvath, J., Hieb, A. R., Jia, W., Grace, L., Barteselli, G., & Stewart, J. M. (2022). The Port Delivery System with ranibizumab: a new paradigm for long-acting retinal drug delivery. *Drug Delivery*, *29*(1), 1326–1334. https://doi.org/10.1080/10717544.2022.2069301

Ratnayaka, J., & Lotery, A. (2020). Challenges in studying geographic atrophy (GA) age-related macular degeneration: The potential of a new mouse model with GA-like features. *Neural Regeneration Research*, *15*(5), 863–864. https://doi.org/10.4103/1673-5374.268972

Resnikoff, S., Pascolini, D., Etya'ale, D., Kocur, I., Pararajasegaram, R., Pokharel, G. P., & Mariotti, S. P. (2004). Global data on visual impairment in the year 2002. *Bulletin of the World Health Organization*, *82*(11), 844–851. https://doi.org//S0042-96862004001100009

Riss, T. L., Moravec, R. A., Niles, A. L., Duellman, S., Benink, H. A., Worzella, T. J., & Minor, L. (2013). Cell Viability Assays. In S. Markossian (Eds.) et. al., *Assay Guidance Manual*. Eli Lilly & Company and the National Center for Advancing Translational Sciences.

Rivera, A., Fisher, S. A., Fritsche, L. G., Keilhauer, C. N., Lichtner, P., Meitinger, T., & Weber, B. H. F. (2005). Hypothetical LOC387715 is a second major susceptibility gene for age-related macular degeneration, contributing independently of complement factor H to disease risk. *Human Molecular Genetics*, *14*(21), 3227–3236. https://doi.org/10.1093/hmg/ddi353

Rizzolo, L. J. (2007). Development and Role of Tight Junctions in the Retinal Pigment Epithelium. *International Review of Cytology*, *258*(07), 195–234. https://doi.org/10.1016/S0074-7696(07)58004-6

Rojo de la Vega, M., Chapman, E., & Zhang, D. D. (2018). NRF2 and the Hallmarks of Cancer. *Cancer Cell*, *34*(1), 21–43. https://doi.org/10.1016/j.ccell.2018.03.022

Rózanowska, M., Jarvis-Evans, J., Korytowski, W., Boulton, M. E., Burke, J. M., & Sarna, T. (1995). Blue light-induced reactivity of retinal age pigment. In vitro generation of oxygen-reactive species. *The Journal of Biological Chemistry*, *270*(32), 18825–18830. https://doi.org/10.1074/jbc.270.32.18825

Rózanowska, M., Wessels, J., Boulton, M., Burke, J. M., Rodgers, M. A. J., Truscott, T. G., & Sarna, T. (1998). Blue light-induced singlet oxygen generation by retinal lipofuscin in non-polar media. *Free Radical Biology and Medicine*, *24*(7-8), 1107–1112. https://doi.org/10.1016/s0891-5849(97)00395-x

Rudolf, M., Malek, G., Messinger, J. D., Clark, M. E., Wang, L., & Curcio, C. A. (2008). Sub-retinal drusenoid deposits in human retina: organization and composition. *Experimental Eye Research*, *87*(5), 402–408. https://doi.org/10.1016/j.exer.2008.07.010

Sachdeva, M. M., Cano, M., & Handa, J. T. (2014). Nrf2 signaling is impaired in the aging RPE given an oxidative insult. *Experimental Eye Research*, *119*, 111–114. https://doi.org/10.1016/j.exer.2013.10.024

Saini, J. S., Corneo, B., Miller, J. D., Kiehl, T. R., Wang, Q., Boles, N. C., Blenkinsop, T. A., Stern, J. H., & Temple, S. (2017). Nicotinamide Ameliorates Disease Phenotypes in a Human iPSC Model of Age-Related Macular Degeneration. *Cell Stem Cell*, *20*(5), 635–647.e7. https://doi.org/10.1016/j.stem.2016.12.015

Sarks, J., Tang, K., Killingsworth, M., Arnold, J., & Sarks, S. (2006). Development of atrophy of the retinal pigment epithelium around disciform scars. *British Journal of Ophthalmology*, *90*(4), 442–446. https://doi.org/10.1136/bjo.2005.083022

Scholl, H. P. N., Charbel Issa, P., Walier, M., Janzer, S., Pollok-Kopp, B., Börncke, F., Fritsche, L. G., Chong, N. V., Fimmers, R., Wienker, T., Holz, F. G., Weber, B. H. F., & Oppermann, M. (2008). Systemic complement activation in age-related macular degeneration. *PloS ONE*, *3*(7), e2593. https://doi.org/10.1371/journal.pone.0002593

Schutt, F., Bergmann, M., Holz, F. G., & Kopitz, J. (2003). Proteins modified by malondialdehyde, 4-hydroxynonenal, or advanced glycation end products in lipofuscin of human retinal pigment epithelium. *Investigative Ophthalmology & Visual Science*, *44*(8), 3663–3668. https://doi.org/10.1167/iovs.03-0172

Seddon, J. M., Cote, J., & Rosner, B. (2003). Progression of age-related macular degeneration: association with dietary fat, transunsaturated fat, nuts, and fish intake. *Archives of Ophthalmology (Chicago, Ill. : 1960)*, *121*(12), 1728–1737. https://doi.org/10.1001/archopht.121.12.1728

Seddon, J. M., Cote, J., Page, W. F., Aggen, S. H., & Neale, M. C. (2005). The US Twin Study of Age-Related Macular Degeneration. *Archives of Ophthalmology*, *123*(3), 321. https://doi.org/10.1001/archopht.123.3.321

Sikorski, E. M., Hock, T., Hill-Kapturczak, N., & Agarwal, A. (2004). The story so far: Molecular regulation of the heme oxygenase-1 gene in renal injury. *American Journal of Physiology - Renal Physiology*, *286*(3 55-3). https://doi.org/10.1152/ajprenal.00297.2003

Singh, R., Phillips, M. J., Kuai, D., Meyer, J., Martin, J. M., Smith, M. A., Perez, E. T., Shen, W., Wallace, K. A., Capowski, E. E., Wright, L. S., & Gamm, D. M. (2013). Functional analysis of serially expanded human iPS cell-derived RPE cultures. *Investigative Ophthalmology & Visual Science*, *54*(10), 6767–6778. https://doi.org/10.1167/iovs.13-11943 (a)

Singh, R., Shen, W., Kuai, D., Martin, J. M., Guo, X., Smith, M. A., … Gamm, D. M. (2013). iPS cell modeling of best disease: Insights into the pathophysiology of an inherited macular degeneration. *Human Molecular Genetics*, *22*(3), 593–607. https://doi.org/10.1093/hmg/dds469 (b)

Singh, R., Kuai, D., Guziewicz, K. E., Meyer, J., Wilson, M., Lu, J., … Gamm, D. M. (2015). Pharmacological Modulation of Photoreceptor Outer Segment Degradation in a Human iPS Cell Model of Inherited Macular Degeneration. *Molecular Therapy : The Journal of the American Society of Gene Therapy*, *23*(11), 1700–1711. https://doi.org/10.1038/mt.2015.141

Skelly, A., Bezlyak, V., Liew, G., Kap, E., & Sagkriotis, A. (2019). Treat and Extend Treatment Interval Patterns with Anti-VEGF Therapy in nAMD Patients. *Vision (Basel, Switzerland)*, *3*(3), 41. https://doi.org/10.3390/vision3030041

Smith, W., Assink, J., Klein, R., Mitchell, P., Klaver, C., Klein, B., Hofman, A., Jensen, S., Wang J. J., de Jong, P. (2001). Risk factors for incident age-related macular degeneration: Pooled findings from 3 continents. *Ophthalmology*, *111*(7), 1280–1287. https://doi.org/10.1016/j.ophtha.2003.11.010

Solomon, S. D., Lindsley, K., Vedula, S. S., Krzystolik, M. G., & Hawkins, B. S. (2019). Anti-vascular endothelial growth factor for neovascular age-related macular degeneration. *The Cochrane Database of Systematic Reviews*, *3*(3), CD005139. https://doi.org/10.1002/14651858.CD005139.pub4

Somasundaran, S., Constable, I. J., Mellough, C. B., & Carvalho, L. S. (2020). Retinal pigment epithelium and age-related macular degeneration: A review of major disease mechanisms. *Clinical & Experimental Ophthalmology*, *48*(8), 1043–1056. https://doi.org/10.1111/ceo.13834

Spaide, R. F., Jaffe, G. J., Sarraf, D., Freund, K. B., Sadda, S. R., Staurenghi, G., Waheed, N. K., Chakravarthy, U., Rosenfeld, P. J., Holz, F. G., Souied, E. H., Cohen, S. Y., Querques, G., Ohno-Matsui, K., Boyer, D., Gaudric, A., Blodi, B., Baumal, C. R., Li, X., Coscas, G. J., … Fujimoto, J. (2020). Consensus Nomenclature for Reporting Neovascular Age-Related Macular Degeneration Data: Consensus on Neovascular Age-Related Macular Degeneration Nomenclature Study Group. *Ophthalmology*, *127*(5), 616–636. https://doi.org/10.1016/j.ophtha.2019.11.004

Sparrow, J. R., & Boulton, M. (2005). RPE lipofuscin and its role in retinal pathobiology. *Experimental Eye Research*, *80*(5), 595–606. https://doi.org/10.1016/j.exer.2005.01.007

Sparrow, J. R., Hicks, D., & Hamel, C. P. (2010). The retinal pigment epithelium in health and disease. *Current Molecular Medicine*, *10*(9), 802–823. https://doi.org/10.2174/156652410793937813

Srinivasan, B., Kolli, A. R., Esch, M. B., Abaci, H. E., Shuler, M. L., & Hickman, J. J. (2015). TEER measurement techniques for in vitro barrier model systems. *Journal of Laboratory Automation*, *20*(2), 107–126. https://doi.org/10.1177/2211068214561025

Stevenson, B. R., Siliciano, J. D., Mooseker, M. S., & Goodenough, D. A. (1986). Identification of ZO-1: A high molecular weight polypeptide associated with the tight junction (Zonula Occludens) in a variety of epithelia. *Journal of Cell Biology*, *103*(3), 755–766. https://doi.org/10.1083/jcb.103.3.755

Stradiotto, E., Allegrini, D., Fossati, G., Raimondi, R., Sorrentino, T., Tripepi, D., Barone, G., Inforzato, A., & Romano, M. R. (2022). Genetic Aspects of Age-Related Macular Degeneration and Their Therapeutic Potential. *International Journal of Molecular Sciences*, *23*(21), 13280. https://doi.org/10.3390/ijms232113280

Strauss, O. (2005). The retinal pigment epithelium in visual function. *Physiological Reviews*, *85*(3), 845–881. https://doi.org/10.1152/physrev.00021.2004

Strunz, T., Kiel, C., Sauerbeck, B. L., & Weber, B. H. F. (2020). Learning from Fifteen Years of Genome-Wide Association Studies in Age-Related Macular Degeneration. *Cells*, *9*(10), 2267. https://doi.org/10.3390/cells9102267

Suárez-Barrio, C., Del Olmo-Aguado, S., García-Pérez, E., de la Fuente, M., Muruzabal, F., Anitua, E., Baamonde-Arbaiza, B., Fernández-Vega-Cueto, L., Fernández-Vega, L., & Merayo-Lloves, J. (2020). Antioxidant Role of PRGF on RPE Cells after Blue Light Insult as a Therapy for Neurodegenerative Diseases. *International Journal of Molecular Sciences*, *21*(3), 1021. https://doi.org/10.3390/ijms21031021

Swaroop, A., Chew, E. Y., Bowes Rickman, C., & Abecasis, G. R. (2009). Unraveling a Multifactorial Late-Onset Disease: From Genetic Susceptibility to Disease Mechanisms for Age-Related Macular Degeneration. *Annual Review of Genomics and Human Genetics*, *10*(1), 19–43. https://doi.org/10.1146/annurev.genom.9.081307.164350

Takahashi, K., & Yamanaka, S. (2006). Induction of Pluripotent Stem Cells from Mouse Embryonic and Adult Fibroblast Cultures by Defined Factors. *Cell*, *126*(4), 663–676. https://doi.org/10.1016/j.cell.2006.07.024

Takahashi, K., Tanabe, K., Ohnuki, M., Narita, M., Ichisaka, T., Tomoda, K., & Yamanaka, S. (2007). Induction of Pluripotent Stem Cells from Adult Human Fibroblasts by Defined Factors. *Cell*, *131*(5), 861–872. https://doi.org/10.1016/j.cell.2007.11.019

Takayama, K., Kaneko, H., Kataoka, K., Kimoto, R., Hwang, S. J., Ye, F., Nagasaka, Y., Tsunekawa, T., Matsuura, T., Nonobe, N., Ito, Y., & Terasaki, H. (2016). Nuclear Factor (Erythroid-Derived)-Related Factor 2-Associated Retinal Pigment Epithelial Cell Protection under Blue Light-Induced Oxidative Stress. *Oxidative Medicine and Cellular Longevity*, 2016, 8694641. https://doi.org/10.1155/2016/8694641

Tarau, I. S., Berlin, A., Curcio, C. A., & Ach, T. (2019). The Cytoskeleton of the Retinal Pigment Epithelium: from Normal Aging to Age-Related Macular Degeneration. *International Journal of Molecular Sciences*, *20*(14), 3578. https://doi.org/10.3390/ijms20143578

Thomas, C. J., Mirza, R. G., & Gill, M. K. (2021). Age-Related Macular Degeneration. *The Medical Clinics of North America*, *105*(3), 473–491. https://doi.org/10.1016/j.mcna.2021.01.003

Thimmulappa, R. K., Lee, H., Rangasamy, T., Reddy, S. P., Yamamoto, M., Kensler, T. W., & Biswal, S. (2006). Nrf2 is a critical regulator of the innate immune response and survival during experimental sepsis. *The Journal of Clinical Investigation*, *116*(4), 984–995. https://doi.org/10.1172/JCI25790

Tomany, S. C., Wang, J. J., Van Leeuwen, R., Klein, R., Mitchell, P., Vingerling, J. R., Klein, B. E., Smith, W., & De Jong, P. T. V. M. (2004). Risk factors for incident age-related macular degeneration: pooled findings from 3 continents. *Ophthalmology*, *111*(7), 1280–1287. https://doi.org/10.1016/j.ophtha.2003.11.010

Vogt, S. D., Curcio, C. A., Wang, L., Li, C. M., McGwin, G., Jr, Medeiros, N. E., Philp, N. J., Kimble, J. A., & Read, R. W. (2011). Retinal pigment epithelial expression of complement regulator CD46 is altered early in the course of geographic atrophy. *Experimental Eye Research*, *93*(4), 413–423. https://doi.org/10.1016/j.exer.2011.06.002

Voisin, A., Monville, C., Plancheron, A., Béré, E., Gaillard, A., & Leveziel, N. (2019). Cathepsin B pH-Dependent Activity Is Involved in Lysosomal Dysregulation in Atrophic Age-Related Macular Degeneration. *Oxidative Medicine and Cellular Longevity*, *2019*, 5637075. https://doi.org/10.1155/2019/5637075

Volland, S., Esteve-Rudd, J., Hoo, J., Yee, C., & Williams, D. S. (2015). A comparison of some organizational characteristics of the mouse central retina and the human macula. *PLoS ONE*, *10*(4), 1–13. https://doi.org/10.1371/journal.pone.0125631

Waisbourd, M., Loewenstein, A., Goldstein, M., & Leibovitch, I. (2007). Targeting vascular endothelial growth factor: A promising strategy for treating age-related macular degeneration. *Drugs and Aging*, *24*(8), 643–662. https://doi.org/10.2165/00002512-200724080-00003

Warwick, A., & Lotery, A. (2018). Genetics and genetic testing for age-related macular degeneration. *Eye (London, England)*, *32*(5), 849–857. https://doi.org/10.1038/eye.2017.245

Wang, L., Kondo, N., Cano, M., Ebrahimi, K., Yoshida, T., Barnett, B. P., Biswal, S., & Handa, J. T. (2014). Nrf2 signaling modulates cigarette smoke-induced complement activation in retinal pigmented epithelial cells. *Free Radical Biology & Medicine*, *70*, 155–166. https://doi.org/10.1016/j.freeradbiomed.2014.01.015 (a)

Wang, J., Iacovelli, J., Spencer, C., & Saint-Geniez, M. (2014). Direct effect of sodium iodate on neurosensory retina. *Investigative Ophthalmology & Visual Science*, *55*(3), 1941–1953. https://doi.org/10.1167/iovs.13-13075 (b)

Westenskow, P. D., Moreno, S. K., Krohne, T. U., Kurihara, T., Zhu, S., Zhang, Z. N., Zhao, T., Xu, Y., Ding, S., & Friedlander, M. (2012). Using flow cytometry to compare the dynamics of photoreceptor outer segment phagocytosis in iPS-derived RPE cells. *Investigative Ophthalmology & Visual Science*, *53*(10), 6282–6290. https://doi.org/10.1167/iovs.12-9721

Winkler, T. W., Grassmann, F., Brandl, C., Kiel, C., Günther, F., Strunz, T., Weidner, L., Zimmermann, M. E., Korb, C. A., Poplawski, A., Schuster, A. K., Müller-Nurasyid, M.,

Peters, A., Rauscher, F. G., Elze, T., Horn, K., Scholz, M., Cañadas-Garre, M., McKnight, A. J., Quinn, N., … Weber, B. H. F. (2020). Genome-wide association meta-analysis for early age-related macular degeneration highlights novel loci and insights for advanced disease. *BMC Medical Genomics*, *13*(1), 120. https://doi.org/10.1186/s12920-020-00760-7

Wong, W. L., Su, X., Li, X., Cheung, C. M. G., Klein, R., Cheng, C. Y., & Wong, T. Y. (2014). Global prevalence of age-related macular degeneration and disease burden projection for 2020 and 2040: a systematic review and meta-analysis. *The Lancet Global Health*, *2*(2), e106–e116. https://doi.org/10.1016/S2214-109X(13)70145-1

Wu, J., Seregard, S., & Algvere, P. V. (2006). Photochemical Damage of the Retina. *Survey of Ophthalmology*, *51*(5), 461–481. https://doi.org/10.1016/j.survophthal.2006.06.009

Xie, X., Feng, J., Kang, Z., Zhang, S., Zhang, L., Zhang, Y., Li, X., & Tang, Y. (2017). Taxifolin protects RPE cells against oxidative stress-induced apoptosis. *Molecular Vision*, 23, 520–528.

Yamanaka, S. (2012). Induced pluripotent stem cells: Past, present, and future. *Cell Stem Cell*, *10*(6), 678–684. https://doi.org/10.1016/j.stem.2012.05.005

Yeligar, S. M., Machida, K., & Kalra, V. K. (2010). Ethanol-induced HO-1 and NQO1 are differentially regulated by HIF-1alpha and Nrf2 to attenuate inflammatory cytokine expression. *The Journal of Biological Chemistry*, *285*(46), 35359–35373. https://doi.org/10.1074/jbc.M110.138636

Yoon, J. M., Shin, D. H., Kong, M., & Ham, D. I. (2022). Age-related macular degeneration eyes presenting with cuticular drusen and reticular pseudodrusen. *Scientific Reports*, *12*(1), 5681. https://doi.org/10.1038/s41598-022-09608-9

Young, R. W. (1967). The renewal of photoreceptor cell outer segments. *The Journal of Cell Biology*, *33*(1), 61–72. https://doi.org/10.1083/jcb.33.1.61

Young, R. W., & Bok, D. (1969). Participation of the retinal pigment epithelium in the rod outer segment renewal process. *The Journal of Cell Biology*, *42*(2), 392–403. https://doi.org/10.1083/jcb.42.2.392

Young, R. W. (1978). The daily rhythm of shedding and degradation of rod and cone outer segment membranes in the chick retina. *Investigative Ophthalmology & Visual Science*, *17*(2), 105–116.

Yu, D. Y., & Cringle, S. J. (2001). Oxygen distribution and consumption within the retina in vascularised and avascular retinas and in animal models of retinal disease. *Progress in Retinal and Eye Research*, *20*(2), 175–208. https://doi.org/10.1016/s1350-9462(00)00027-6

Zeiss, C. J. (2010). Review paper: Animals as models of age-related macular degeneration: An imperfect measure of the truth. *Veterinary Pathology*, *47*(3), 396–413. https://doi.org/10.1177/0300985809359598

Zhang D. D. (2006). Mechanistic studies of the Nrf2-Keap1 signaling pathway. *Drug Metabolism Reviews*, *38*(4), 769–789. https://doi.org/10.1080/03602530600971974

Zhang, H., Liu, Y. Y., Jiang, Q., Li, K. R., Zhao, Y. X., Cao, C., & Yao, J. (2014). Salvianolic acid A protects RPE cells against oxidative stress through activation of Nrf2/HO-1 signaling. *Free Radical Biology and Medicine*, *69*, 219–228. https://doi.org/10.1016/j.freeradbiomed.2014.01.025

Zhang, X. Y., Ng, T. K., Brelén, M. E., Wu, D., Wang, J. X., Chan, K. P., Yung, J. S. Y., Cao, D., Wang, Y., Zhang, S., Chan, S. O., & Pang, C. P. (2016). Continuous exposure to non-lethal doses of sodium iodate induces retinal pigment epithelial cell dysfunction. *Scientific Reports*, *6*, 37279. https://doi.org/10.1038/srep37279

Zhao, Z., Chen, Y., Wang, J., Sternberg, P., Freeman, M. L., Grossniklaus, H. E., & Cai, J. (2011). Age-related retinopathy in NRF2-deficient mice. *PloS ONE*, *6*(4), e19456. https://doi.org/10.1371/journal.pone.0019456

Zhao, H., Wang, R., Ye, M., & Zhang, L. (2019). Genipin protects against H2O2-induced oxidative damage in retinal pigment epithelial cells by promoting Nrf2 signaling. *International Journal of Molecular Medicine*, *43*(2), 936–944. https://doi.org/10.3892/ijmm.2018.4027

Zhou, P., Kannan, R., Spee, C., Sreekumar, P. G., Dou, G., & Hinton, D. R. (2014). Protection of retina by αB crystallin in sodium iodate induced retinal degeneration. *PLoS ONE*, *9*(5), 1–15. https://doi.org/10.1371/journal.pone.0098275

List of Abbreviations

Abbreviation	Meaning
ACTB	Beta actin
AMD	Age-related macular degeneration
ARPE-19	Adult RPE cell line-19
BL	Blue light
CD46	Membrane cofactor protein
CNV	Choroidal neovascularization
DAPI	4′,6-diamidino-2-phenylindole
GA	Geographic atrophy
H	High risk
hiPSC-RPE	Human iPSC-derived RPE
HMOX1	Heme oxygenase 1
HNE	4-Hydroxynonenal
HPRT1	Hypoxanthine phosphoribosyltransferase 1
iPSCs	Induced pluripotent stem cells
KEAP1	Kelch-like ECH-associated protein 1
L	Low risk
LDH	Lactate dehydrogenase
LED	Light-emitting diode
mRNA	Messenger ribonucleic acid
MTT	3-(4,5-dimethylthiazol-2-yl)-2,5-diphenyltetrazolium bromide
NLRP3	Nucleotide-binding oligomerization domain-like receptor family, pyrin domain-containing protein 3
NQO1	NAD(P)H dehydrogenase [quinone] 1
NRF2	Nuclear factor erythroid 2-related factor 2
NV-AMD	Neovascular AMD
PBMCs	Peripheral blood mononuclear cells
POS	Photoreceptor outer segments
PQ	Paraquat
qRT-PCR	Quantitative real-time polymerase chain reaction
ROS	Reactive oxygen species
RPE	Retinal pigment epithelium
SD	Standard deviation
SI	Sodium iodate
TEER	Transepithelial electrical resistance
TF	Transcription factor
VEGFA	Vascular endothelial growth factor A
ZO-1	Tight junction protein 1; Zonula occludens 1

List of Figures

List of Tables

Acknowledgements

I would like to thank my supervisor, Professor Dr. Bernhard Weber, for introducing me to such an exciting field of research. The skills I was able to acquire and sharpen during my time in your laboratory have been invaluable to me and will certainly be beneficial to my future career. It was a privilege to have worked at the Institute of Human Genetics. Especially valuable and intellectually stimulating was the practice of presenting my work to you and the team at regular intervals. Thank you very much for supporting me and providing constructive feedback along the way.

Special thanks and great appreciation as well to Dr. Karolina Plößl. I am so glad to have worked alongside an extremely diligent, conscientious, well-organized and passionate scientist. Thank you so much for teaching me such a wide range of skills and methods regarding laboratory work, data analysis and result presentation, as well as how to efficiently organize experiments. I really appreciate the time and effort you spent in supporting me with my dissertation. It was an absolute pleasure to work with you.

Thank you very much to Dr. Christina Kiel for helping me with the statistical analysis of my data.

The entire team of the Institute of Human Genetics was extremely supportive and collegial. It was so pleasant and rewarding to be part of a team that works so well together.

Selbstständigkeitserklärung

Ich erkläre hiermit, dass ich die vorliegende Arbeit ohne unzulässige Hilfe Dritter und ohne Benutzung anderer als der angegebenen Hilfsmittel angefertigt habe. Die aus anderen Quellen direkt oder indirekt übernommenen Daten und Konzepte sind unter Angabe der Quelle gekennzeichnet. Insbesondere habe ich nicht die entgeltliche Hilfe von Vermittlungs- bzw. Beratungsdiensten (Promotionsberater oder andere Personen) in Anspruch genommen. Niemand hat von mir unmittelbar oder mittelbar geldwerte Leistungen für Arbeit erhalten, die im Zusammenhang mit dem Inhalt der vorgelegten Dissertation stehen. Die Arbeit wurde bisher weder im In- noch im Ausland in gleicher oder ähnlicher Form einer anderen Prüfungsbehörde vorgelegt.

Regensburg, den 07. Februar 2023 Emily Webster